

國立交通大學  
材料科學與工程學系  
博士論文

半導體微影奈米尺寸的穩定性控制  
**The Stability Control of Semiconductor  
Photo Lithography in Nano Size**



研究生:郭養國  
指導教授:朝春光 博士

中華民國九十三年 十二月

## ■ Abstract (中文)

一個新的 Reticle 設計，利用鑽石高熱傳導，在傳統的 pellicle-reticle 底端增加一層鑽石薄膜，鑽石材料取代 pellicle。這個方法將會幫助未來微影(photo-lithography)製程進展到 35nm 以下，光罩(reticle)因長時間受到光熱能的影響而產生微量膨脹變形問題獲得改善。曝光能量是影響關鍵尺寸 (Critical Dimension)的重要因素，曝光能量會改變線寬(Line-Width)與白邊(white wall)的大小，且線寬與白邊這兩者與曝光能量為線性關係( $R^2 > 0.85$ )，但是如果曝光能量太高或太低將會使線寬不穩定。曝光能量之所以能影響關鍵尺寸的原因是光阻(Photo-Resist)吸收到比較高的能量時與顯影液接觸會產生比較劇烈的中和(Neutralized)反應，所以越高曝光能量時線寬會越小，且關鍵尺寸會因為邊緣受到高的能量而產生光阻吸收能量不均勻的現象，因為這個原因所以要得到更小的關鍵尺寸並不能把曝光能量刻意的加高，如果要使用這種方式，則必須更改用適合這種能量的光阻。如果要取得更小的線寬則必須使用解析度(resolution)較佳的光阻與波長較短的光源。但是高曝光能量卻能使得光阻底部吸收到更多的反射能量而使得白邊變小。但是如果曝光能量太低，將使得光阻吸收到能量不足而無法與 TMAH(Tetramethylammonium Hydroxide)產生中和反應，而無法形成圖形。

## ■ Abstract (English)

A new reticle is designed that takes advantage of the high value of thermal conductivity of diamond to add a layer of diamond film to the bottom of traditional pellicle-reticle; that is, the new reticle replaces the pellicle with a diamond material. This method may help maintain the future manufacturing process of photo-lithography below 35 nm and can improve the problem of slightly out of shape reticle caused by the long-term effects of light and thermal energy. Exposure dose is one of the most important factors that affects CD (Critical Dimension) bar since it can change the dimension of line-width and white wall. In this work, both line-width and white wall present a linear relationship ( $R^2 > 0.85$ ) with respect to the exposure dose. However, too high or too low of exposure dose would impose the instability of line-width. The reason for exposure dose to affect CD bar is that when absorbing high energy the photo-resist (PR) can produce more severely neutralized reaction as it in contact with developer. Therefore, the higher the exposure dose the smaller is the line-width. Also, CD bar would reveal inhomogeneous phenomenon caused by absorbing high energy via the edge of PR. Due to this reason, increasing the exposure dose intentionally is not an appropriate method to obtain a smaller CD bar. When it comes to using exposure energy to obtain the

desirable CD, PR capable of being exposed with higher energy should be considered. If it becomes necessary to obtain much smaller line width, then it is necessary to use PR of better resolution in conjunction with a light source containing a much lower wavelength. But, higher exposure dose would cause the bottom of PR to absorb more reflective energy and make white wall become smaller. On the contrary, if exposure dose becomes too low, PR would not form a pattern due to the fact that the absorption of exposure energy by PR is not strong enough to produce a neutralized reaction when in contact with TMAH (Tetramethylammonium Hydroxide).



## 誌 謝

在這段時間中能夠順利取得博士文憑，最主要要感謝指導教授朝春光博士的細心指導與協助，使得論文得以順利完成。

其次我要感謝我的口試委員：交通大學材料系系主任張翼博士，工研院光電所副主任許榮宗博士，清華大學材料系林樹均博士，中科院游欽宏博士，國家豪微米研究室柯富祥博士，在口試期間的指導。

接下來要感謝的是美國 Duane Morris 專利事務所 Randy 與 Won Joon Kouh 在專利技術上的協助，使之能夠在專利技術上的突破。

求學期間，家人默默地關懷與付出，是我精神上的支柱，尤其是老婆與祐祐是我精神上最大的支柱，我會好好珍惜。

**List of paper**

Abstract (中文).....

Abstract(English) .....

誌謝.....

Table of Figures.....A

List of Figures.....B

Chapter 1 Introduction.....1

Chapter 2 paper review.....4

Chapter 3 The traditional reticle level detects the method.....7

    Introduction.....7

    Summary of the reticle level detects the method.....7

Chapter 4 The traditional thermal of slightly out of shape reticle detects the method.....26

    Introduction.....26

    Summary of the reticle thermal detects the method.....26

Chapter 5

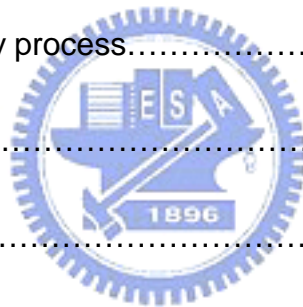
    Improvement in instable analysis of heat inflation induced line-width after replacing pellicle with diamond film on reticle

(photo-masks) .....	40
Introduction.....	40
The heat conduction equation.....	41
Comparisons between traditional pellicle-reticle model and diamond films-reticle thermal conductivity mode.....	42
Experimental method.....	44
Results.....	45
Diamond Reticle thermal conductivity.....	45
Diamond Reticle Intensity.....	46
Effects of improved oxide layer on diamond reticle on CD (Critical Dimension) bar.....	46
Conclusions.....	47
List of Table.....	48
 Chapter 6	
Analysis of instability in a Critical Dimension Bar due to focus and exposure.....	51
Introduction.....	51
Experimental.....	52
Equipment.....	52

Results and Discussion.....	56
Symmetrical Multiprocessing Best Focus.....	56
Focus.....	59
DOF (Depth Of Focus) .....	61
Exposure dose.....	62
Conclusions.....	64

Chapter 7

Analysis of instability line width and white wall created by the photolithography process.....	74
Introduction.....	74
Experimental.....	75
Equipment.....	75
Experimental.....	78
Results and Discussion.....	78
Focus and Exposure Theory.....	78
The impact of exposure dose on CD Bar.....	80
Standing wave.....	83
The impact of focus on white wall.....	85
Conclusions.....	87





List of Table.....88

Chapter 8

Analysis of the Effects of Reflectance and Refraction Generated by  
Wafers Made from Fused Silica, ALONy and TiSixNy Under  
Different Light Sources on Pattern Length and Best  
Focus.....101

Introduction.....101

Experimental.....102

Results and Discussion.....103

    Method used to obtain the best focus.....103

    Focus Exposure Theory.....104

    Influence of Wafer Surface Materials on Best Focus  
    Variation.....106

    Influence of Wafer Surface Materials on DOF (Depth of  
    Focus) Variation.....108

    Influence of Exposure Dose on Pattern Length Variation for  
    Different Wafer Surface Materials.....109

    Astigmatism.....111

Conclusions.....112



Chapter 9 Conclusions.....121

References.....123



■ **List of Table**

Table 5.1 Thermal properties of film and substrate .....48

Table 5.2 Various types of reticle intensity.....48

Table 7.1 Sensitivity of photo-resist used in experiment.....88



■ List of Figures

Figure 3.1 is a schematic illustration of one embodiment of the apparatus of the present invention.....18

Figures 3.2 are schematic illustrations of the apparatus of Figure 1 in different scenarios for various ways in which the surface being monitored can deviate from the reference plane. ....19

Figures 3.3 are schematic illustrations of the apparatus of Figure 1 in different scenarios for various ways in which the surface being monitored can deviate from the reference plane. ....20

Figures 3.4 are schematic illustrations of the apparatus of Figure 1 in different scenarios for various ways in which the surface being monitored can deviate from the reference plane. ....21

Figure 3.5 is a schematic illustration of another embodiment of the apparatus of the present invention. ....22

Figure 3.6 is a schematic illustration of an exemplary reticle stage employing four apparatuses of the present invention on four corners of the reticle stage.....23

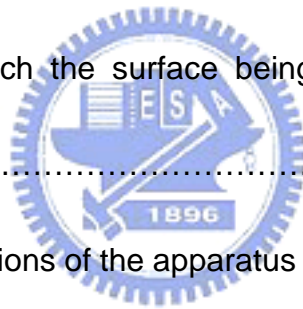


Figure 3.7 is a sectional schematic illustration of another embodiment of the apparatus of the present invention. ....24

Figure 3.8 is an exploded view of the apparatus of Figure 3.7.....25

Figure 4.1 is a schematic view of an illustrative embodiment of an optical reticle thermal detector according to the present invention, illustrating implementation of the invention when the reticle is in an undistorted condition.....37

Figure 4.2 is a schematic view of a reticle, illustrating reflection of light from the reticle when the reticle is in the undistorted condition (solid lines) and when the reticle is thermally distorted (dashed lines) .....37

Figure 4.3 is a schematic view of an illustrative embodiment of an optical reticle thermal detector according to the present invention, illustrating implementation of the invention when the reticle is in a thermally-distorted condition.....38

Figure 4.4 is a schematic view of an illustrative embodiment of a mechanical reticle thermal detector according to the present invention.....38

Figure 4.5 is a schematic view of an illustrative embodiment of an electromechanical reticle thermal detector according to the present invention.....39

Figure 5.1 Route Map of Laser Beam Used in Experiment.....49

Figure 5.2 Traditional reticle and diamond film reticle composite.....49

Figure 5.3 Variances of Line-Width/Diameter of Wafer CD Bar/Via in Different Types of Reticles Following Continuing 200 hour photo exposure.....50

Figure 6.1 I-line symmetrical multiprocessing focus. Pattern length changes observed using an Applied Materials SEM Vision. (a) At focus=0 $\mu\text{m}$ , the pattern had the same shape as that on the reticle; (b) at a focus of -0.8 $\mu\text{m}$ , the pattern was shortened; (c) at focus=-1.2 $\mu\text{m}$ , the pattern was shortened and completely transformed; (d) at focus=-1.6 $\mu\text{m}$ , the pattern irregularly contracted into a shape that resembled an ellipse.....65

Figure 6.2 DUV symmetrical multiprocessing focus. Pattern length changes observed using an Applied Materials SEM Vision: (a) At focus=0 $\mu\text{m}$ , the pattern had the same shape as that on the reticle, but was longer; (b) at focus=-0.8 $\mu\text{m}$ , the pattern was shortened; (c) at focus=-1.2 $\mu\text{m}$ , the pattern was shortened and completely transformed; d) at focus=-1.6 $\mu\text{m}$ , the pattern became an irregular shapes.....66

Figure 6.3 Process latitude smiley curve of pattern length-focus, with an I-line stepper and a positive resist.....67

Figure 6.4 The process latitude smiley curve pattern length-focus, with a DUV stepper and a positive resist. ....68

Figure 6.5 I-line light source, PFI-58 resist, exposure dose =200  $mJ / cm^2$ , focus=0 $\mu\text{m}$ : Observed with the Applied Materials SEM at a scanning angle of +45°: line-width=0.682  $\mu\text{m}$ , white wall, and three -dimensional picture.....69

Figure 6.6 I-line light source, PFI 58 Resist, Exposure =200  $mJ / cm^2$ ; Figures of white wall and Independent Proximity When (a) Focus=+0.4  $\mu\text{m}$ , (b) Focus=-0.4  $\mu\text{m}$ ,

under multiplying rate 50KV of HITACHI S-9200 CD SEM and Line-Width=0.2  $\mu$  m. No matter it is 0  $\mu$  m or 0  $\mu$  m, there is regular triangle while wall.....70

Figure 6.7 Deep UV light source, Exposure =30  $mJ/cm^2$ , Figures of white wall and Independent Proximity When Focus=0, under multiplying rate 50KV of HITACHI S-9200 CD SEM and Line-Width=0.2  $\mu$  m. The independent proximity of Deep UV is smaller than I-line. ....71

Figure 6.8 I-line light source, the figure of linear relationship of (a) PFI-58 Resist, (b) IX950 Resist and (c) PFI56A6 Resist Exposure- Line Width.....72

Figure 7.1 (a) Stepper Exposure Diagram, (b) Influence of Focus on Exposure Area. (c) Focus Locations following Reflectance and Refraction on Photo Resist and Wafer Surface by Light Source.....89

Figure 7.2 (a) SEPR 451, (b) SEPR-432 and (c) SEPR-450H, correlation diagram of exposure dose and line width, (d) Graphs showing exposure dose vs. white wall for three different PR. ....91

Figure 7.3 DUV light source, SEPR 451 photo resist, exposure time =40  $mJ/cm^2$ , focus=0 $\mu$ m. Observed with the Hitachi SEM at a magnification voltage of 50Kv. i) line-width, ii) white wall. ....95

Figure 7.4 DUV light source, SEPR 432 photo resist, exposure dose =30  $mJ/cm^2$ , Observed with the Applied Materials SEM at a scanning angle of +45°: (a) focus=0  $\mu$ m, (b) focus=+1.0 $\mu$ m CD Bar three -dimensional picture.....95

Figure 7.5 Collapse of CD bar for SEPR 451 PR at exposure dose of  $80 \text{ mJ/cm}^2$ , picture taken by Applied Materials SEM Vision. ....96

Figure 7.6 Exposure dose becomes too low ( $10 \text{ mJ/cm}^2$ ) for SEPR-450H PR, observed with the Hitachi SEM at a magnification voltage of 100Kv. PR would not form a pattern.....97

Figure 7.7 (a) high exposure dose ( $50 \text{ mJ/cm}^2$ ) makes CD bar become smaller. (b)Instability of CD bar caused by high exposure dose ( $60 \text{ mJ/cm}^2$ ) for SEPR-432 PR, by Applied Materials SEM Vision. ....99

Figure 7.8 (a) add top ARC to SEPR 432, (b) add bottom ARC to SEPR 432, (c) SEPR 432 without adding any ARC, graphs showing standing wave as side wall of CD bar was observed via Applied Materials SEM Vision.....100

Figure 8.1 Stepper Exposure Diagram, Best Focus Locations following Refraction on Photo Resist and Wafer Surface by Auto Focus Light Source.....114

Figure 8.2 Pattern Length Focus Process Latitude Smiley Curve Obtained by Deep UV Together with SEPR 432 Photo Resist from Wafers Made using (a) fused silica, (b)  $AlO_xN_y$  or (c)  $TiSi_xN_y$  via Matrix Exposure.....115

Figure 8.3 Observed with the Applied Materials SEM at a scanning angle of  $+45^\circ$ , (a) Fused silica wafer Exposure Dose= $46 \text{ mJ/cm}^2$  and focus= $0.0\mu\text{m}$ , (b)  $AlO_xN_y$  wafer Exposure Dose= $56 \text{ mJ/cm}^2$  and focus= $-0.45\mu\text{m}$  (c)  $TiSi_xN_y$  wafer Exposure Dose= $56 \text{ mJ/cm}^2$  and focus= $-0.15\mu\text{m}$ .....117



Figure 8.4 Collapse of CD bar for (a)  $AlO_xN_y$  wafer at exposure dose of  $56 \text{ mJ/cm}^2$  and focus= $-0.65\mu\text{m}$  (b)  $TiSi_xN_y$  wafer at exposure dose of  $56 \text{ mJ/cm}^2$  and focus= $-0.45\mu\text{m}$ , picture taken by Applied Materials SEM Vision.....118



## Chapter 1

### Introduction

The fabrication of various solid state devices requires the use of planar substrates, or semiconductor wafers, on which integrated circuits are fabricated. The final number, or yield, of functional integrated circuits on a wafer at the end of the IC fabrication process is of utmost importance to semiconductor manufacturers, and increasing the yield of circuits on the wafer is the main goal of semiconductor fabrication. After packaging, the circuits on the wafers are tested, wherein non-functional dies are marked using an inking process and the functional dies on the wafer are separated and sold. IC fabricators increase the yield of dies on a wafer by exploiting economies of scale. Over 1000 dies may be formed on a single wafer which measures from six to twelve inches in diameter.

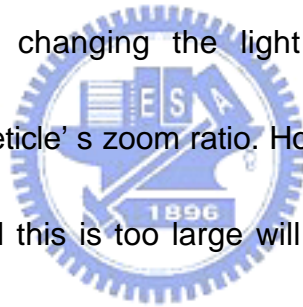
The issue of how to transfer a pattern onto a wafer during photolithography is very important. Normally, the resist is treated as a pattern-transferring medium. Such a medium should have a very smooth surface to reduce the focus error. In this experiment, spin coating is used. The velocity of the center differs from that of the outer edges of a rotating disk, so a perfectly smooth surface cannot be obtained. Therefore, resist temperature, cooling

temperature, heating temperature, cup temperature, cup humidity and exhaust pressure were controlled to eliminate this imperfection to yield an acceptable error. A lower cooling temperature yields a thicker center, such that the surface of the wafer protrudes at the center. A lower cooling temperature also corresponds to a thicker center, with the same effect. The cup temperature was set to the cooling temperature so that thickness distribution would be the same as. A higher heating temperature yields a thinner photo resist. Higher the humidity yields a thinner photo resist.

Resist is a photo-sensitive material. If exposed to common white light, a chemical reaction occurs and photolithography cannot be performed. The photolithography process is like the development of a photographic film in that it must be performed in a darkroom. The photolithographic process is further limited since a yellow light source does not promote the resist to react chemically. Accordingly, photolithography should be performed in an environment with a yellow light source. The commonly used light sources in the stepper include the G-line, the I-line and DUV (deep ultraviolet). The G-line wavelength is ~436nm, the I-line  $\lambda=350\sim450\text{nm}$ , and DUV  $\lambda=100\sim300\text{nm}$ . The wavelength of the I-line changes according to the internal composition and gas pressure of the mercury arc lamp used, varying within 350~450nm. This study

employs a superior UV lamp produced by Ushio Inc., which has a  $\lambda$  of 350nm. DUV wavelengths differ according to the laser gas composition: KrF  $\lambda$ =248nm, ArF  $\lambda$ =193nm and F<sub>2</sub>  $\lambda$ =157nm. In this work , the DUV stepper's laser light source, KrF  $\lambda$ =248nm, was used.

Photolithographic experiments depend on several kinds of measurement instruments. Moreover, the optical process involved is complex. The main aim is to reduce the line-width and make the CD bar even more stable, which is usually achieved by changing the light source. This research seeks to achieve the same results without changing the light source . One method of improvement involves the reticle's zoom ratio. However, a difference between the reticle's zoom ratio and this is too large will cause the photolithographic process not to be ideal. In these experiments, the compression ratio applied to the pattern on the reticle and the wafer was 5:1. The compression ratio applied to the DUV was the same as for the I-line.



## Chapter 2

### paper review

Recently, interest in the research and applications of diamond has increased significantly due to the development of the Chemical Vapor Deposition (CVD) technique for producing diamond films. Since diamond has the highest thermal conductivity of all known substances, it has numerous potential applications. However, this high thermal conductivity creates a problem in measuring the thermal conductivity of diamond materials <sup>1,2</sup>.

Numerous techniques exist for measuring the thermal conductivity of solid materials <sup>3~6</sup>. This study proposes a two layer model based on the principle of heat diffusion to determine the thermal conductivity for various CVD diamond thin films based on the effective thermal diffusivity of a diamond film on a silicon substrate measured by using a holographic interferometric technique <sup>7</sup>.

The main sources of distortion for soft pellicle systems include temperature changes and the attachment of curved frames to non-flat reticles, with the latter being the inevitable consequence of the stressed chrome pattern <sup>8,9</sup>.

According to the research by A. Mikkelsen in 2001 <sup>10</sup>, the reticle oxide layer thickness may reach 20nm, adding 5nm to the wafer, if optical reducing ratio is used.

Wafer throughput in micro-lithography depends on the sensitivity of the resist film to radiation. A lower exposure time required to produce a latent Image in the resist corresponds to a higher throughput<sup>11</sup>. The focus affects line-width: a focus of 0  $\mu$  m yields the lowest line-width, the width increases with the focus distance. Positive and negative foci yield symmetrical results<sup>12</sup>. The primary factor that dominates the gradient of the exposure/line-width relationship is the resist's internal chemical composition<sup>13</sup>.

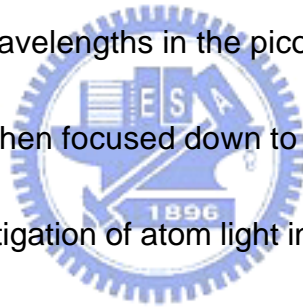
Resist spin coating has been successfully modeled using a detailed non-Newtonian analysis, which allows local fluid viscosity to vary with concentration and shear rate<sup>14</sup>. The cleavage of a butylester is acid-catalyzed and yields carboxylic acid and isobutene after exposure to the PAC (Photo Active Component) and PEB (Post-Exposure Back)<sup>15</sup>. When an acid generator is present in a CAMP (Chemically Amplified) resist formulation, the mechanism for producing a lithographic pattern is simple. The strong acid formed causes deprotection at a relatively low temperature with an activation energy of around 11 to 14 kcal/mol<sup>16</sup>.

Wafer throughput in micro-lithography depends on the sensitivity of the resist film to radiation. A lower exposure time required to produce a latent Image in the resist corresponds to a higher throughput<sup>17</sup>. The designed by

Watanabe et al.<sup>18</sup> showed that the focus margin for 0.3 $\mu\text{m}$  lithography with a KrF excimer stepper is  $\pm 0.08\mu\text{m}$  for DOF (Depth of Focus) of  $\pm 0.5\mu\text{m}$ . It is possible for an ArF excimer laser stepper to achieve 0.13 $\mu\text{m}$  lithography with a DOF of  $\pm 0.5\mu\text{m}$  by using the recently developed technique of super resolution.

The wafer surface profile is structure of the device and has irregularities of 0.3 to 1 $\mu\text{m}$ . As optical lithography will not reach the necessary resolution for future demands in microengineering. Now lithographic techniques have to be ready to produce nanostructures in a parallel way. Atoms with thermal kinetic energies have de Broglie wavelengths in the picometer regime and so they do not suffer from diffraction when focused down to a nanometer scale spot size.

In the last decade the investigation of atom light interaction has shown, that the trajectories of neutral atoms can be efficiently manipulated with laser light and that optical elements for neutral atoms can be built using the resonant interaction with laser light<sup>18 - 21</sup>.



## Chapter 3

### The traditional reticle level detects the method

#### ■ Introduction

In an apparatus for monitoring any deviation of a planar surface from its desired position, a light source and a light detector are positioned so that when the surface is at the desired position a beam of light projected by the light source is reflected by the surface and fully registers on the light detector causing the light detector to generate a peak output signal. When the surface deviates from its desired position, the reflected beam of light does not fully register on the light detector, causing the light detector to generate less than peak output signal.

#### ■ Summary of the reticle level detects the method

According to an embodiment of the present invention, depicted in Figure 3.1 is an optical level detector configured for monitoring whether a planar surface has deviated from its desired position, represented by a reference plane. Reference plane only represents a desired position for the planar surface and does not represent a physical surface. Optical level detector is

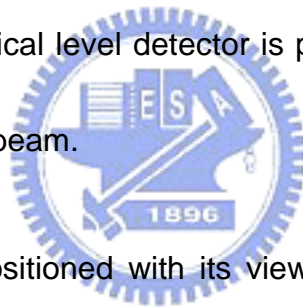


positioned at a known distance  $X$  from the reference plane . The absolute value of the distance  $X$  is not important but it is important that the distance  $X$  be fixed and does not change once the optical level detector is set up.

Associated with the reference plane is an incidence axis and a reflection axis . The incidence axis represents the path of an incident light beam from a light source incident to the reference plane and defines a reference incidence angle  $\theta_1$  between the reference plane and the incidence axis. When a planar surface is placed at the reference plane, the incidence beam will be reflected by the planar surface and returned towards the optical level detector as a reflected beam. The reference reflection axis represents the path of the reflected light beam when the planar surface is placed at the position defined by the reference plane, i.e. the desired position for the planar surface. The reference reflection axis defines a reference reflection angle  $\theta_2$ , which is equal to the incidence angle  $\theta_1$ , between the reference plane and the reference reflection axis. Therefore, by positioning a light detector in line with the reference reflection axis, one may detect whether the planar surface has deviated from the reference plane.

In the embodiment of the present invention illustrated in Figure 3.1, the light source is provided in the optical level detector for projecting a narrow beam of

light, the incidence beam, on to the planar surface. The light source is preferably a laser or a light emitting diode but any other light source may be adopted for this purpose. The light source projects the incidence beam along its projection axis. In this embodiment of the present invention, the light source is positioned such that the projection axis is coincident with the incidence axis. Thus, the incidence beam propagates along the path defined by the incidence axis and on to the planar surface. The incidence beam is reflected by the planar surface and travels back to the optical level detector as a reflected beam. The optical level detector is provided with a light detector for receiving this reflected beam.



The light detector is positioned with its viewing axis coincident with the reference reflection axis so that when the planar surface is in its desired position, the reflected light beam falls squarely on the light detector. The light detector is preferably a device such as a photocell that converts the light energy of the reflected beam into an electrical signal that can be readily detected and monitored. The voltage level of a typical photocell's output signal will vary proportionally with the intensity or the amount of light shone on the photocell. Thus, when the reflected beam falls completely on the light detector (i.e. fully registers with the light detector), the output signal of the light detector

will be at the peak voltage value possible with the reflected beam. If the reflected beam falls on the light detector only partially (i.e. does not fully register with the light detector), the output signal of the light detector will be at some voltage value less than the peak value.

This ensures that when a planar surface is in its desired position, i.e. at the position represented by the reference plane, the reflected beam will be coincident with the viewing axis and the reflected beam will completely register with the light detector. In this scenario, the output signal of the light detector will exhibit a peak voltage value for the given planar surface and its light reflecting characteristics. It should be noted that the peak voltage value of the light detector in this context does not necessarily mean the absolute peak voltage value that the light detector is capable of producing. It refers to the peak voltage value that the light detector will produce in the given configuration of the optical level detector.

If the planar surface deviates from its desired position, the reflected beam will not be coincident with the reflection axis and, in turn, not coincident with the viewing axis of the light detector. Thus the reflected beam will not completely register with the light detector. Depending on the degree of the deviation, the reflected beam could completely miss the light detector or only

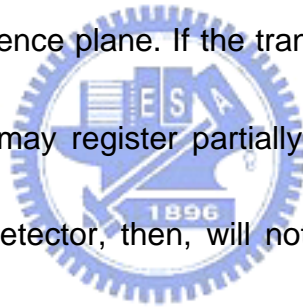
partially register with the light detector. In either case, the resulting output signal of the light detector will exhibit a voltage value that is less than the peak value.

The exemplary configuration of Figure 3.1 represents the situation where the planar surface is in its desired position. Thus, the angle of incidence for the incidence beam with respect to the planar surface is same as the reference incidence angle  $\theta_1$ . And, correspondingly, the angle of reflection for the reflected beam with respect to the planar surface is same as the reference reflection angle  $\theta_2$ .



Thus, the optical level detector of the present invention can be used to determine whether a planar surface has deviated from its desired position, represented by the reference plane by monitoring the output signal of the light detector. The output signal can be monitored using any suitable circuits or devices that can measure the voltage level of the output signal. Such circuits or devices are well known to one of ordinary skill in the field and they need not be discussed in detail here. Figures 3.2 and 3.3 illustrate some examples of a number of different situations in which a planar surface may deviate from the reference plane which can be detected by the optical level detector.

In Figure 3.2, the planar surface has deviated from the reference plane by an angular translation represented by angle  $\beta$ . The incidence beam will strike the planar surface at an incidence angle  $\alpha_1$  and the reflected beam leaves the planar surface at a reflected angle  $\alpha_2$ . As illustrated, the resulting reflected beam also has been angularly translated from the viewing axis of the light detector by the angle  $\beta$ . The reflected beam is not coincident with the viewing axis and no longer registers with the light detector. The resulting output signal of the light detector will be zero volts, signifying that the planar surface has deviated from the reference plane. If the translation angle  $\beta$  is sufficiently small, the reflected beam may register partially with the light detector. The output signal of the light detector, then, will not be zero volts but it will be something less than the peak value, still signifying that the planar surface has deviated from the reference plane.



In Figure 3.3, the planar surface has deviated from the reference plane by a linear translation represented by  $Y$ . The incidence beam will strike the planar surface at an incidence angle  $\alpha_1$  and the reflected beam leaves the planar surface at a reflected angle  $\alpha_2$ . The planar surface is parallel to the reference plane and the incidence angle  $\alpha_1$  and the reflected angle  $\alpha_2$  are same as the reference incidence angle  $\alpha_1$  and the reference reflected angle  $\alpha_2$ ,

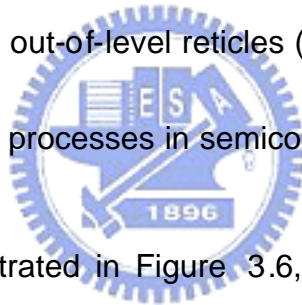
respectively. However, the reflected beam will be translated accordingly as represented by  $Y'$  and thus the reflected beam will not be coincident with the viewing axis of the light detector. Again, the reflected beam will not fully register with the light detector and the output signal of the light detector will be some value less than the peak value, signifying that the planar surface has deviated from the reference plane.

In another embodiment of the present invention, the light source and the light detector may be mounted in the optical level detector such that they are not coincident with the projection axis and the viewing axis, respectively, to accommodate different mounting configurations. For example, in Figure 3.4, the light source and the light detector are mounted in horizontal configuration, but by employing reflectors and respectively, the incidence beam and the reflected beam are made to travel along the desired paths. The reflectors may be mirrors, prisms or other suitable reflectors. The light source and the light detector may be configured in many different orientations as long as the reflectors are used to direct the incidence beam and the reflected beam to propagate along the desired paths.

In certain applications, a plurality of the optical level detector may be utilized to monitor positions of a plurality of surface regions on a planar surface.

For example, as illustrated in Figure 3.5, a planar surface may have a surface region **A** that is on the reference plane but the remainder of the planar surface represented by surface region **B** may be deviated from the reference plane. If one optical level detector was monitoring the surface region **A**, the planar surface may seem as though it is on the reference plane. Thus, two or more optical level detectors may be utilized to monitor a plurality of surface regions on the planar surface to better detect any deviations from the reference plane.

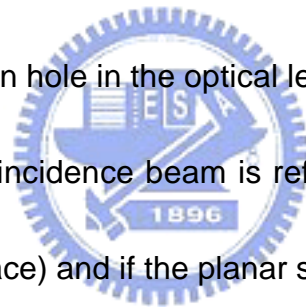
The inventor has applied the optical level detector of the present invention in such a manner in detecting out-of-level reticles (or photo lithographic masks) during the photolithography processes in semiconductor wafer manufacturing.



In one application, illustrated in Figure 3.6, four optical level detectors similar to the embodiments described herein may be mounted on a reticle stage of a stepper tool. The reticle stage has a reticle holding well for holding a reticle in place. Each of the four optical level detectors may be positioned near each of the four corners of the reticle holding well, as identified by the reference numbers. The optical level detectors are used to monitor whether or not a reticle (not shown) placed on the reticle holding well is properly leveled. Each of the four optical level detectors may be configured, for example, so that their light detectors generate peak output signal values when the reticle is

properly leveled in the reticle holding well. The output signals of the light detectors may be monitored individually. Alternatively, the optical level detectors may be connected in series and monitor the total voltage of the output signals.

Figure 3.7 illustrates a sectional view of an optical level detector as implemented by the inventor on the reticle stage according to another embodiment of the present invention. The light source is attached to the optical level detector by a light source holding plate. The light from the light source passes through a pin hole in the optical level detector and emerges as the incidence beam. The incidence beam is reflected by the planar surface (representing a reticle surface) and if the planar surface does not deviate from the reference plane, the reflected beam will be coincident with the reference reflection axis. In this example, the light detector is positioned in the optical level detector in a configuration similar to that discussed in reference to Figure 3.4. The light detector is provided such that its viewing axis is horizontally oriented and not coincident with the reference reflection axis. A reflector is provided at an appropriate orientation so that when the planar surface is at the desired location and does not deviate from the reference plane, the reflected beam will be deflected towards the light detector and fully register with the light





detector through the hole provided in the optical level detector. As with the other embodiments of the present invention discussed herein, when the planar surface deviates from the reference plane, the reflected beam will no longer be in proper alignment with the reference reflection axis and the reflected beam will not fully register with the light detector. By monitoring the electrical output signal of the light detector, one can thus detect whether or not the planar surface is at the desired location represented by the reference plane.

In the particular configuration implemented by the inventor, the optical level detector is mounted on to the reticle stage by a set of connecting hardware that allows the height of the optical level detector to be adjusted relative to the reticle surface (the planar surface). The set of connecting hardware comprises a vertically actuating guide bearing that allows the height of the optical level detector to be adjusted and an L-bracket for attaching the whole assembly on to the reticle stage. The guide bearing is a standard slide/bed type comprising a slide and a bed. To adjust and control the height of the optical level detector attached to the guide bearing, a worm gearing set up is used. The slide is provided with wormgear teeth and a worm is situated in the bed. The worm has a thumb screw to enable a human operator to adjust the height of the optical level detector by turning the thumb screw. These connecting hardware may

be viewed in more detail in the exploded view of the assembly illustrated in Figure 3.8. As discussed in reference to Figure 3.6, four of the optical level detector may be installed near the four corners of the reticle holding well using the connecting hardware described herein to verify that the reticle is properly leveled in the reticle holding well before the stepper is operated. The vertically actuating guide bearing may be of other types of guide bearing well known in the art and not necessarily limited to the slide/bed type described herein.

The use of the optical level detector of the present invention has simplified the stepper tool operator's task of verifying that the reticle is properly level in the reticle stage. While the foregoing invention has been described with reference to the above embodiments, various modifications and changes can be made without departing from the spirit of the invention. Accordingly, all such modifications and changes are considered to be within the scope of the appended claims.

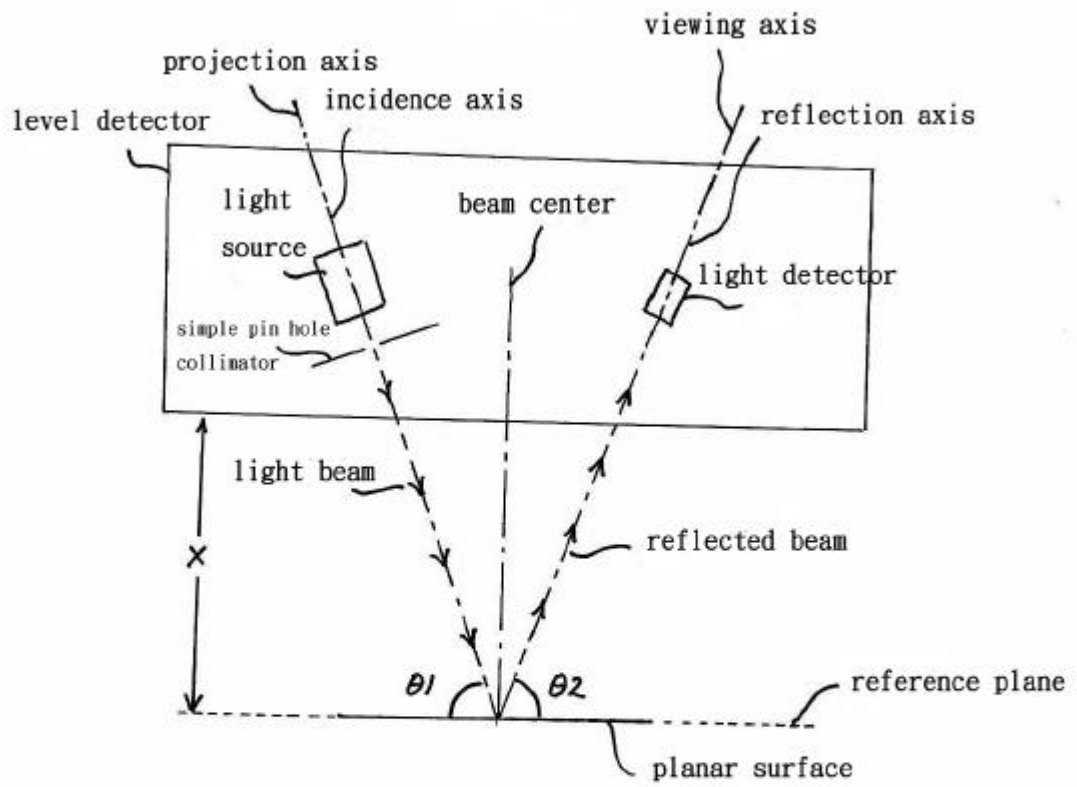
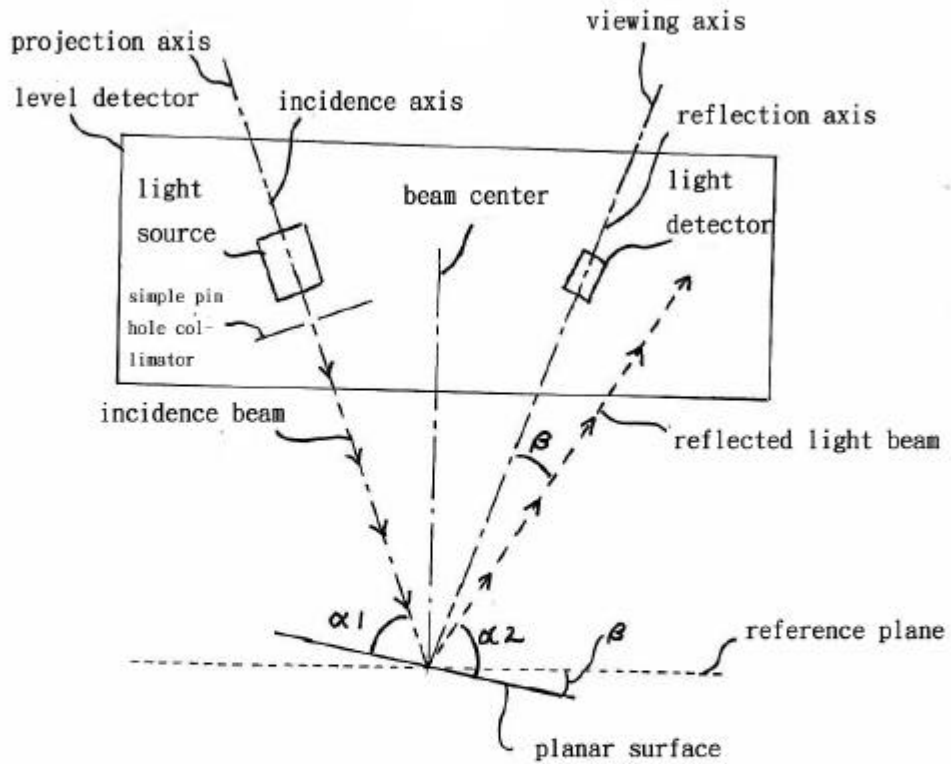
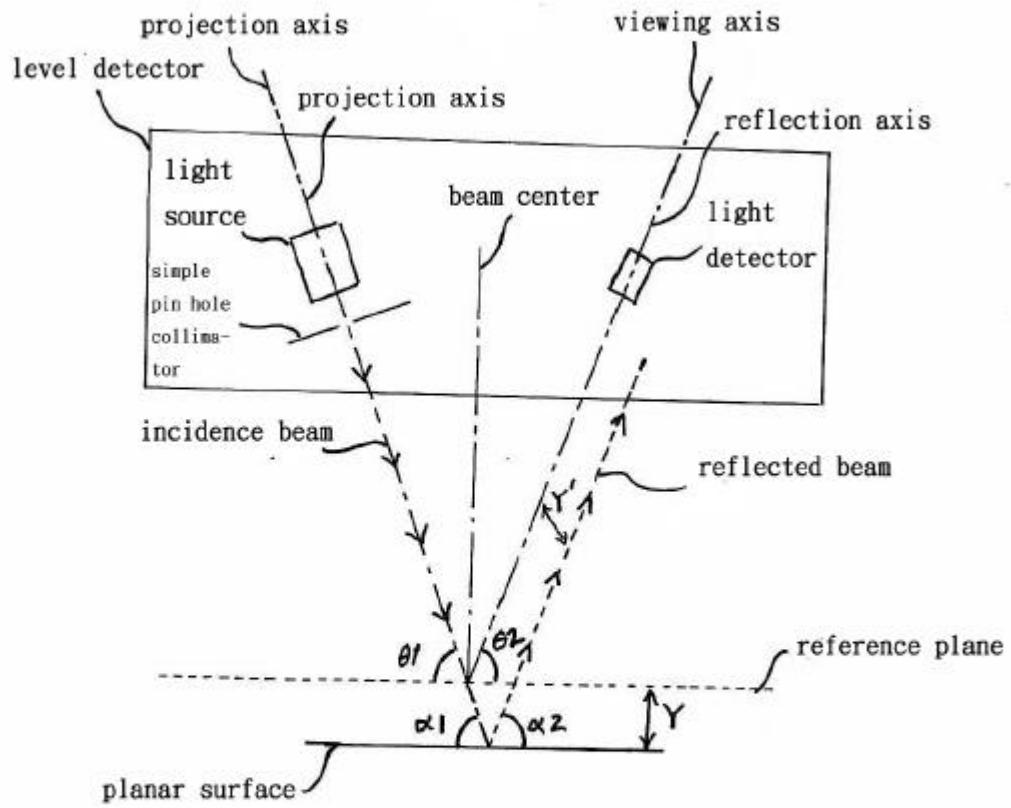


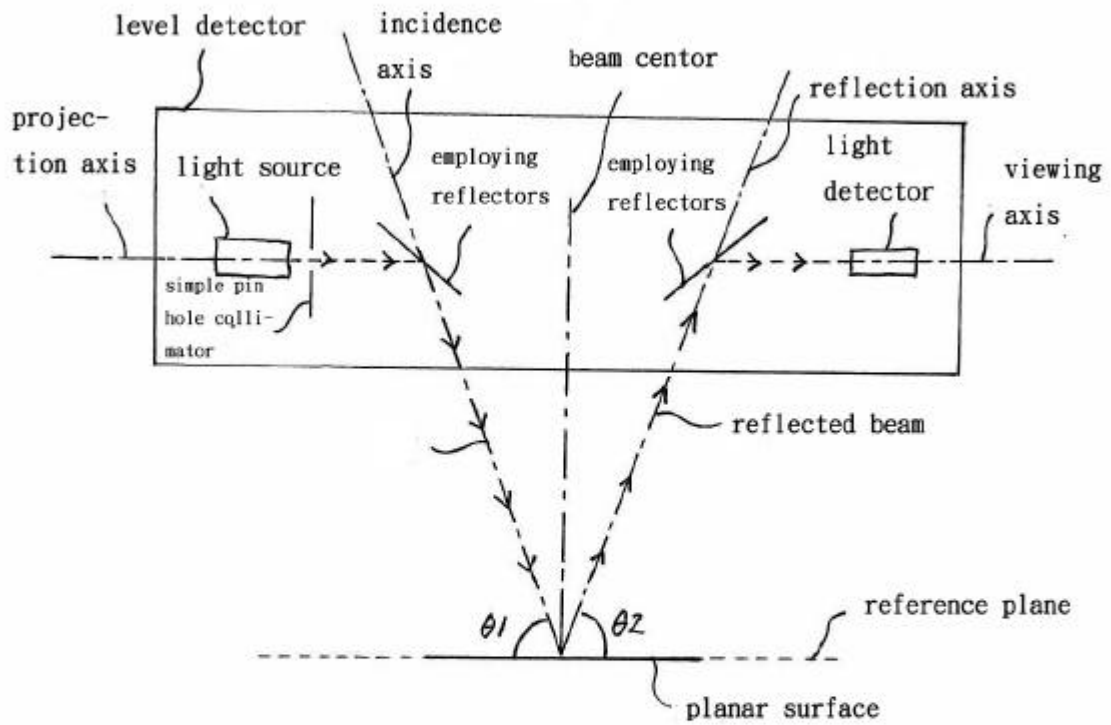
Figure 3.1 is a schematic illustration of one embodiment of the apparatus of the present invention.



Figures 3.2 are schematic illustrations of the apparatus of Figure 3.1 in different scenarios for various ways in which the surface being monitored can deviate from the reference



Figures 3.3 are schematic illustrations of the apparatus of Figure 3.1 in different scenarios for various ways in which the surface being monitored can deviate from the reference plane.



Figures 3.4 are schematic illustrations of the apparatus of Figure 3.1 in different scenarios for various ways in which the surface being monitored can deviate from the reference plane.

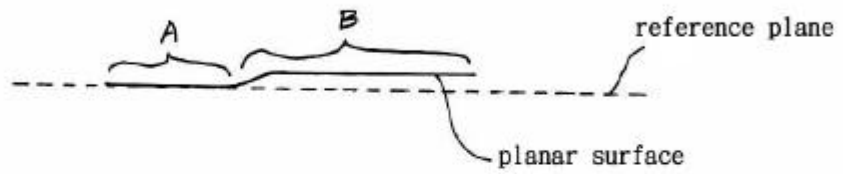


Figure 3.5 is a schematic illustration of another embodiment of the apparatus of the present invention.

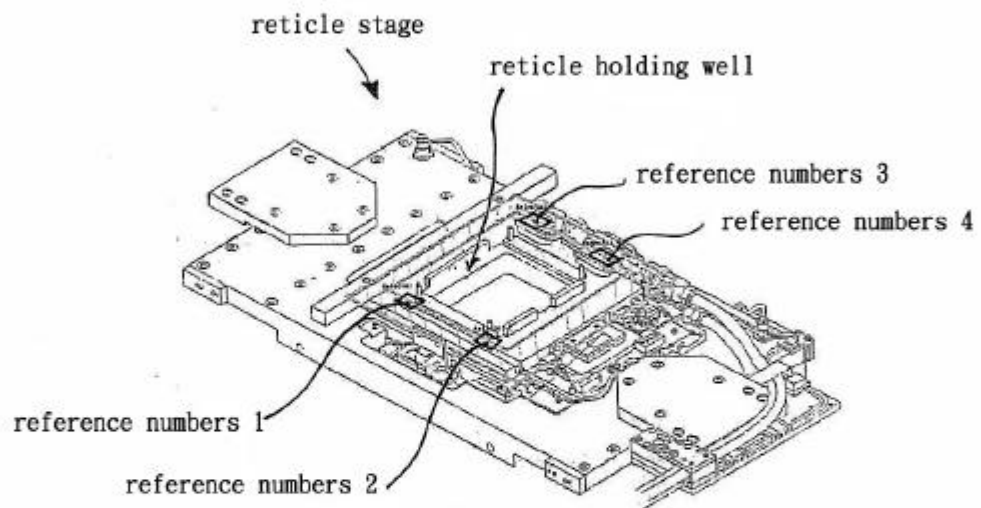


Figure 3.6 is a schematic illustration of an exemplary reticle stage employing four apparatuses of the present invention on four corners of the reticle stage.



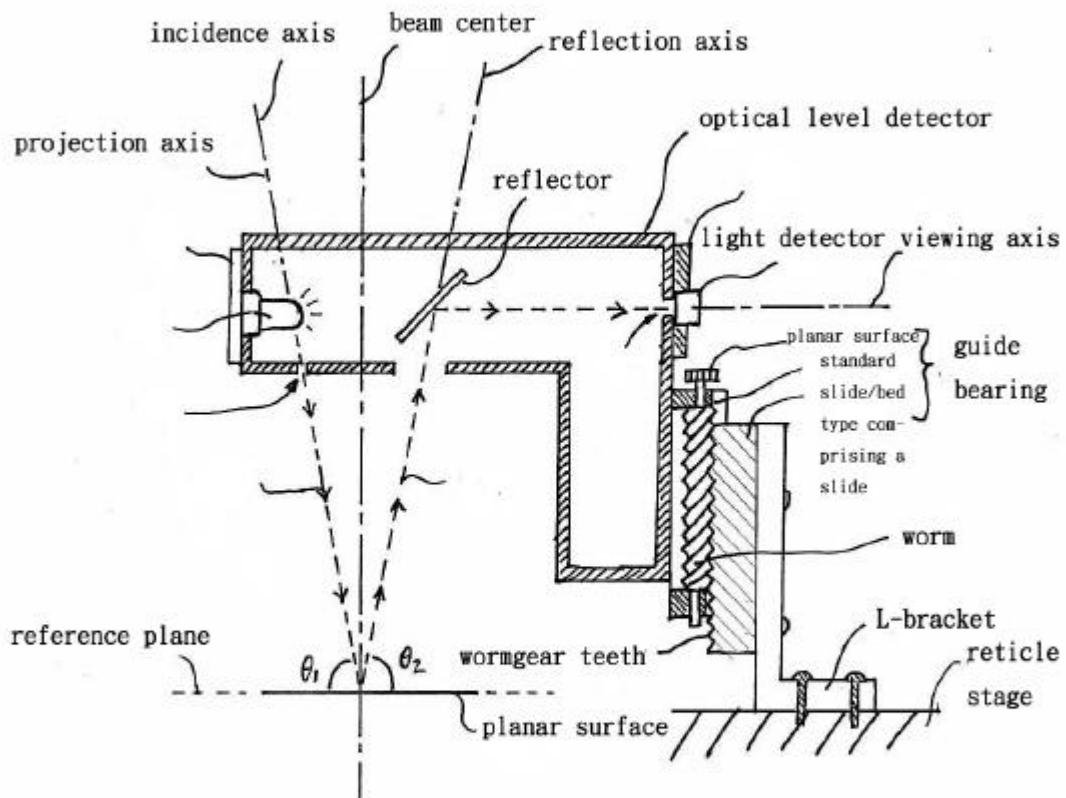


Figure 3.7 is a sectional schematic illustration of another embodiment of the apparatus of the present invention.

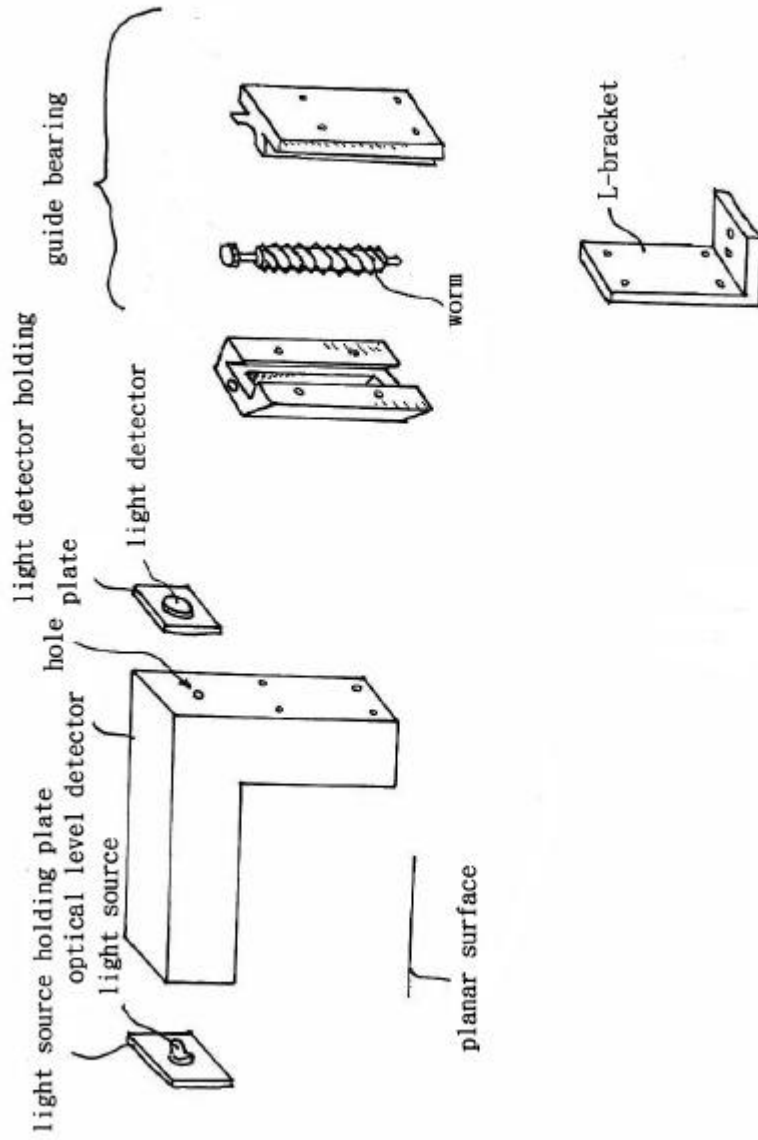


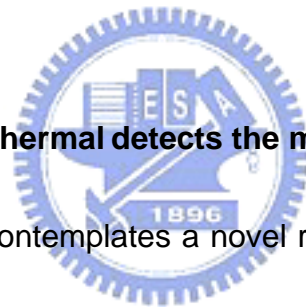
Figure 3.8 is an exploded view of the apparatus of Figure 3.7.

## Chapter 4

### The traditional thermal of slightly out of shape reticle detects the method

#### ■ Introduction

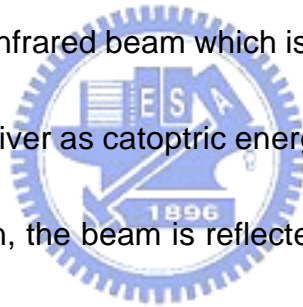
The present invention relates to reticles used in the formation of integrated circuit (IC) patterns or dies on semiconductor wafer substrates. More particularly, the present invention relates to a thermal detector which determines whether a reticle is thermally distorted to an excessive degree prior to exposure of a wafer through the reticle in photolithography.



#### ■ Summary of the reticle thermal detects the method

The present invention contemplates a novel reticle thermal detector which is suitable for determining whether a reticle is distorted typically due to thermal effects from an exposure light source in a stepper or scanner prior to exposure of a semiconductor wafer through the reticle. The reticle thermal detector alerts personnel to the distorted condition of a reticle as the reticle lies on a reticle stage in a stepper or scanner preparatory to a photolithography process. Therefore, the distorted reticle can be removed and a replacement reticle placed on the reticle stage to ensure that a circuit pattern of high integrity is transmitted from the reticle to a wafer with precision during photolithography.

In one embodiment, the reticle thermal detector of the present invention is an optical reticle thermal detector and includes a transmitter such as a laser beam transmitter or a light-emitting diode, for example. A receiver is positioned in spaced-apart relationship with respect to the transmitter, with the transmitter and receiver located on opposite sides of a reticle stage in a stepper or scanner. An alarm connected to the receiver receives an activation signal from the receiver when the receiver fails to receive a beam reflected from the reticle. Prior to exposure of a wafer through a reticle placed on the reticle stage, the transmitter emits a light or infrared beam which is reflected from the surface of the reticle and into the receiver as catoptric energy. As long as the reticle is in an undistorted configuration, the beam is reflected from the reticle at such an angle that the reflected beam enters the receiver and the alarm is not activated. On the other hand, in the event that the reticle is thermally distorted, the distorted reticle deflects the reflected beam from entering the receiver. The receiver, in turn, activates the alarm and thereby alerts personnel to the thermally-distorted condition of the reticle.



In another embodiment, the reticle thermal detector includes a mechanical device which determines whether the reticle is thermally distorted through mechanical means. In the event that the reticle is distorted, the mechanical

device activates the alarm. In still another embodiment, the reticle thermal detector includes an electromechanical device which determines whether the reticle is distorted and activates the alarm in the event that the reticle is distorted. The invention further includes a novel method of enhancing the quality of circuit pattern images formed on a wafer during photolithography by monitoring the distorted state or configuration of a reticle prior to use of the reticle in photolithography.

In still another embodiment, the invention includes an exposure apparatus such as a scanner or stepper which includes a reticle thermal detector. The exposure apparatus includes an exposure device for exposing a wafer. The exposure device includes a light source for emitting light, a reticle stage adjacent to the light source for holding a reticle and a lens adjacent to the reticle stage. The reticle thermal detector includes a mechanism for determining a degree of distortion of the reticle provided adjacent to the reticle stage and an alarm connected to the mechanism for activation by the mechanism when the reticle is distorted.

Referring initially to Figures 4.1-4.3, an illustrative embodiment of an optical reticle thermal detector of the present invention is generally indicated by reference numeral. The optical reticle thermal detector is designed to be

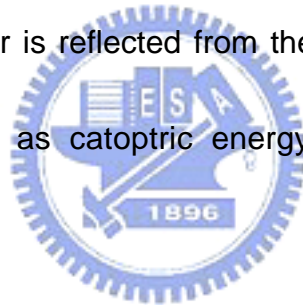
installed in a stepper or scanner which may be conventional and is used to transmit circuit pattern images from a reticle to a semiconductor wafer substrate (not shown) in the photolithography step of semiconductor fabrication. The stepper/scanner includes a reticle stage for holding the reticle; a lens beneath the reticle stage; and a positive focal point, a center focal point and a negative focal point beneath the lens. A light source is disposed above the wafer stage for emitting light through the reticle.

During photolithography, a semiconductor wafer (not shown) is placed on a wafer stage (not shown) at the center focal point. Light is emitted from the light source through the reticle and lens, respectively. When the reticle is in an undistorted configuration, the lens focuses the circuit pattern image defined by the reticle onto the wafer at the center focal point. This results in a circuit pattern of high integrity and quality being formed on the wafer.

On the other hand, throughout extended use, the light from the light source tends to heat the reticle, thus causing the reticle to expand and become thermally distorted. This, in turn, causes the circuit pattern image to become focused above the center focal point (toward the positive focal point) or below the center focal point (toward the negative focal point). Consequently, the circuit pattern image transmitted to the wafer at the center focal point becomes

distorted, resulting in a distorted circuit pattern image of low quality being formed on the wafer.

The optical reticle thermal detector of the present invention includes a transmitter and a receiver which are disposed in spaced-apart relationship with respect to each other on opposite sides of the reticle stage. A computer is connected to the light receiver, typically through computer wiring. An alarm is, in turn, connected to the computer typically through alarm wiring. The transmitter and receiver are positioned in such a manner that an incident beam emitted from the transmitter is reflected from the reticle as a reflected beam which enters the receiver as catoptric energy when the reticle is in an undistorted configuration.



The transmitter may be any light-emitting element known by those skilled in the art, including but not limited to a laser-emitting device or an LED (light-emitting diode), for example. Alternatively, the transmitter may be any device which is suitable for emitting a beam of electromagnetic radiation such as infrared radiation, for example. The receiver may be any device which is capable of receiving a reflected light or radiation beam and responsively transmitting an electrical signal to the computer (or alternatively, transmitting a modulated electrical signal or terminating transmission of an electrical signal to

the computer) in the event that the reflected light or radiation beam is no longer received by the receiver. The alarm may be an audible alarm, a visual alarm, or both an audible and visual alarm. The computer is programmed to activate the alarm in the event that the receiver transmits an electrical signal to the computer, transmits a modulated electrical signal to the computer or terminates transmission of an electrical signal to the computer.

In operation of the optical reticle thermal detector, a reticle is initially placed in the reticle stage of the stepper/scanner, and a semiconductor wafer (not shown) having a photoresist layer deposited thereon is placed on a wafer stage (not shown) in the stepper/scanner. Under circumstances in which the reticle is generally in thermal equilibrium with the environment (such as may occur, for example, upon initial placement of a previously unused reticle in the reticle stage), the reticle is in an undistorted condition, as illustrated by the area bounded by the solid lines and indicated by reference numeral in Figure 4.2. Therefore, the reticle is suitable to transmit a circuit pattern image of high quality onto the wafer (not shown) placed on the wafer stage in the stepper/scanner during a subsequent photolithography process. On the other hand, under circumstances in which the reticle has been heated to an excessive degree, typically by the light from the light source (such as may





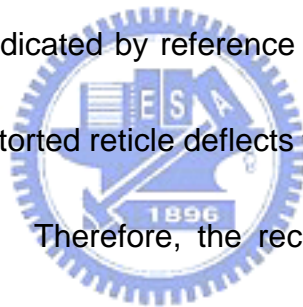
occur throughout prolonged usage of the reticle in the stepper/scanner), the reticle is in an expanded, thermally-distorted configuration, as illustrated by the area bounded by the dashed lines and indicated by reference numeral in Figure 4.2. Therefore, the distorted reticle is not suitable to transmit a high-quality circuit pattern image onto the wafer during a subsequent photolithography process.

Prior to the photolithography process, the thermal state of the reticle is determined by the reticle thermal detector. Accordingly, an incident light or radiation beam is emitted from the transmitter, typically against the upper surface of the reticle. Figure 4.1 illustrates the case in which the reticle is in an undistorted configuration. In that case, a reflected beam is reflected from the reticle and enters the receiver as catoptric energy. As long as the reflected beam enters the receiver, the receiver does not transmit an electrical signal to the computer through the computer wiring. Therefore, the computer refrains from activating the alarm through the alarm wiring and the photolithography process can proceed.

During photolithography, light is emitted from the light source and through the reticle and lens, respectively. The lens focuses the light, in the form of the circuit pattern image in the reticle, onto the wafer (not shown) located at the

center focal point. Due to the undistorted configuration of the reticle, the circuit pattern image transmitted to the wafer has a high resolution and facilitates the etching of high-quality circuits on the wafer during subsequent process steps.

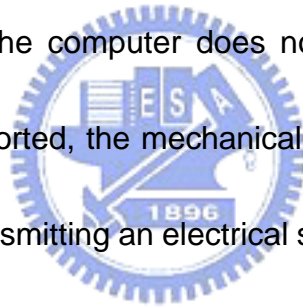
In the event that the reticle has been heated excessively (such as by the heat source after prolonged use in the stepper/scanner, for example), the reticle becomes thermally distorted. This is indicated by the dashed lines in Figure 4.2, in which the enlarged area of the reticle indicated by reference numeral represents the increased size of the distorted reticle relative to the normal, undistorted size (indicated by reference numeral). Consequently, as shown in Figure 4.3, the distorted reticle deflects the reflected light beam away from entering the receiver. Therefore, the receiver transmits an electrical signal to the computer, through the computer wiring. Responsive to the signal from the receiver, the computer transmits an alarm activation signal to the alarm, through the alarm wiring. The alarm broadcasts an audible signal, a visual signal or both an audible and a visual signal to alert personnel to the distorted condition of the reticle. Therefore, the reticle can be removed from the reticle stage and replaced with an undistorted reticle to ensure transmittal of a high-quality circuit pattern image from the reticle onto the semiconductor wafer.



In the configuration of the reticle thermal detector heretofore described, the receiver transmits an electrical signal to the computer 16 and the computer activates the alarm in the event that the reflected beam does not enter the receiver. However, it is understood that alternative operational configurations are possible. For example, the receiver may be adapted to transmit an electrical signal to the computer under circumstances in which the reticle is undistorted (and the reflected beam therefore enters the receiver). In that case, the receiver does not transmit the signal to the computer and the computer consequently activates the alarm if the reflected beam does not enter the receiver (thus indicating that the reticle is distorted). In another alternative configuration, when the reticle is undistorted, the receiver transmits a baseline signal to the computer as long as the reflected beam enters the receiver. If the reticle is distorted, the receiver transmits a modulated electrical signal to the computer, which activates the alarm responsive to receiving the modulated signal from the receiver.

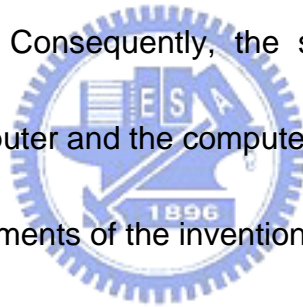
Referring next to Figure 4.4, a mechanical retical thermal detector according to the present invention is generally indicated by reference numeral. The mechanical retical thermal detector includes a mechanical device which engages a reticle when the reticle rests on a reticle stage of a stepper/scanner

(Figure 4.1). A computer is connected to the mechanical device typically through computer wiring. An alarm, which may be an audible alarm, a visual alarm or both, is connected to the computer typically through alarm wiring. The mechanical device may be any device which is capable of detecting an abnormal thickness of the reticle when the reticle is in a thermally distorted configuration and transmitting an electrical signal (or alternatively, transmitting a modulated electrical signal or terminating transmission of the signal) to the computer in the event that the reticle is distorted. Accordingly, in the event that the reticle is undistorted, the computer does not activate the alarm. In the event that the reticle is distorted, the mechanical device causes the computer to activate the alarm by transmitting an electrical signal, transmitting a modified electrical signal or terminating transmission of an electrical signal to the computer. The reticle can then be replaced by an undistorted reticle prior to photolithography.



Referring next to Figure 4.5, an electromechanical retical thermal detector according to the present invention is generally indicated by reference numeral. The electromechanical retical thermal detector includes at least one, and typically, multiple piezoelectric sensors which engage a reticle when the reticle rests on a reticle stage of a stepper/scanner (Figure 4.1). A computer is

connected to the piezoelectric sensors typically through computer wiring. An alarm, which may be an audible alarm, a visual alarm or both, is connected to the computer typically through alarm wiring. The piezoelectric sensors are capable of sensing pressure exerted by the reticle when the reticle is in an expanded, thermally distorted configuration, in which case the piezoelectric sensors generate and transmit an electrical signal to the computer through the computer wiring. Consequently, the computer activates the alarm through the alarm wiring. In the event that it is undistorted, the reticle does not exert pressure on the sensors. Consequently, the sensors do not transmit an electrical signal to the computer and the computer does not activate the alarm. While the preferred embodiments of the invention have been described above, it will be recognized and understood that modifications can be made in the invention and the appended claims are intended to cover all such modifications which may fall within the spirit and scope of the invention.



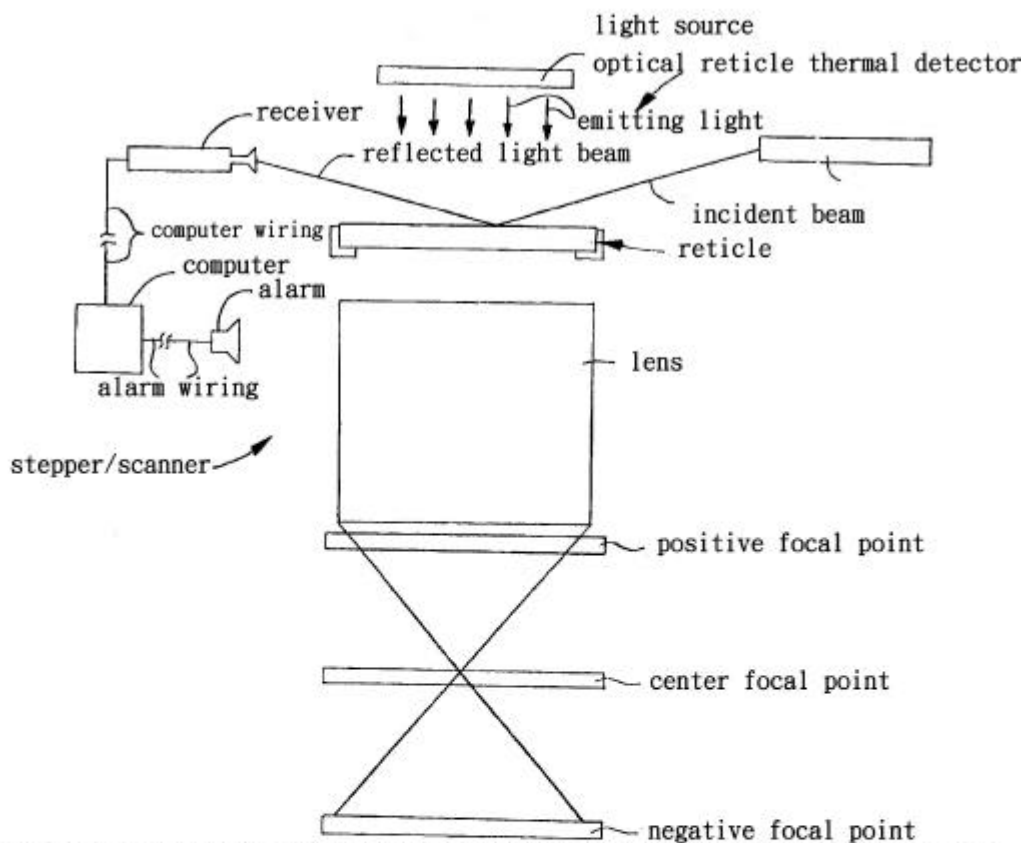


Figure 4.1 is a schematic view of an illustrative embodiment of an optical reticle thermal detector according to the present invention, illustrating implementation of the invention when the reticle is in an undistorted condition.

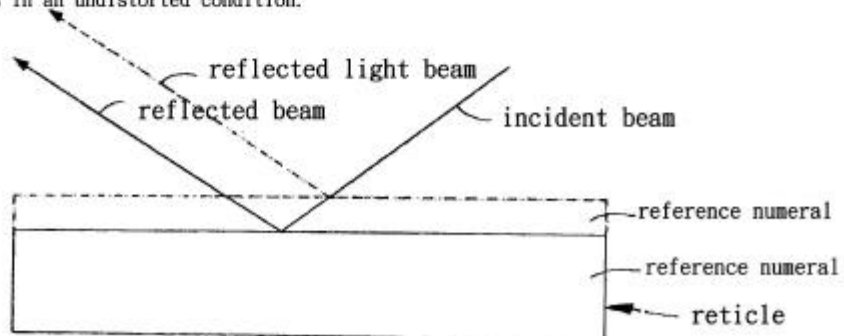


Figure 4.2 is a schematic view of a reticle, illustrating reflection of light from the reticle when the reticle is in the undistorted condition (solid lines) and when the reticle is thermally distorted (dashed lines).

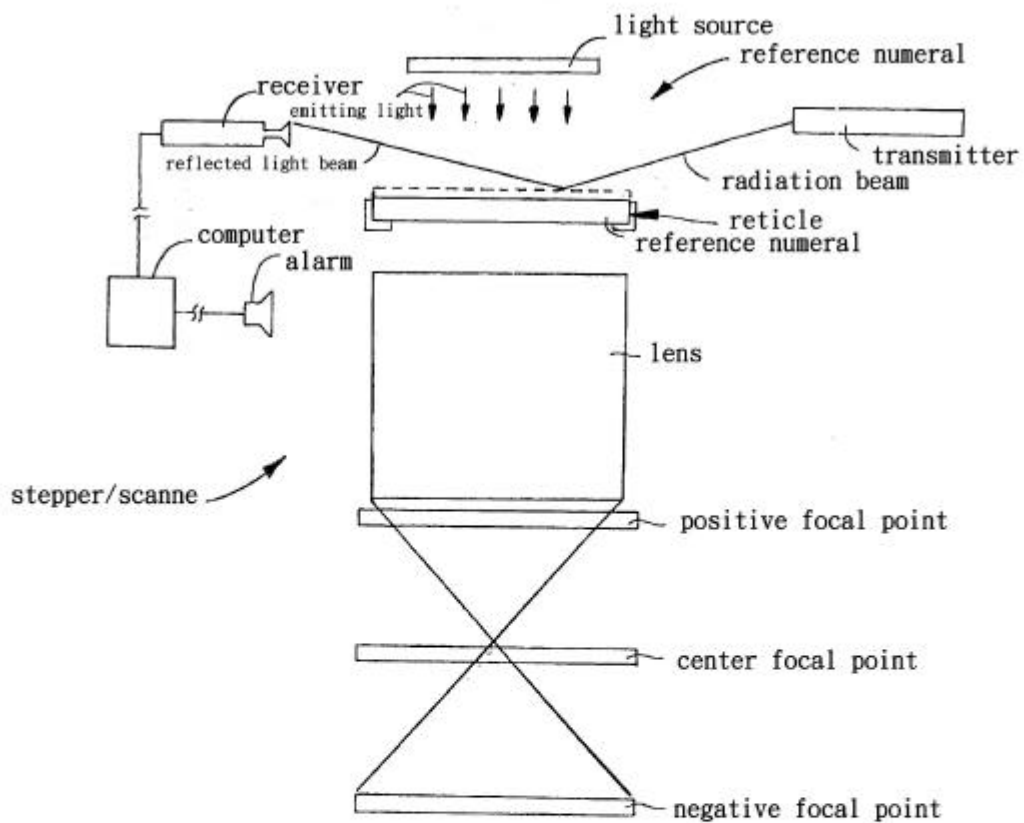


Figure 4.3 is a schematic view of an illustrative embodiment of an optical reticle thermal detector according to the present invention, illustrating implementation of the invention when the reticle is in a thermally-distorted condition.

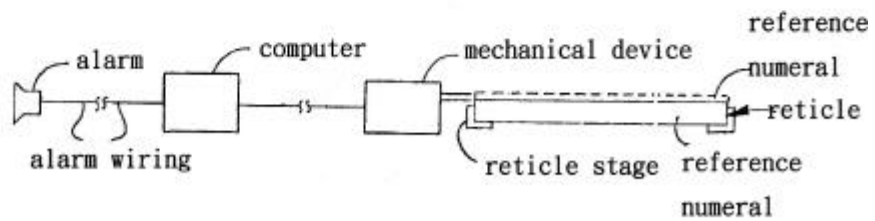


Figure 4.4 is a schematic view of an illustrative embodiment of a mechanical reticle thermal detector according to the present invention.

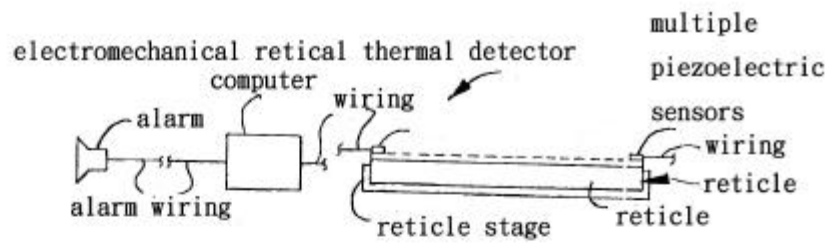


Figure 4.5 is a schematic view of an illustrative embodiment of an electromechanical retical thermal detector according to the present invention.



## Chapter 5

### Improvement in instable analysis of heat inflation induced line-width after replacing pellicle with diamond film on reticle (photo-masks)

#### ■ Introduction

Recently, interest in the research and applications of diamond has increased significantly due to the development of the Chemical Vapor Deposition (CVD) technique for producing diamond films. Since diamond has the highest thermal conductivity of all known substances, it has numerous potential applications. However, this high thermal conductivity creates a problem in measuring the thermal conductivity of diamond materials <sup>1,2</sup>. Numerous techniques exist for measuring the thermal conductivity of solid materials <sup>3~6</sup>. This study proposes a two layer model based on the principle of heat diffusion to determine the thermal conductivity for various CVD diamond thin films based on the effective thermal diffusivity of a diamond film on a silicon substrate measured using a holographic interferometric technique <sup>7</sup>. The main sources of distortion for soft pellicle systems include temperature changes and the attachment of curved frames to non-flat reticles, with the latter being the inevitable consequence of the stressed chrome pattern <sup>8,9</sup>.

## ■ The heat conduction equation

For one dimensional heat flow along the y direction, the rate change of heat transfer can be expressed as

$$\frac{dQ}{dt} = -k_s A \frac{dT}{dy} \quad (1)$$

where  $k_s$  denotes the thermal conductivity along the y direction in the unit of  $W m^{-1} K^{-1}$ ,  $dT/dy$  represents the temperature distribution along the y direction of  $K m^{-1}$ , A is the cross sectional area of the sample perpendicular to the heat transfer direction of  $m^2$ , and  $dQ/dt$  denotes the thermal power of W. Notably, thermal conductivity,  $k_s$ , is a heat transfer value per unit temperature gradient per unit time through unit cross section, which is perpendicular to the heat transfer direction. The temperature gradient through the unit cross section then can be measured by introducing a known quantity of heat to the solid material to determine the value of  $k_y$  from Eqn. (1).

Modeling of thermal conductivity in a solid begins with the diffusion equation:

$$\nabla^2 T - \frac{1}{a} \frac{\partial T}{\partial t} = -\frac{1}{k_s} Q(x, y, z, t) \quad (2)$$

When  $a$  denotes the thermal diffusivity, for a long, thin film of a homogeneous material, with one end of the thin film held at a constant temperature and the other end heated at a known rate, the steady state, one dimensional temperature distribution is determined by the familiar expression

from Eqn. (2).

Fourier's law, Eqn. (1), can be used to determine the conduction heat transfer rate. That is,

$$q_y = -kA \frac{dT}{dy} = \frac{kA}{L} (T_{material,1} - T_{material,2}) \quad (3)$$

Particularly, an analogy exists between heat diffusion and electrical charge. Just as an electrical is associated with the conduction of electricity, a thermal resistance may be associated with the conduction of heat. Defining resistance as the ratio of a driving potential to the corresponding transfer rate,

Eqn. 3 shows that the thermal resistance for conduction is

$$R \equiv \frac{T_{material,1} - T_{material,2}}{q_y} = \frac{L}{kA} \quad (4)$$



#### ■ Comparisons between traditional pellicle-reticle model and diamond films-reticle thermal conductivity model

Equivalent thermal circuits may also be used for more complex systems, such as composite walls. Such walls may involve numerous series and parallel thermal resistances due to layers of different materials. Consider the series composite wall of Fig. 5.1 (a) and (b). The one dimensional heat transfer rate for this system can be expressed as

$$q_y = \frac{T_1 - T_n}{\sum R} \quad (5)$$

Consider the traditional pellicle-reticle of a two-layer composite, as illustrated in Fig. 5.1 (a) Each layer is characterized by an individual thickness,  $y$  density, heat capacity, and thermal conductivity,  $k$ . where  $T_1 - T_3$  is the overall temperature difference and the summation includes all thermal resistances.

Consequently,

$$q_y = \frac{T_1 - T_3}{\left( \frac{L_{quartz}}{k_{quartz}A} + \frac{L_{chromium}}{k_{chromium}A} \right)} \quad (6)$$

Alternatively, the heat transfer rate can be related to the temperature difference and resistance associated with each element.

$$q_y = \frac{T_1 - T_2}{\left( \frac{L_{quartz}}{k_{quartz}A} \right)} = \frac{T_2 - T_3}{\frac{L_{chromium}}{k_{chromium}A}} \quad (7)$$

Consider the diamond film-reticle thermal resistances of a three-layer composite, as shown in Fig. 5.1 (b),

$$q_{y'} = \frac{T_1' - T_4'}{\left( \frac{L_{quartz}}{k_{quartz}A} + \frac{L_{chromium}}{k_{chromium}A} + \frac{L_{diamond}}{k_{diamond}A} \right)} \quad (8)$$

Alternatively, the heat transfer rate can be related to the temperature difference and resistance associated with each element.

$$q_{y'} = \frac{T_1 - T_2}{\left(\frac{L_{\text{quartz}}}{k_{\text{quartz}}A}\right)} = \frac{T_2' - T_3'}{\frac{L_{\text{chromium}}}{k_{\text{chromium}}A}} = \frac{T_3' - T_4'}{\frac{L_{\text{diamond}}}{k_{\text{diamond}}A}} \quad (9)$$

The initial temperature is the same for the traditional pellicle-reticle and diamond-reticle, so  $T_1 = T_1'$ . However, due to the effects of the thermal conductivity of diamond film,  $T_2 \neq T_2', T_3 \neq T_3'$ . Putting Table 1 into Eqns. 7 and 9 demonstrates that a diamond film-reticle has better heat radiation.

#### ■ Experimental method

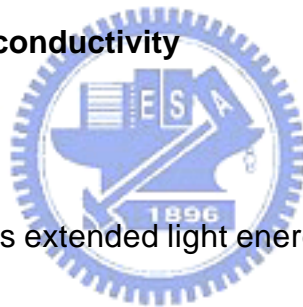


A 10  $\mu$  m thick layer of diamond film (Type a) is deposited on a chromium layer on the bottom of a reticle via CVD using Cymer KrF Laser as the source of photo exposure. Figure 5.2 describes the laser route in which the Cymer machine shoots a highly homogeneous light that could control uniformity below 0.3% via a fly eye. The homogeneous laser light obtains zero order and 1<sup>st</sup> order light via annular aperture. The laser beam of zero order and 1<sup>st</sup> order light could be controlled under experimental size following going through a reticle blind. Subsequently, through the main condenser lens, the main condenser lens is the final optical element for the exposure beam before

entering the reticle and reduction projection, the condenser lens to ensure beam telecentricity. The final lens is the projection lens. The main function of the projection lens is to reduce the laser ratio to 4:1 and project it onto the wafer surface.

## ■ Results

### Diamond Reticle thermal conductivity



When the reticle receives extended light energy, it will be out of shape due to thermal inflation. The CD (Critical Dimension) Bar from coating positive resist on the wafer of inflated reticle thus will shrink. Figure 5.3 may prove that traditional pellicle-reticle is four times the quantity of out-of-shape than diamond thin film under continuing photo exposure for 200 hours. At this point, the temperature of the traditional pellicle-reticle increases from 23.01 to 24.34 while the temperature of the diamond thin film reticle increases from 23.00 to 23.03. The increase of 1.33 reduces the CD bar by 0.05  $\mu\text{m}$ . If this shape change is applied to photo-lithography of 35nm line width, 30nm

of CD Bar can be obtained. Figure 5.3 shows that the increase of just 0.03 has almost no effect on 35nm process. This result demonstrates that diamond is a new and ideal replacement for pellicle in both theory and practice.

### **Diamond Reticle Intensity**

Table 2 shows that the value of measurement of intensity of reticle of quartz and chromium is  $227.6 \text{ mW/cm}^2$  and following adding a layer of pellicle, the value of intensity reduces by 0.483% while the value of intensity of diamond-reticle reduce by 17.97%. The loss of energy after light increase the medium of diamond is the weakness that will make throughput of scanner slow down.

### **Effects of improved oxide layer on diamond reticle on CD (Critical Dimension) bar**

According to the research by A. Mkkelson in 2001<sup>10</sup>, the reticle oxide layer thickness may reach 20nm, adding 5nm to the wafer, if optical reducing

ratio is used. The 35nm via(hole)-process increases the size to 40nm and reduces the CD bar to 30nm.

Because chromium wire of diamond-reticle is wrapped up between diamond and quartz, the chromium does not contact with air, and no oxide phenomenon occurs. The design of diamond-reticle provides a method of preventing reticle from producing an oxide layer.

## ■ Conclusions

Today's photo manufacturing process has not had ability to produce 35nm line-width, so the experiment used 0.11  $\mu\text{m}$  manufacturing technology to act as quantity of transformation of thermal inflation and applied the quantity of transformation to future 35nm manufacturing process.

Presently, the tolerable standard of error of margin of semiconductors is 3 sigma. In the 65nm process, the error of margin 5nm is within 3 sigma while the error margin in 35nm process exceeds 3 sigma. Therefore, when a semiconductor process is developed to 35nm, the slight shape change due to heat must be resolved. However, until now, no paper or patent has offered a solution. Diamond film reticle may provide a solution for achieving slight shape change in the future.



■ List of Table

**Table 5.1**

Thermal properties of film and substrate [HITACHI PD 5000 Manual]

Material	Thickness	Thermal conductivity ( $W / m K$ )
Quartz	6.30 mm	4.8
Chromium pattern	100 nm	93.7
Pellicle	0.08 mm	-
CVD Diamond film (Type a)	10 $\mu m$	1193

**Table 5.2**

Various types of reticle intensity

	No Pellicle-reticle	Pellicle-reticle	Diamond film-reticle
Intensity ( $mW / cm^2$ )	227.6	226.5	186.7

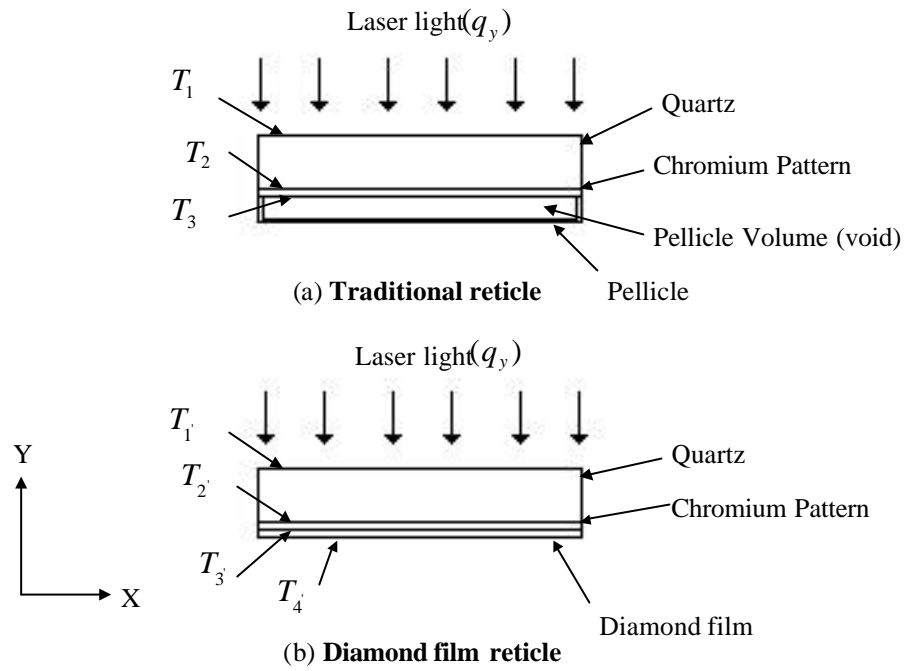


**Figure 5.1 Route Map of Laser Beam Used in Experiment**

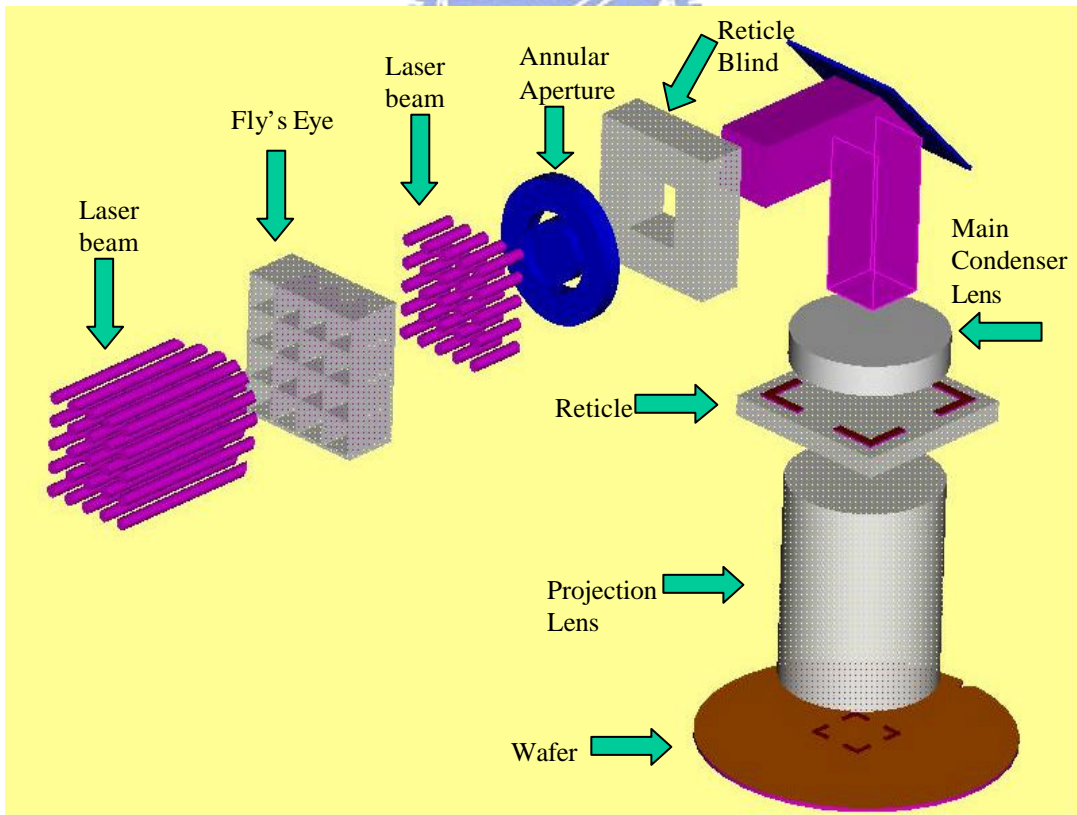


**Figure 5.2 Traditional reticle and diamond film reticle composite**

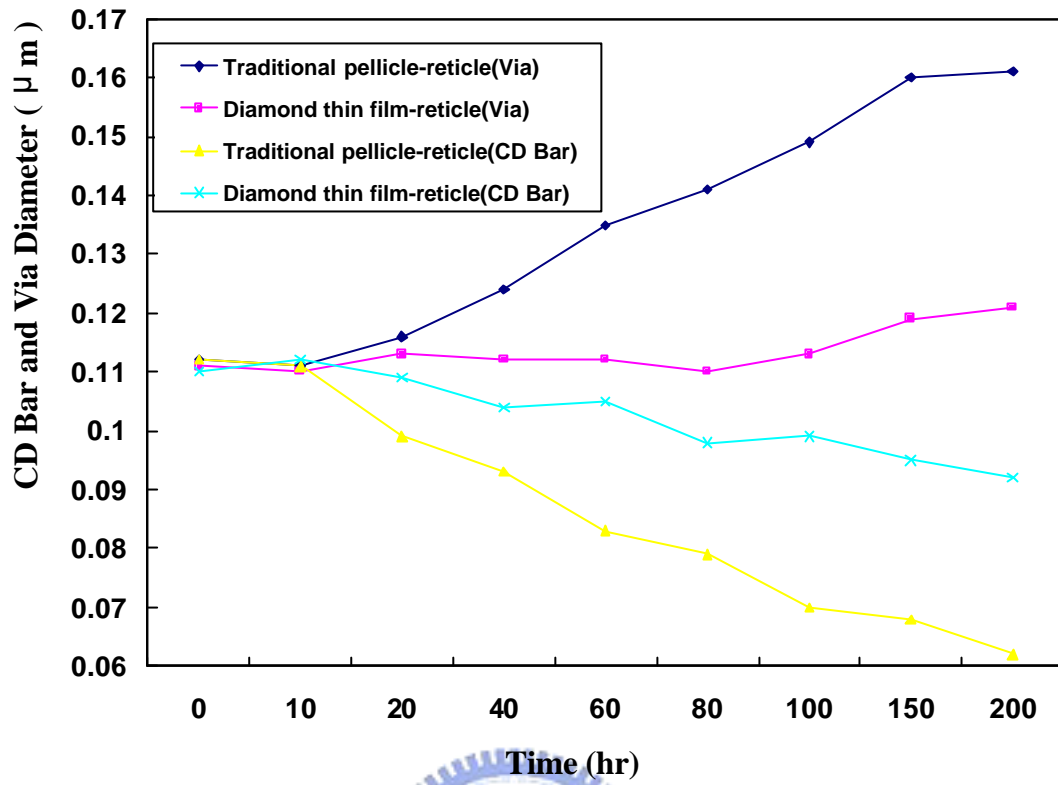


Figure 5.3 Variances of Line-Width/Diameter of Wafer CD Bar/Via in Different Types of Reticles Following Continuing 200 hour photo exposure.

## Chapter 6

### Analysis of instability in a Critical Dimension Bar due to focus and exposure

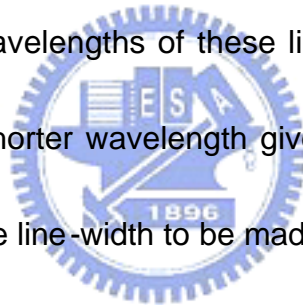
#### ■ Introduction

In the photolithography processing of semiconductor, line-width is smaller and smaller. Therefore, the requirements of process window are stricter than before. Among them, the control of focus and exposure dose is one of the most important factors that may affect line-width. Bad control of focus and exposure may not only affect line-width, but also cause the increment of rejects of products. The research explored mainly the effects of focus and exposure dose on line-widths of different photo resists. The research obtained related coefficients of exposure dose-line width and focus-line width by coating photo resist of different components on the surface of silica wafer. The results of research found that focus might not only change line-width but also had positive-negative symmetric relationship with line-width. It also found that there was linear relationship between exposure dose and line-width.

## ■ Experimental

### Equipment

The steppers were a Nikon I-line and DUV. The major function of a stepper is to apply the exposure pattern to the surface of a wafer that has already been coated with a layer of resist. The main difference between an I-line stepper and a DUV stepper is that they use different light sources. The light source used by an I-line stepper is a UV lamp  $\lambda=365\text{nm}$ , while the light source used by a DUV stepper is a KrF excimer laser  $\lambda=248\text{nm}$ . The differences between the wavelengths of these light sources lead to different resolutions. Generally, a shorter wavelength gives a better resolution, and a better resolution enables the line-width to be made narrower.



The exposure field used by the I-line stepper was a 6inch/22mm square of glass material. The LNA (Lens Numerical Aperture)=0.60 and the INA (Input Numerical Aperture)=0.38. The NAs (numerical apertures) were fixed.

The exposure field used by the DUV stepper was a 6inch/22mm square of glass material. LNA=0.60 and INA=0.45. The Nikon stepper has two numerical apertures. The INA is the front-end of the lens through which the arc lamp or

the laser light passes. The INA did not affect the experiment. The LNA is a device of Aperture in Projection LENS. Numerical Aperture in this experiment means LNA. Hence,  $LNA=NA$  ( $s=INA/LNA$ , I-line and DUV Illumination aperture used conventional types). Generally, the NA of the DUV can be opened wider because the resolution of the resist used with DUV is higher than with the I-line.

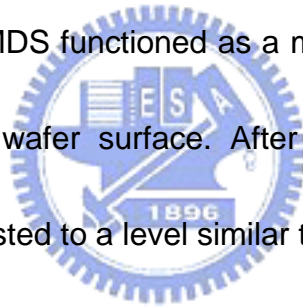
For SEM (scanning electron microscopy), the microscopes used were a Hitachi S-9200, a KLA\_Tencor 8100, and an Applied Materials' SEM Vision. The Hitachi S-9200's primary function was to measure the pattern's line-width and to capture a top view of the image. The error correction method involved a standard wafer that, after etching, had a line-width of  $0.3\mu\text{m}\pm 10\%$ . The line-width of this standard wafer was measured and if the result was within  $0.3\mu\text{m}\pm 10\%$ , that was considered to meet our requirements. The error between the results obtained by the KLA\_Tencor and those obtained by the Hitachi S-9200 was not allowed to exceed  $\pm 10\%$ .

The Applied Materials SEM Vision was not used to measure line-width because its top view measurement was worse than those made with the

Hitachi S-9200 or the KLA\_Tencor 8100. The Applied Materials SEM Vision was used mainly to view a pattern in three–dimensions. This SEM provides the advantage of having an E-beam that measure the wafer' s surface at  $\pm 45^\circ$  and  $0^\circ$ . This SEM therefore enables a pattern to be observed in three dimensions .

The TEL CLEAN ACT-8 machine was used for spin coating and as a developer. The main functions of the ACT-8 are {1} priming, {2} spin coating, {3} soft baking, and {4} developing

{1} A layer of HMDS (Hexamethyldisilazane)  $(CH_3)_3SiNHSi(CH_3)_3$  is sprayed onto the wafer. HMDS functioned as a medium that strengthened the bond between resist and wafer surface. After suitable priming, the wafer surface energy can be adjusted to a level similar to the resist surface energy to increase the adhesive strength between the wafer surface and the resist. {2} After dehydration baking and priming, the liquid resist must be evenly applied to the wafer surface. The resist was dripped onto the center of the wafer and distributed over its surface by the centrifugal force due to high-speed rotation. A higher rotation speed yields a thinner and more uniform resist liquid. The resist includes a very volatile organic solvent. After the resist is sprinkled onto the wafer surface, the stickiness of the resist changes with the volatility of the solvent. Failing to complete the coating before the solvent becomes volatile



yields poor uniformity. {3} The main purpose of the soft baking was to eliminate the solvent that remains in the resist after spin coating, to transform the resist from a semi-solid to a solid film. {4} The main purpose of developing was to display the pattern that followed the exposure and leave the required pattern after the developer reacts.

After the coating process is completed, the thickness of the resist must be known. Therefore, a KLA\_Tencor PROMETRIX UV-1280SE was used to measure the thickness of the resist film, by applying optical methods to measure accurately the thickness of the resist from the center of the wafer to the edges of the wafer after the resist has solidified.



## **Experimental**

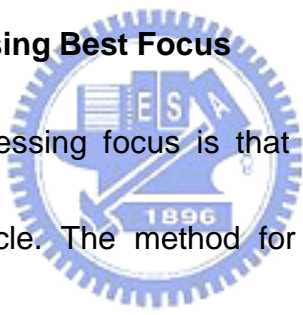
The matrix was exposed by marking off the X (horizontal) and Y (vertical) axes on the surface of the wafer and then changing the focus and the exposure dose to vary the CD bar. Once the resist material was checked, the optimal focus and exposure dose for the resist were determined. Different resists correspond to different optimal focal centers. The focus and exposure dose are two variables that simultaneously influence the line-width's cross-sectional pattern. Consequently, a CD-SEM had to be used to measure or observe changes in the pattern. The optimal focus is the center point of the



acceptable DOF (Depth of Focus) range. The experiments showed that a focus nearer to zero yielded an image of better quality. The optimal exposure dose is one that—with a fixed focus—makes the pattern on the wafer the same as the pattern on the reticle. Also, a smaller white wall enables more requirements to be met. The best situation involved no white wall. A negative white wall may have caused the CD bar to collapse.

## ■ Results and Discussion

### **Symmetrical Multiprocessing Best Focus**



Symmetrical multiprocessing focus is that which yield a pattern most similar to that on the reticle. The method for measuring the symmetrical multiprocessing focus was to take a wafer coated with a positive resist (PFI 58 Resist) and to expose 17 sets of patterns on its surface. Each pattern consisted of nine horizontal patterns and nine vertical patterns, each of which included five rhomboids. The length to width ratio of the rhomboids on the reticle was 30:1. However, their shape changed with the focus. The length of each rhombus was measured and the longest one found. The focus this longest rhombus was the best focus because as the focus changed, all the rhomboid patterns changed shape accordingly due to defocusing and the

changing area of exposure. Defocusing can be divided into positive and negative. For a positive resist, the positive defocusing cross-section of a CD-bar is a regular triangle. Severe defocusing causes the sharp cornered pattern to become smoother and rounder. A negative defocusing cross-section CD bar is an undercutting, which, if severe will cause the CD-Bar to collapse and the sharp -cornered pattern to become smoother and rounder. Therefore, when the focus is at zero, the rhombuses are longest, and when the focus shifts to positive or negative, contraction and deformation occur.



The I-line stepper and the DUV stepper in this experiment used the same reticle. However, the differences between the resists used with each stepper caused the I-line stepper to require longer exposure than the DUV stepper. For the I-line stepper, the exposure conditions were exposure dose =165  $mJ / cm^2$  and exposure step=0.2 $\mu m$ . The focus variation ranged from +1.6 $\mu m$  to -1.6 $\mu m$ . The Applied Materials' SEM Vision revealed that the best focus for the I-line stepper was 0 $\mu m$ , at which the ratio between of length to the width of the rhombuses was approximately 30:1. Shifting the focus farther from 0 $\mu m$  caused the rhomboid patterns to become more blurred, contracted and deformed. When the focus was  $\pm 1.6\mu m$ , the five rhomboid patterns contracted

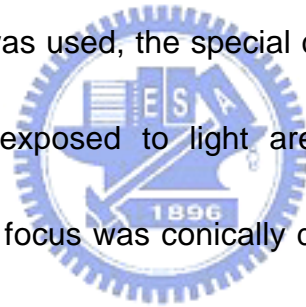
into irregular ellipse forms (Figure 6.1) because of the defocusing effect produced on this area. The pattern changes at negative and positive foci were symmetrical (Figure 6.2).

When measuring the best focus for the DUV stepper, SEPR 432 was used as the positive resist. The exposure conditions were exposure dose =  $30 \text{ mJ} / \text{cm}^2$  and exposure step =  $0.2 \mu\text{m}$ . The focus variation ranged from  $+1.6 \mu\text{m}$  to  $-1.6 \mu\text{m}$ . The Applied Materials SEM Vision was used to observe that the patterns at negative and positive focus were symmetrical. However, the pattern of the DUV stepper was better than for the I-line stepper. When the focus was zero, the pattern was a 30:1 rhombus. When the focus was  $\pm 1.6$ , the five rhomboid patterns contracted into irregular shapes (Figure 6.3) because the DUV's defocusing effect is stronger than the I-line's defocusing effect. Consequently, the shapes obtained were smoother and rounder than with the I-line. The patterns at negative and positive focus were symmetrical (Figure 6.4).

When the I-line stepper focus was  $0 \mu\text{m}$  and the DUV stepper focus was also  $0 \mu\text{m}$ , the two corresponding patterns were expected to be identical. However, in this experiment, the DUV stepper's rhombus pattern was longer than the I-line stepper's because exposure dose impacts pattern length. A

longer exposure dose causes the resist to undergo a more intense chemical reaction. However, the difference between the two patterns was satisfactory for this experiment, and the pattern lengths in each of the two cases did not have to be equal. After a long exposure, contact with the developer causes a more intense chemical reaction. Therefore, for both the H-line stepper and the DUV stepper, increased exposure dose yields a longer pattern.

The focus also affects the length of the pattern. When focus =  $0\mu\text{m}$ , the pattern is longest, and when the focus is  $\pm 1.6\mu\text{m}$  the pattern is shortest, because a positive resist was used, the special characteristic of which is that areas of resist that are exposed to light are washed away during the development reaction. The focus was conically distributed, and the negative focus and positive focus were symmetrical. At a focus of  $0\mu\text{m}$ , the exposed areas were fewest and no defocusing was observed. At a focus of  $\pm 1.6\mu\text{m}$ , however, more areas of the positive resist were exposed, and, because of serious defocusing, the pattern was shortened and contracted, becoming irregular.



## **Focus**

The best focus determines the present, actual focus, which varies with the

best focus as standard. According to M. E. Preil and W. H. Arnold (1992), focus influences line-width. Their experimental method was to vary the focus from -1.2~ to 1.2 $\mu\text{m}$  and observe the changes. They found that at a focus of 0 $\mu\text{m}$ , the line-width was smallest; that a longer focus yielded a larger the line-width, and that positive and negative foci were symmetrical. In this work, the best focus was used to arrive at results that were the opposite of those obtained by Preil and Arnold because the process latitude smiley curve was different. Restated, a different resist was used herein.

Varying the focus over  $\pm 1.6\mu\text{m}$  revealed that the I-line's best focus curve included clear variations within  $\pm 0.4\mu\text{m}$ , as shown in Figure 6.2. Therefore, the I-line focus was varied within  $\pm 0.4\mu\text{m}$  and the variation of line-width measured. A white wall was observed simultaneously. In Figure 6.5 and 6.6, when the focus was varied between  $\pm 0.4\mu\text{m}$ , a white wall in the shape of a regular triangle appeared regardless of whether the focus was positive or negative, which result contradicts theory. With a positive focus the white wall is expected to be a regular triangle, but according to theory, at a negative focus, the white wall will be an under-cut. However, producing an undercutting with a negative focus was found to be difficult, contrary to expectations, because during the development process, the surface of the water came into contact

with the developer for a longer period than did the base, so the chemical reaction took longer at the surface than at the base. Making an undercutting required that the focus be continuously maintained negative. However, a focus nearer to  $0\mu\text{m}$  is generally preferred. Using a negative resist switches the orientation of the white wall.

### **DOF (Depth of Focus)**

Better imaging effects are obtained by deepening the DOF a consistently before acronyms. The factor that most strongly influences the DOF is the resist window, which was obtained herein by changing the focus and determining the size of the DOF from the changes in the focus and the line-width. The focus varied from  $+0.4\mu\text{m}$  to  $-0.4\mu\text{m}$ , and the Hitachi S-9200 revealed the patterns obtained at each focus. Given a specific exposure dose, with a line-width and white wall between the positive focus and the negative focus, the DOF for this kind of resist can be obtained,

$$DOF = K_2 \frac{I}{NA^2};$$

$$R = \frac{K_1 I}{NA} \dots [1]$$

$$DOF = K_3 \frac{R^2}{I} \dots [2]$$

## Exposure dose

Figure 6.6 was a UV lamp, while that used to obtain Figure 6.7 was a laser, but the line-widths are clearly identical. The top edge of the CD bar in Figure 6.6 is less stable than that in Figure 6.7, and the top edge of the CD bar in Figure 6.6 is semicircular showing independent proximity. In Figure 6.7, the same reticle was used; its borders were found to be more stable than in Figure 6.6, and the top edge of the CD bar was almost a right angle, because the wavelength of a UV lamp is higher than that of a lasers, so the resolution is poorer, such that an pattern identical to that on the reticle is harder to obtain.

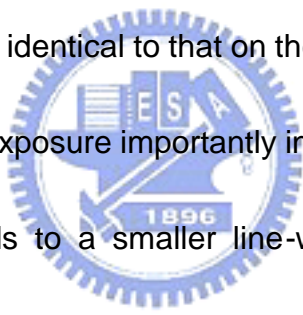


Figure 6.8 shows that exposure importantly influences line-width. A higher exposure dose corresponds to a smaller line-width, according to a linear relationship. The experiment revealed that the gradient of the exposure/line-width relation did not change with the thickness of the resist. Birol Kuyel and Harry Sewell (1990) noticed that line-width and the thickness of the resist followed a wave . The main factor that influenced the gradient of the exposure/line-width relation was the resist's sensitivity composition. Generally, the extent to which the composition induces a stronger chemical reaction with the developer influences the slope .

Figure 6.8 showed that a higher the exposure dose corresponds to a smaller line-width, mainly because increasing the time for which the resists is exposed increases add to the force of the chemical reaction between the resist and the developer. Consequently , the developer will remove even more exposed resist, reducing the line-width.

A better resolution enables a smaller line-width to be obtained, such that at the appropriate exposure dose no variations will be produced. Therefore, the line-width can be reduced only by improving the resolution. Figure 6.1. showed that the resolution was related to NA,  $\lambda$  and k (k= permittivity). In this experiment, NA was usually set between 0.5 and 0.7, although the NA was used to control the resolution, the effect was not great. Changing the wavelength and k to adjust the resolution was more effective. However, at present, UV lamps and KrF lasers are our only available light sources. Increasing k will be the simplest method of improving. The current method is to switch to a different resist or to apply an ARC (anti-reflection coating) to the surface of the resist. The goal is to reduce both k and the optical proximity effect. The transmission rate of the ARC material on the surface layer must be increased to allow the light beam to pass through it and fall onto the resist



beneath, reducing refraction. However, the addition of a layer of ARC to the surface of the resist beyond the scope of this work.

## ■ Conclusions

The focus and exposure of dose in photolithography process is the important condition to determine figure. It is very hard to determine which is the best focus and exposure dose in photolithography process. In semiconductor plants (Fab), they usually use a frequently used PR as basic standard while other PRs co-work with it. But this method was proved probably wrong. The experiment found that the patterns of focus are symmetrical and process latitude smiley curve will not change because of different elements of PR but location or figure of best focus will do. Exposure dose will change size of CD Bar, that is, higher exposure dose will make CD bar smaller, but too high exposure dose will make CD Bar not stable or even cause the collapse of CD Bar. Therefore, it is not correct to use exposure dose to change line width. There is linear relationship between exposure dose and line width. According to the results of our experiment,  $R^2 > 0.9$ , so their relationship could be consider as linear relationship ( $R^2 > 0.9$  is called high positive correlation in statistics).

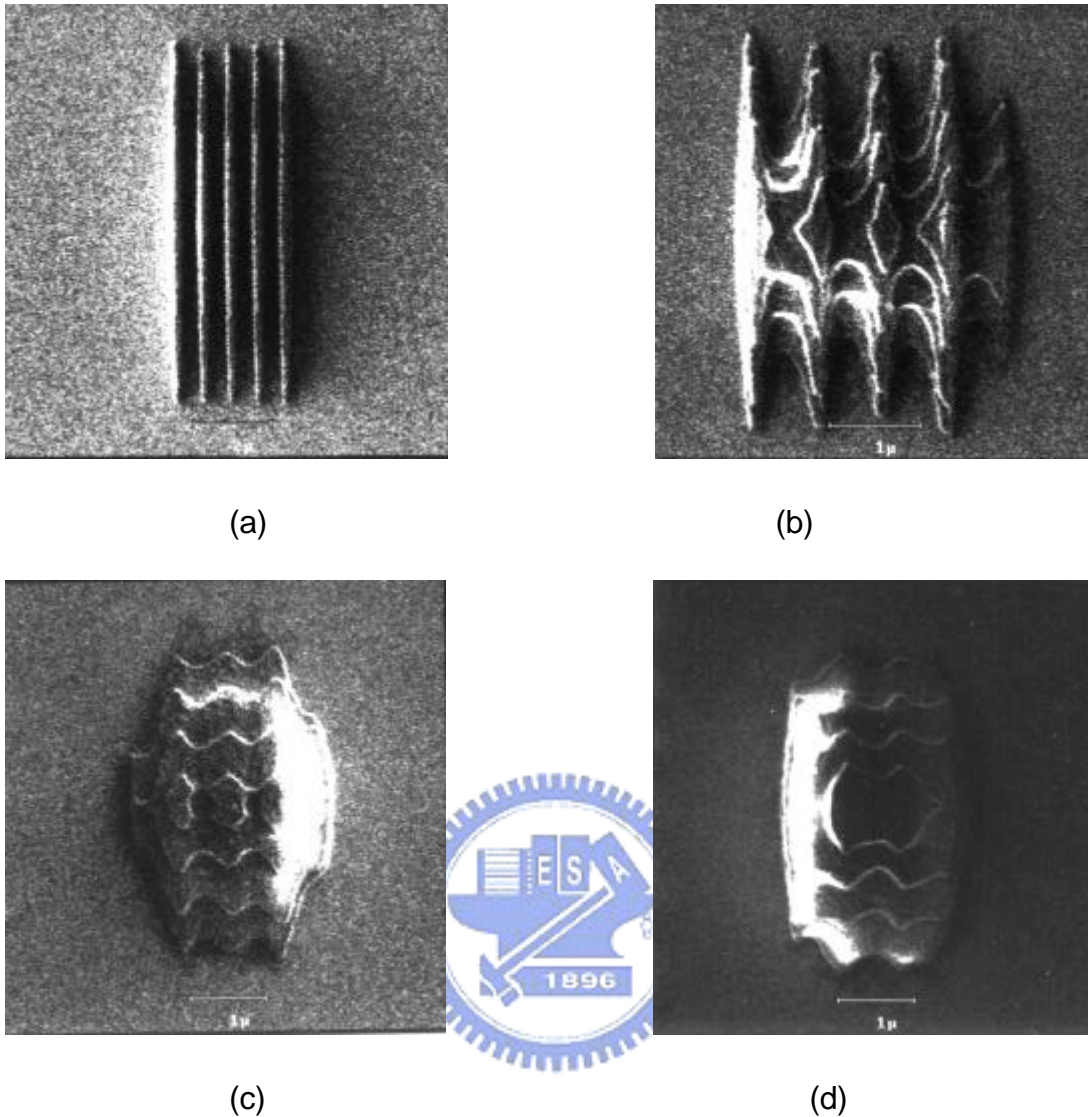


Figure 6.1 I-line symmetrical multiprocessing focus. Pattern length changes observed using an Applied Materials SEM Vision. (a) At focus=0 $\mu\text{m}$ , the pattern had the same shape as that on the reticle; (b) at a focus of -0.8 $\mu\text{m}$ , the pattern was shortened; (c) at focus=-1.2 $\mu\text{m}$ , the pattern was shortened and completely transformed; (d) at focus=-1.6 $\mu\text{m}$ , the pattern irregularly contracted into a shape that resembled an ellipse.

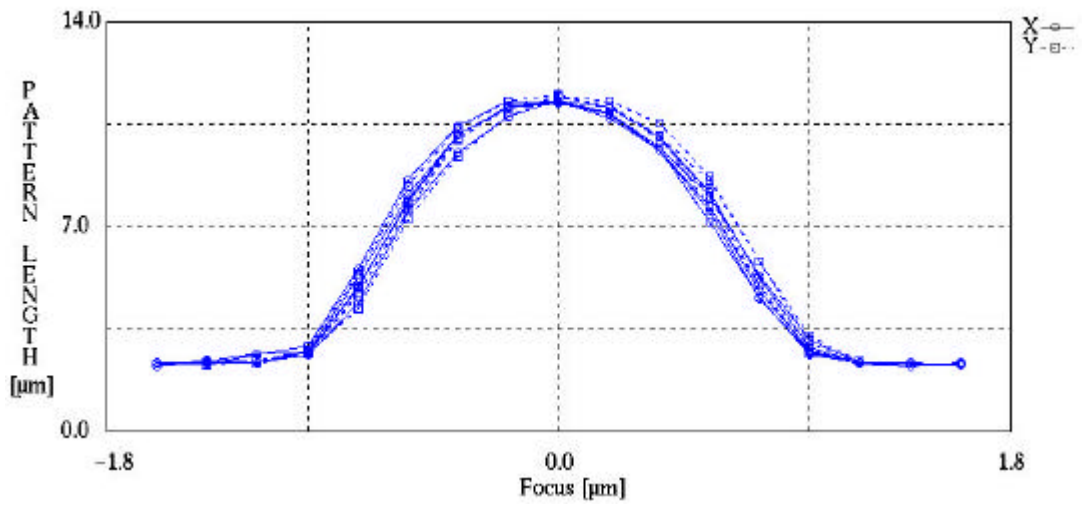
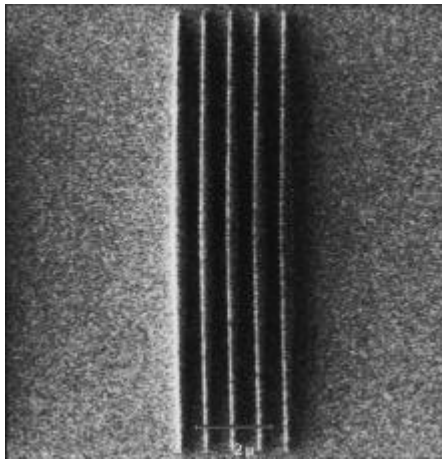


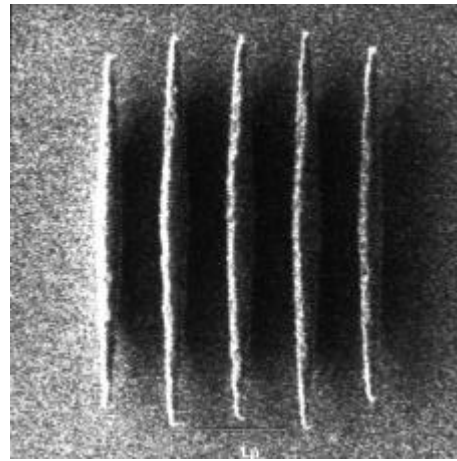
Figure 6.2 Process latitude smiley curve of pattern length-focus, with an I-line

stepper and a positive resist.

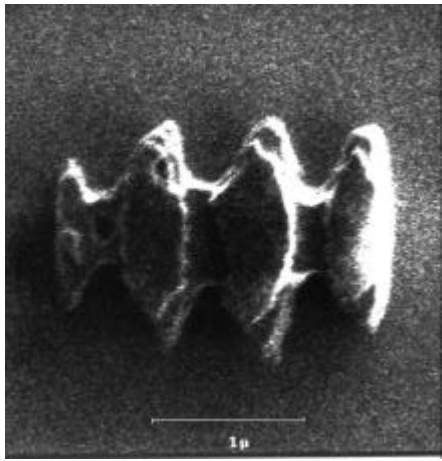




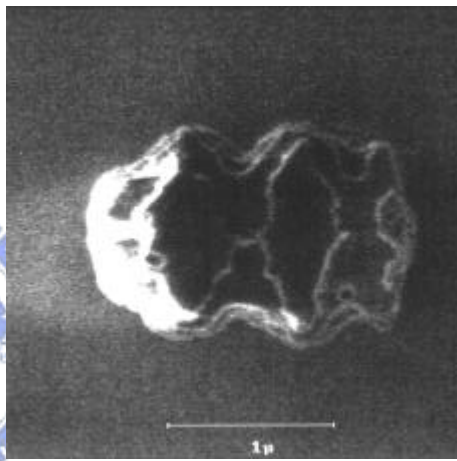
(a)



(b)



(c)



(d)

Figure 6.3 DUV symmetrical multiprocessing focus. Pattern length changes observed using an Applied Materials SEM Vision: (a) At focus= $0\mu\text{m}$ , the pattern had the same shape as that on the reticle, but was longer; (b) at focus= $-0.8\mu\text{m}$ , the pattern was shortened; (c) at focus= $-1.2\mu\text{m}$ , the pattern was shortened and completely transformed; d) at focus= $-1.6\mu\text{m}$ , the pattern became an irregular shapes.

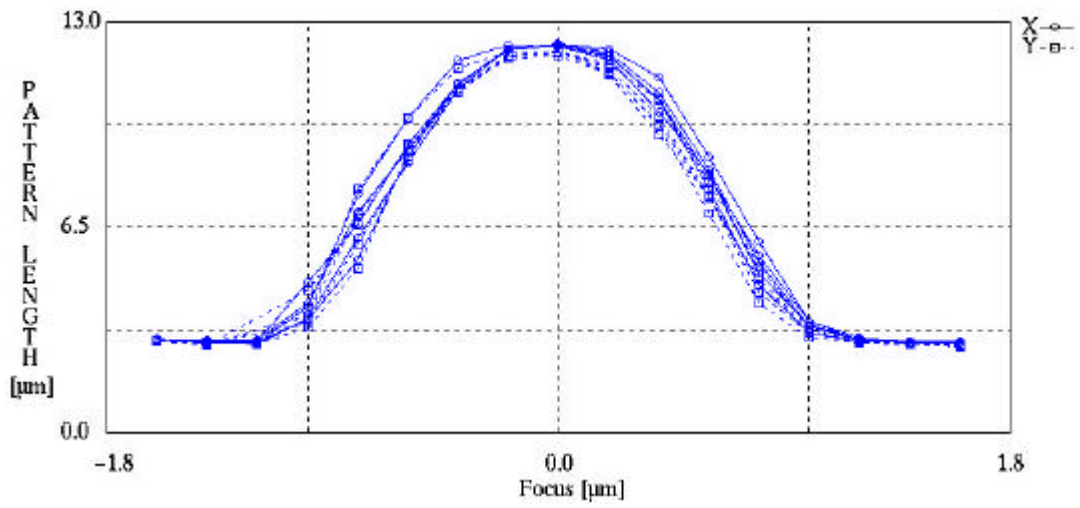


Figure 6.4 The process latitude smiley curve pattern length-focus, with a DUV stepper and a positive resist.



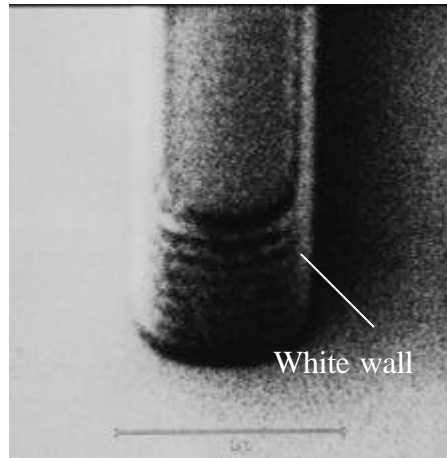
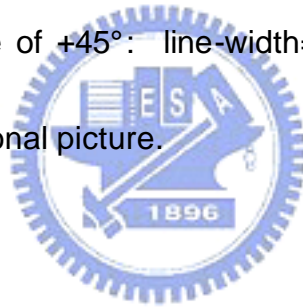


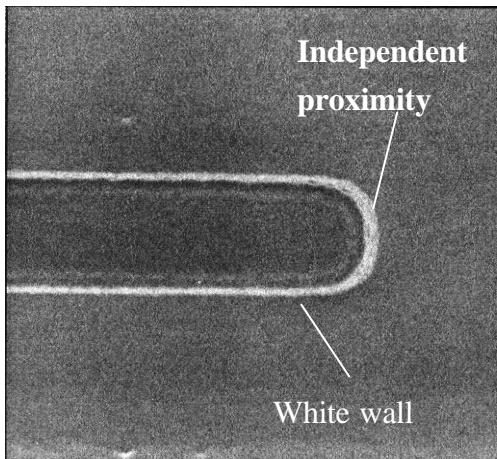
Figure 6.5 I-line light source, PFI-58 resist, exposure dose =  $200 \text{ mJ} / \text{cm}^2$ ,

focus =  $0 \mu\text{m}$ : Observed with the Applied Materials SEM at a

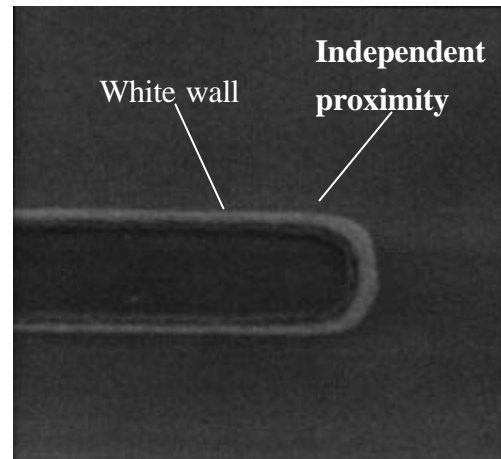
scanning angle of  $+45^\circ$ : line-width =  $0.682 \mu\text{m}$ , white wall, and

three-dimensional picture.





(a)



(b)

Figure 6.6 I-line light source, PFI 58 Resist, Exposure =  $200 \text{ mJ} / \text{cm}^2$ ; Figures

of white wall and Independent Proximity When (a) Focus =  $+0.4 \mu\text{m}$ ,

(b) Focus =  $-0.4 \mu\text{m}$ , under multiplying rate 50KV of HITACHI

S-9200 CD SEM and Line-Width =  $0.2 \mu\text{m}$ . No matter it is  $0 \mu\text{m}$  or

$0 \mu\text{m}$ , there is regular triangle while wall.

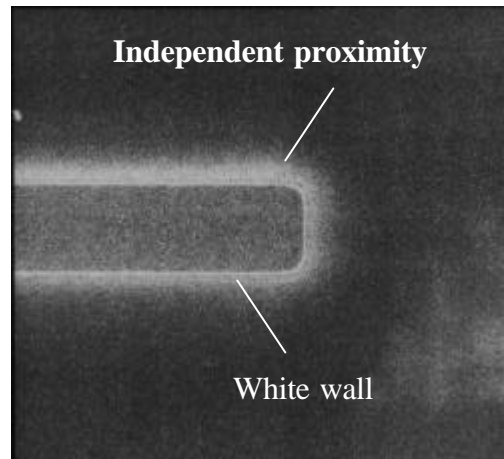


Figure 6.7 Deep UV light source, Exposure =  $30 \text{ mJ} / \text{cm}^2$ , Figures of white wall and Independent Proximity When Focus=0, under multiplying rate 50KV of HITACHI S-9200 CD SEM and Line-Width=  $0.2 \mu \text{m}$ .

The independent proximity of Deep UV is smaller than I-line.





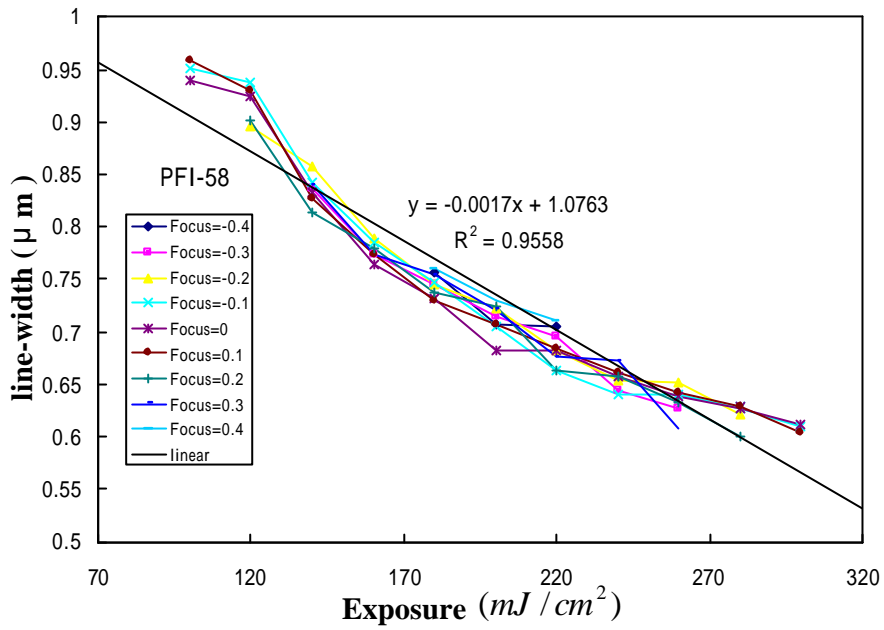


Fig. 6.8 (a)

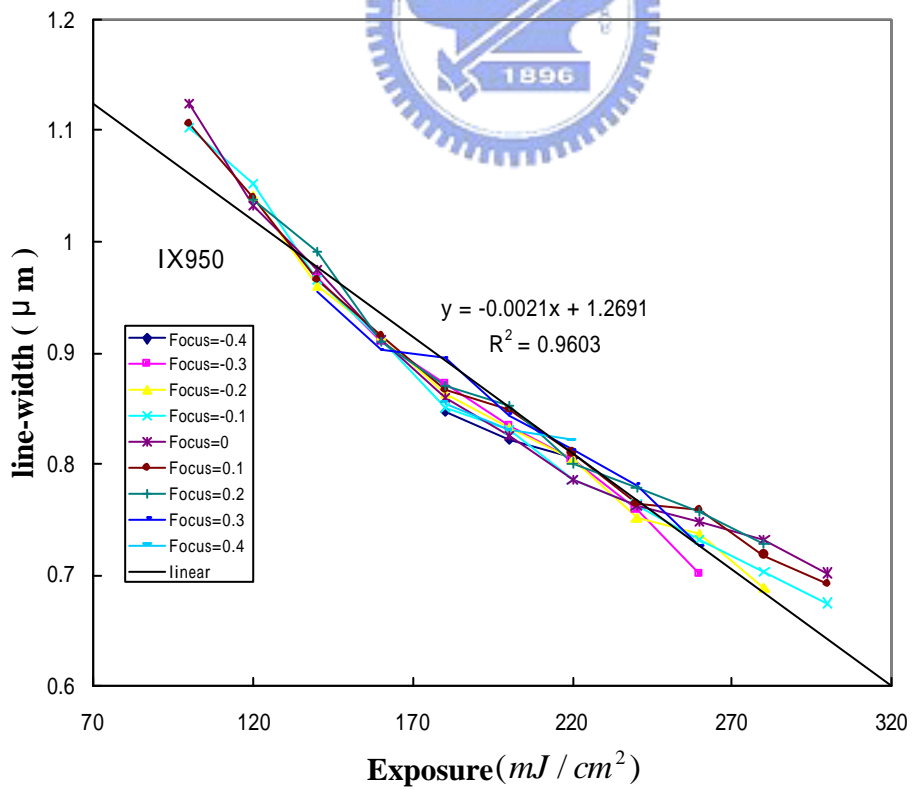


Fig. 6.8 (b)

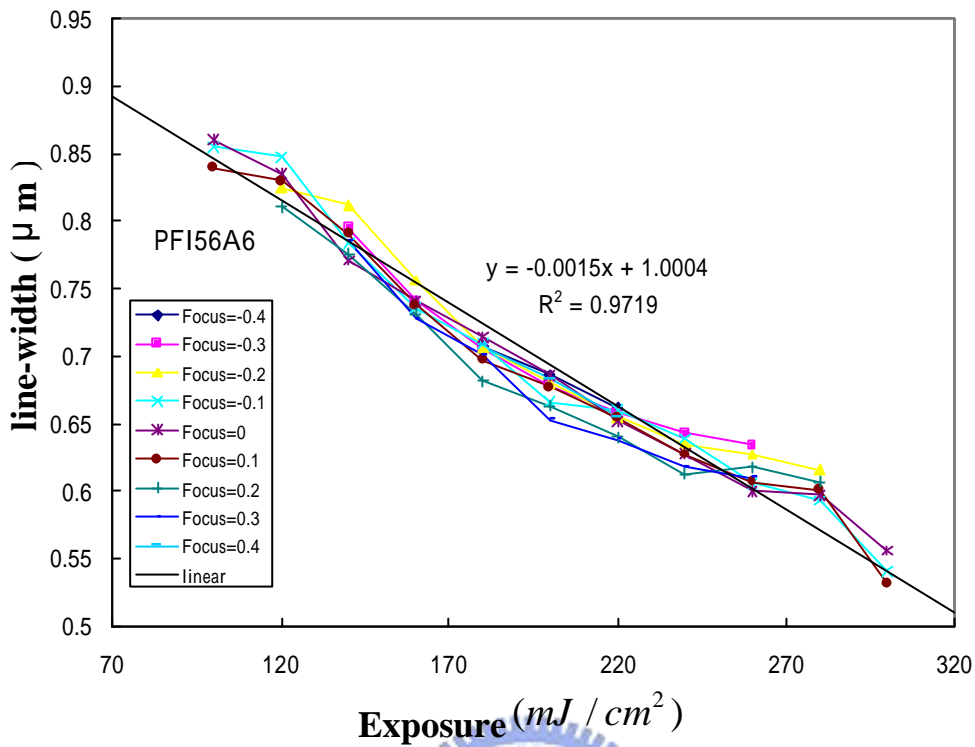


Fig. 6.8 (c)

Figure 6.8 I-line light source, the figure of linear relationship of (a) PFI-58 Resist, (b) IX950 Resist and (c) PFI56A6 Resist Exposure- Line Width.

## Chapter 7

### Analysis of instability line width and white wall created by the photolithography process

#### ■ Introduction

In the photolithography processing of semiconductor, line-width is smaller and smaller. Therefore, the requirements of process window are stricter than before. In the small line-width, the formation of serious white wall will affect line-width and cause rejects in following process. The study conducted research on the control of best focus in which particularly explored the relationship between exposure dose and line-width and the phenomenon of white wall generated by focus. The research obtained related coefficients of exposure dose-line width and exposure dose-white wall by coating photo resist of different components with the same thickness on the surface of fused silica wafer. The results of research found that exposure dose might not only change line-width but also had important effects on white wall. Among others, the most important factor for exposure dose is the component of sensitivity of photo resist.

## ▪ Experimental

### Equipment

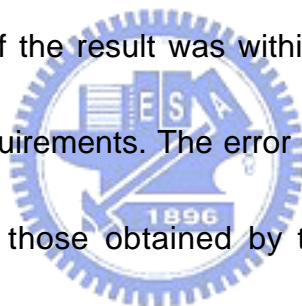
The steppers were a Nikon I-line and DUV. The major function of a stepper is to apply the exposure pattern to the surface of a wafer that has already been coated with a layer of resist. The main difference between an I-line stepper and a DUV stepper is that they use different light sources. The light source used by an I-line stepper is a UV lamp  $\lambda=365\text{nm}$ , while the light source used by a DUV stepper is a KrF excimer laser  $\lambda=248\text{nm}$ . The differences between the wavelengths of these light sources lead to different resolutions. Generally, a shorter wavelength gives a better resolution, and a better resolution enables the line-width to be made narrower.

The exposure field used by the I-line stepper was a 6inch/22mm square of glass material. The LNA (Lens Numerical Aperture)=0.60 and the INA (Input Numerical Aperture)=0.38. The NAs (numerical apertures) were fixed.

The exposure field used by the DUV stepper was a 6inch/22mm square of glass material. LNA=0.60 and INA=0.45. The Nikon stepper has two numerical apertures. The INA is the front-end of the lens through which the arc lamp or the laser light passes. The INA did not affect the experiment. The LNA is the NA close to the edge of the wafer and directly affects the experiments. Hence,

$LNA=NA$  (  $=INA/LNA$ , Illumination aperture used annular type). Generally, the NA of the DUV can be opened wider because the resolution of the resist used with DUV is higher than with the I-line.

For SEM (scanning electron microscopy), the microscopes used were a Hitachi S-9200, and a Applied Materials' SEM Vision. The Hitachi S-9200's primary function was to measure the pattern's line-width and the capture a top view of the image. The error correction method involved a standard wafer that, after etching, had a line-width of  $0.3\mu\text{m}\pm 10\%$ . The line-width of this standard wafer was measured and if the result was within  $0.3\mu\text{m}\pm 10\%$ , then the was considered to meet our requirements. The error between the results obtained by the nikon stepper and those obtained by the Hitachi S-9200 was not allowed to exceed  $\pm 10\%$ .

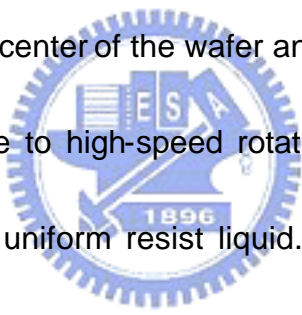


The applied materials SEM vision investigation used APPLIED materials SEM Vision to observe the free-space diagram of pattern and the composition of EDX measurement materials rather than using measurement of line-width. The main advantage of this approach is that E-beam can measure the wafer surface under  $\pm 45^\circ$ , thus indicating the free-space diagram and pattern variation.

The TEL CLEAN ACT-8 machine was used for spin coating and as a

developer. The main functions of the ACT-8 are {1} priming, {2} spin coating, {3} soft baking, and {4} developing

{1} A layer of HMDS (Hexamethyldisilazane) is sprayed onto the wafer. HMDS functioned as a medium that strengthened the bond between resist and wafer surface. After suitable priming, the wafer surface energy can be adjusted to a level similar to the resist surface energy to increase the adhesive strength between the wafer surface and the resist. {2} After dehydration baking and priming, the liquid resist must be evenly applied to the wafer surface. The resist was dripped onto the center of the wafer and distributed over its surface by the centrifugal force due to high-speed rotation. A higher rotation speed yields a thinner and more uniform resist liquid. The resist includes a very volatile organic solvent. After the resist is sprinkled onto the wafer surface, the stickiness of the resist changes with the volatility of the solvent. Failing to complete the coating before the solvent becomes volatile yields poor uniformity.



{3} The main purpose of the soft baking was to eliminate the solvent that remains in the resist after spin coating, to transform the resist from a semi-solid to a solid film. {4} The main purpose of developing was to display the pattern that followed the exposure and leave the required pattern after the developer reacts.

After the coating process is completed, the thickness of the resist must be known. Therefore, a KLA\_Tencor PROMETRIX UV-1280SE was used to measure the thickness of the resist film, by applying optical methods to measure accurately the thickness of the resist from the center of the wafer to the edges of the wafer after the resist has solidified.

### ■ Experimental

This experiment is designed to use matrix exposure to lay out horizontal and vertical axes and to utilize the combination of exposure to obtain variant conditions between line width and white wall. PR is subject to different optimal focus point resulting from different properties in terms of thickness and sensitivity. In this experiment, in order to attain the optimal focal point, each PR was calibrated to a focus of less than  $\pm 0.1 \mu\text{m}$  before experiment. Then, matrix exposure method was used to set up the focus at the best focal position. By changing exposure dose, the results of experiment are obtained.

### ■ Results and Discussion

#### Focus and Exposure Theory

Figure 7.1 clearly illustrates a cone shaped distribution and positive and

negative symmetry of light sources from the lens to the wafer surface. Given focus=+1.4  $\mu$  m and focus=-1.4  $\mu$  m , the exposure area of CD Bar exceeds focus=0  $\mu$  m. Consequently, the size of CD Bar is not different given focus=0  $\mu$  m and focus=  $\pm$ 1.4  $\mu$  m. Pattern length is longest when focus=0  $\mu$  m, because exposure area is smallest and pattern length is shortest when focus=  $\pm$ 1.4  $\mu$  m because exposure area is maximized. However, these phenomenon only occur on positive resist. For negative resist opposite results are obtained. Positive resist is characterized by the lighted area producing photo-acid and alkali developer, which is eliminated following neutralization because of the balance between acid and alkali. DUV light source has a cone shape distribution, and positive and negative symmetry exists between the lens and the wafer surface. When exposure location is on the top of the cone, then this investigation assumes focus=0  $\mu$  m. The focus distance increases with the distance of the exposure location from the top of the cone., The cone area is smallest when focus=0  $\mu$  m, and thus the lighted area is less than for focus=  $\pm$  1.4  $\mu$  m while the pattern length is longer or bigger. The lighted area of positive resist increases given focus=  $\pm$ 1.4  $\mu$  m. Besides, probably because of the serious defocus or the reduced capacity to display diagram borders, pattern length is reduced and an irregular pattern forms given focus=  $\pm$ 1.4  $\mu$  m.





## The impact of exposure dose on CD Bar

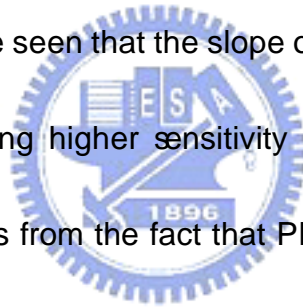
Exposure dose is a main factor in influencing line-width. In this research, it is found that the higher the exposure dose the smaller is the line width. At the same time, exposure dose can affect white wall, i.e., the higher the exposure dose the smaller is the white wall. Furthermore, both exposure dose–line width and exposure dose-white wall contribute to the characteristics of linear relationship.

From Fig. 7.2, it can be seen by comparison that these three PR produce three different line widths and white walls when exposing them at the same energy. However, these three PR curves appear the same trend. That is, the higher the exposure dose, the smaller are the line width and the white wall. Under the same PR thickness, the main factor that affects the slope of exposure dose-line width and white wall is the sensitivity of PR. In other words, under the same energy, the higher the sensitivity, the smaller the line width becomes. In this experiment, under the condition of having the fixed film thickness of PR, the varied relationship of energy with respect to line width and white wall is studied. All three PR thickness are controlled at  $7500 \pm 200 \text{ \AA}$  and the homogeneity of PR is at  $3 \sigma < 0.03 \mu\text{m}$ .

From Fig. 7.2, it is found that line-width measured after exposed with high

dose is much smaller than that when exposed with low dose, which is consistent with the results obtained from measuring white wall and line-width. In addition, line-width and exposure dose present the linear relationship, and white wall and exposure dose contribute to the linear relationship as well. When exposure dose is low, line-width is wider than that exposed at high dose. This can be attributed to the facts that at high exposure dose, the absorption of high energy of PR enhances the reaction capability of neutralization. Therefore, there will be more areas to be neutralized. Those impurities after neutralization can be rapidly washed away by DI water. However, too high of exposure dose can cause line-width to become very small. As a result, the aspect ratio becomes too large. Therefore, CD bar can't hold back the turbulent force caused by DI water as neutralized area is washed, causing CD bar to collapse. From Fig. 7.3, it is revealed that SEPR 451 PR can cause CD bar to collapse at Dose= $80 \text{ mJ/cm}^2$ . This resulted from the facts that the sensitivity of SEPR 451 is higher than that of the other two PR and can cause aspect ratio to become higher than that of the other two PR even at the same exposure dose. After development, SEPR 451 can't support the impact of turbulent force and collapse. High energy can make light penetrate through the bottom of PR with high reflective energy coming out from bottom. Therefore, the area to be

neutralized at the bottom of CD bar is increased. Hence, white wall decreases as the exposure is increased, and it maintains a linear relationship with respect to exposure dose. From Fig. 7.2, it can be seen that the linear slope of exposure dose-white wall and dose-line width is different using the same PR. By comparing the slope of exposure dose-line width with that of exposure-white wall for three different PR, the slope of exposure dose-line width is higher, so is the slope of exposure-white wall. The main reason contributing to this trend is due to the sensitivity of PR. By comparing the table1 with Fig 7.2, it can be seen that the slope of exposure dose-line width is much steeper for PR having higher sensitivity as compared to that having lower sensitivity. This arises from the fact that PR with higher sensitivity after its exposing to light source becomes relatively easy to produce neutralized reactions. Also, it can be found from Fig. 7.2 that the sensitivity between SEPR 451 and SEPR-450H is off by 1.96 times. When exposure dose is at  $20 \text{ mJ/cm}^2$ , line width can be off by 1.03 times. However, as exposure dose reaches to  $65 \text{ mJ/cm}^2$ , line width can be different by 0.42 times. The outcome attained from this observation indicates that the higher the exposure dose, the more important the factor of sensitivity that can affect on line width. As exposure dose is at  $20 \text{ mJ/cm}^2$ , white wall is off by 1.46 times. While exposure



dose reaches at  $65 \text{ mJ/cm}^2$ , line width is off by 0.68 times. The ratio of white walls with their exposure doses at 20 or at  $65 \text{ mJ/cm}^2$  is 2.12. The ratio of line widths with their exposure doses at 20 or at  $65 \text{ mJ/cm}^2$  is 2.45. From these two ratios, it can be found that the error caused by the impact of sensitivity with respect to line width and white wall is minimal.

From Fig 7.4, Exposure dose becomes too low, PR would not form a pattern due to the fact that the absorption of exposure energy by PR is not strong enough to produce a neutralized reaction when in contact with TMAH.

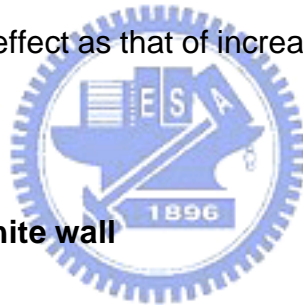
On the contrary, From Fig 7.5 (a), high exposure energy makes CD bar become smaller. From Fig. 7.5 (b), it can be found that too high of exposure dose can make CD bar become unstable. High exposure energy makes CD bar unstable and this step could cause an error if the wrong measurement point were selected. Therefore, the CD SEM measurement method we use is to measure a point for each  $0.2 \mu\text{m}$  in length by selecting a center point on CD bar within a range of  $2 \mu\text{m}$  for ten points. Then, take the average of these ten points to be the value of the line width.

### **Standing wave**

The formation of standing wave is caused by areas having exposed the

strongest light with the formation of the most abundant Indene Carboxylic Acid (ICA). These exposed areas have the fastest dissolvable rate in alkaline solution and their dissolvable areas are the widest ones after development. On the other hand, the areas having exposed the weakest light show the narrowest dissolvable regions. As a result, PR after development forms a periodic contour pattern, i.e., wide and narrow side wall or (white wall). These wave patterns can't be observed by using Hitachi S-9200 or KLA Tencor 8100 CD SEM. In order to observe these phenomena clearly, it is necessary to use Applied Materials SEM Vision to look at them by tilting wafer with  $45^\circ$  and/or use E-beam to examine by twisting wafer with  $\pm 45^\circ$ . From this experiment, it is found that exposure dose doesn't affect the size of standing wave. It can be attributed to the facts that the increment of exposure dose can't change the wavelength of laser. But, coating top ARC (Anti-Reflection Coating) and bottom ARC on the surface or bottom of PR can make the effect of standing wave reduced. From Fig. 7.6(a) and (b) and Fig. 7.6(c), by comparing PR in terms of adding top ARC and bottom ARC to SEPR 432, the standing wave becomes smaller after adding top ARC and bottom ARC to the PR as compared with using SEPR 432 PR along. In fact, we had problem using APPLIED Materials SEM Vision to locate for a periodic contour pattern of white wall with wide and

narrow side wall caused by standing wave. This arises from the facts that the addition of top ARC or bottom ARC can improve the effectiveness of the refractive index and the absorbance of SEPR 432. In addition, different PR would produce different effects of standing wave because different PR possesses different refractive and absorbance. From Fig. 7.6, the contour patterns caused by standing wave resulting from three different types of PR are presented. When the refractive and the absorbance of PR per se are the same as those of top ARC or bottom ARC, the standing wave obtained from the PR produces the same effect as that of increasing top ARC or bottom ARC.



### **The impact of focus on white wall**

Carboxylic acid can be produced after PR is exposed. This acid after its contact with base solution will be neutralized and dissolved. Basically, development process results in a neutralized reaction as PR is sprayed by developer, and it is considered as a severe impact in terms of affecting line width and white wall (Fig. 7.7). In this experiment, the development process used is the same for all wafers. Data obtained through this arrangement can be very accurate. After exposure, TMAH (Tetramethylammonium Hydroxide)  $N(CH_3)_4^+ OH^-$  is used to neutralize wafer by having PR going through

acid-base balanced reactions. The PR surface of wafer will produce different shapes because of the light going through a reticle in generating a cone-shrinking ratio of 4:1. When it is in positive focus, light will project onto the wafer surface with a reverse cone-shrinking ratio of 4:1 causing CD bar to have a shape of positive trapezoid (Fig 7.8. (b)), resulting from the usage of positive PR. If +focus is in the range of greater than the permitted thickness of PR, then CD bar has a shape of equilateral triangle. When it is in negative focus, light will project onto the wafer surface with right circular cone-shrinking ratio of 4:1, thus causing CD bar to have a shape of reverse trapezoid. When the negative focus is greater than the range of permitted thickness of PR, then CD bar would collapse due to the lack of support from bottom. In this experiment, focus is restricted within the range of  $\pm 0.1 \mu\text{m}$ . Therefore, the impact of focus on white wall is reduced to its minimum. Although this factor is reduced, the occurrence of white wall will still take place. The reason is that when TMAH is sprayed on the surface of PR, the neutralized reaction takes place on the surface first, then it extends into the bottom. As a result, the surface of PR has experienced longer time than that of bottom. Consequently, the white wall of CD bar forms a taper side (Fig. 7.8).

## ■ Conclusions

Due to the differences of the composition of sensitizer contained in each PR, as a result, the sensitivity of each PR shows great differences according to its characteristics. Sensitivity is an important factor in terms of absorbing light when PR is exposed. However, photoresists with good sensitivity do not produce the same good results consistently in terms of resolution. Therefore, sensitivity becomes one of the important components of PR. For PRs having the same sensitivity, their CD bars can be changed using different exposure doses. High exposure dose not only makes CD bar smaller, but also causes white wall to be relatively small. In other words, the side wall of CD bar becomes more vertical. Nevertheless, too high of exposure dose can make CD bar either unstable or even collapsible. It is worth mentioning that both exposure dose-line width and exposure dose-white wall appear to have the linear relationship. Statistically, when  $R^2 > 0.7$ , data is regarded as highly correlated. In this experiment, our results indicate that  $R^2 > 0.85$ , therefore, to be considered as a linear correlation.

#### ■ List of Table



Table 7.1 Sensitivity of photo-resist used in experiment

	SEPR 451	SEPR-432	SEPR-450H
Sensitivity	$13.15 \text{ mJ/cm}^2$	$10.57 \text{ mJ/cm}^2$	$6.71 \text{ mJ/cm}^2$



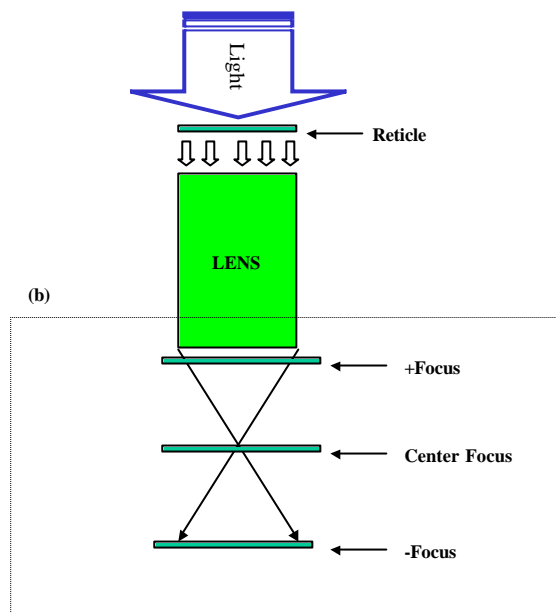


Fig. 7.1 (a)

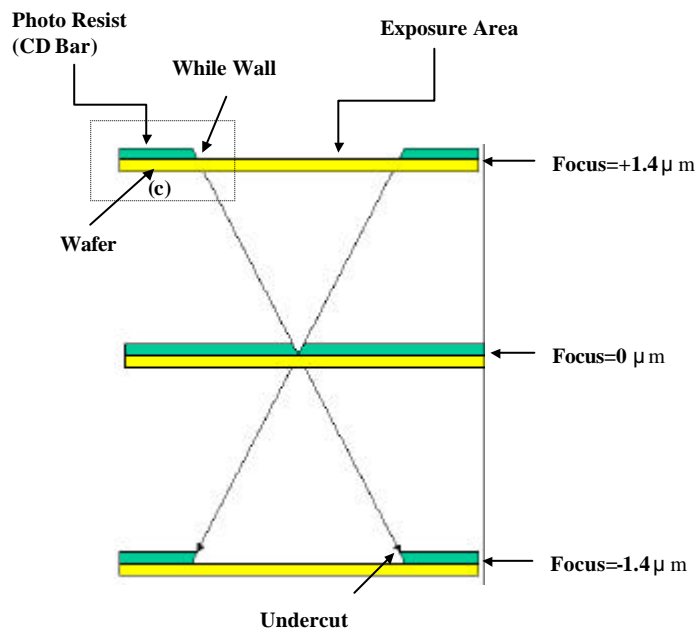
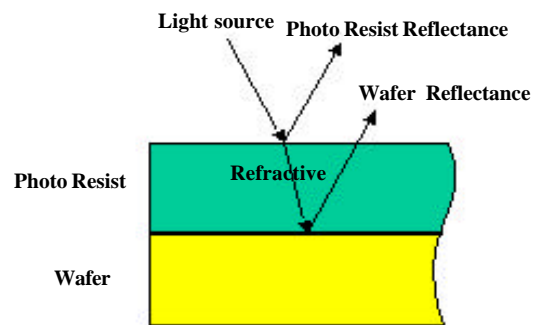


Fig. 7.1 (b)



**Fig. 7.1 (c)**

Figure 7.1 (a) Stepper Exposure Diagram, (b) Influence of Focus on Exposure Area. (c) Focus Locations following Reflectance and Refraction on Photo Resist and Wafer Surface by Light Source.



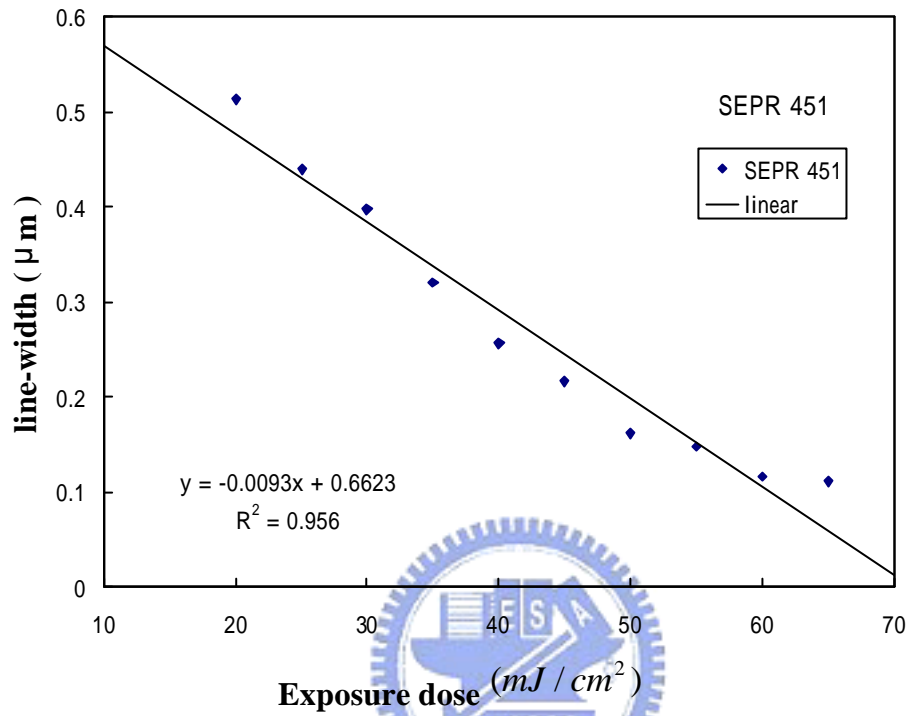
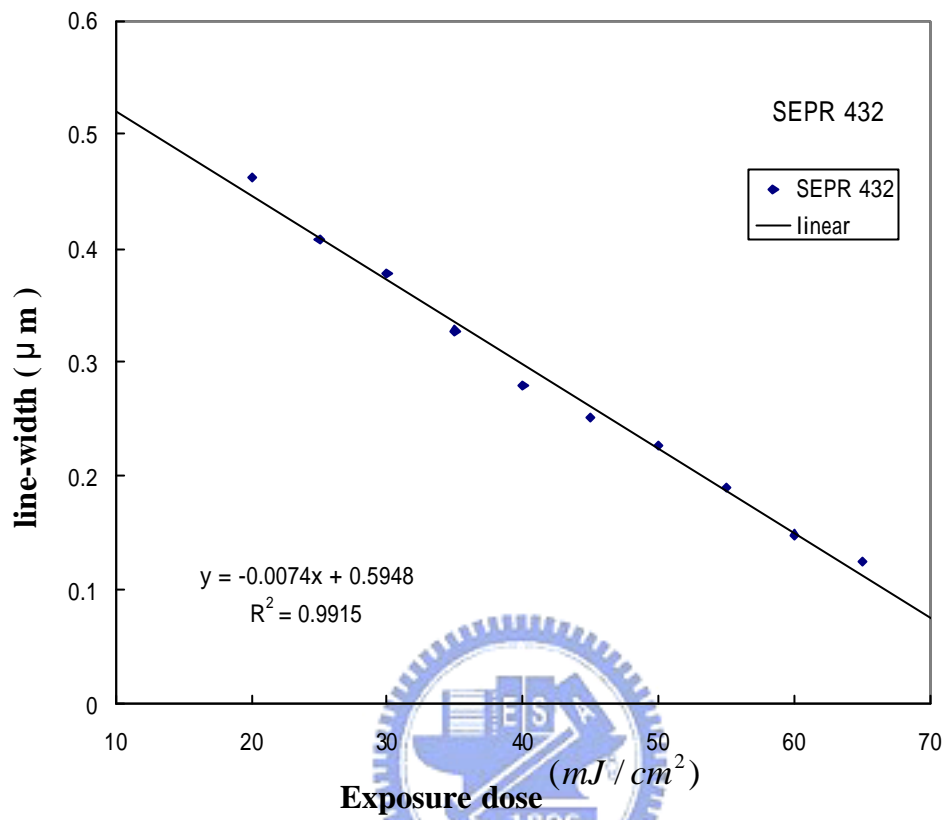


Fig. 7.2 (a)



**Fig. 7.2 (b)**

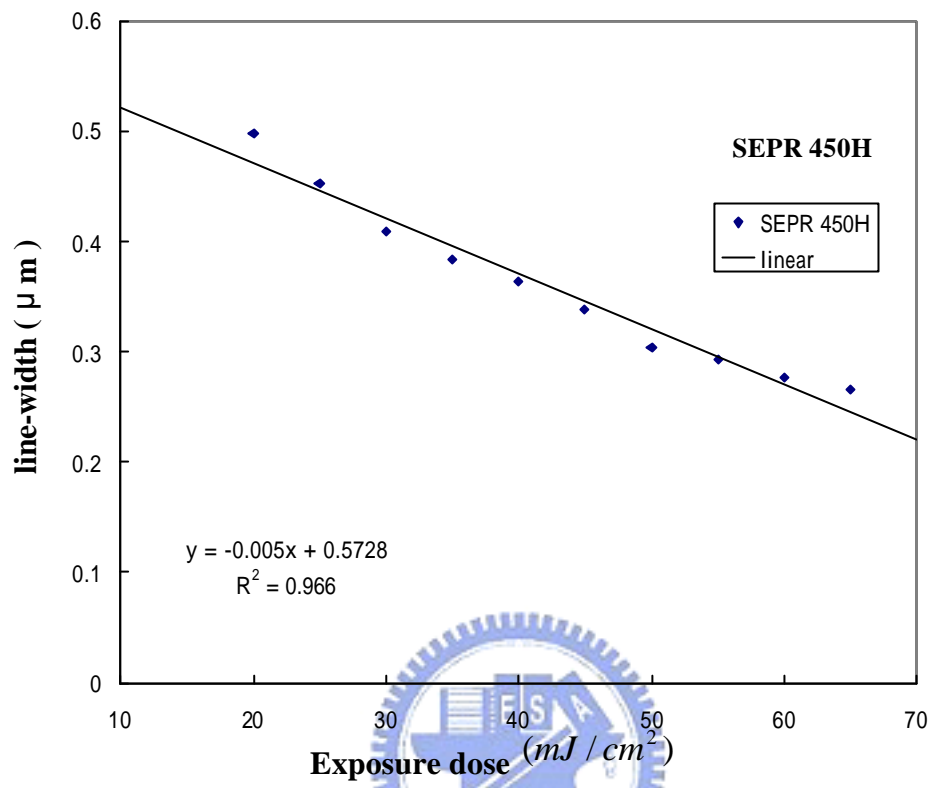


Fig. 7.2 (c)

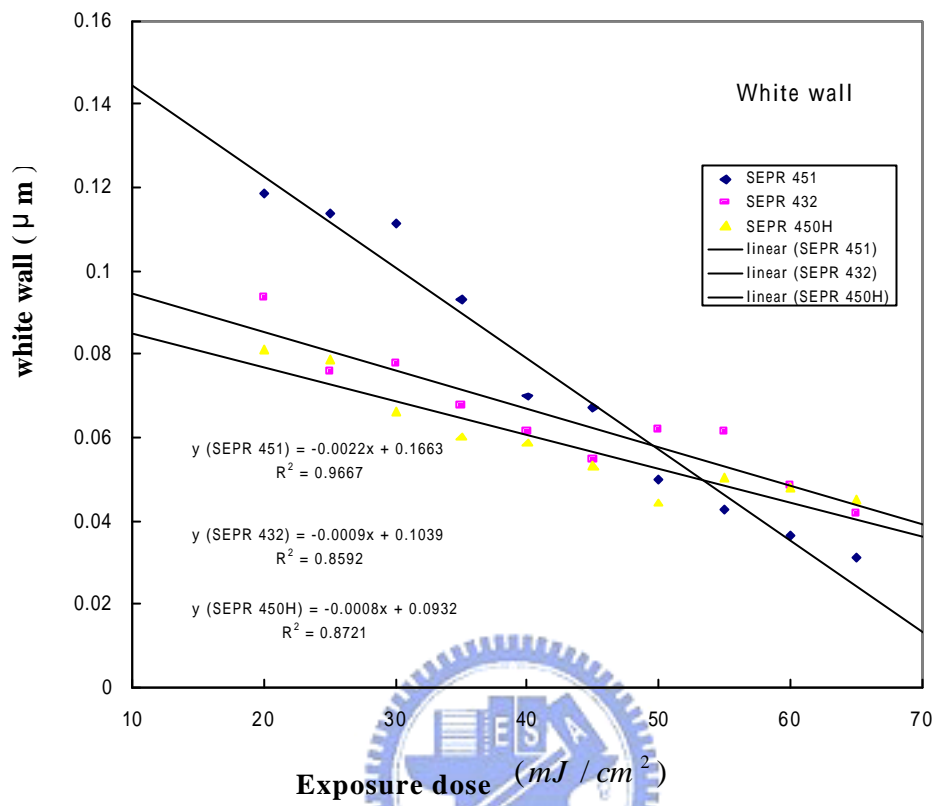


Fig. 7.2 (d)

Figure 7.2 (a) SEPR 451, (b) SEPR-432 and (c) SEPR-450H, correlation diagram of exposure dose and line width, (d) Graphs showing exposure dose vs. white wall for three different PR.

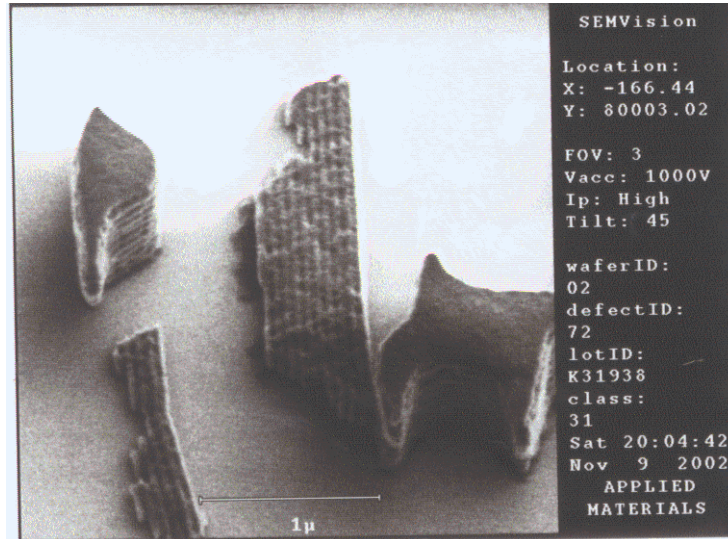


Figure 7.3 Collapse of CD bar for SEPR 451 PR at exposure dose of 80  $mJ/cm^2$ , picture taken by Applied Materials SEM Vision.

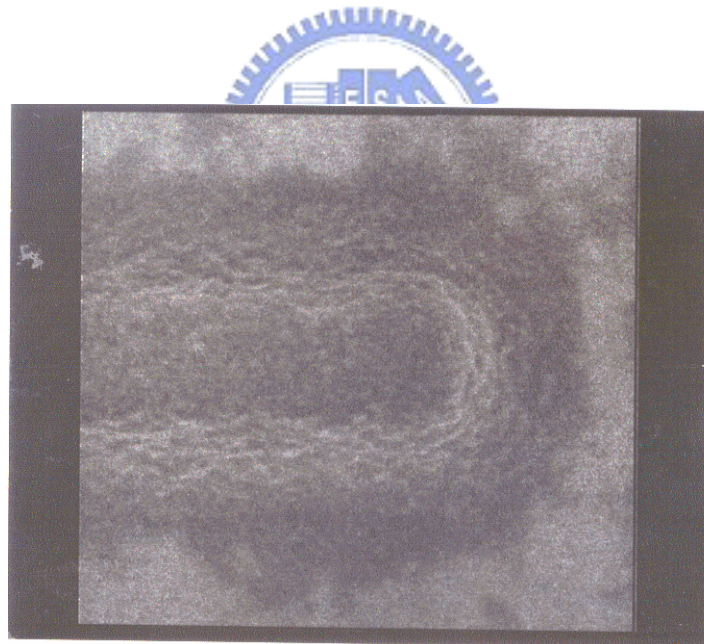
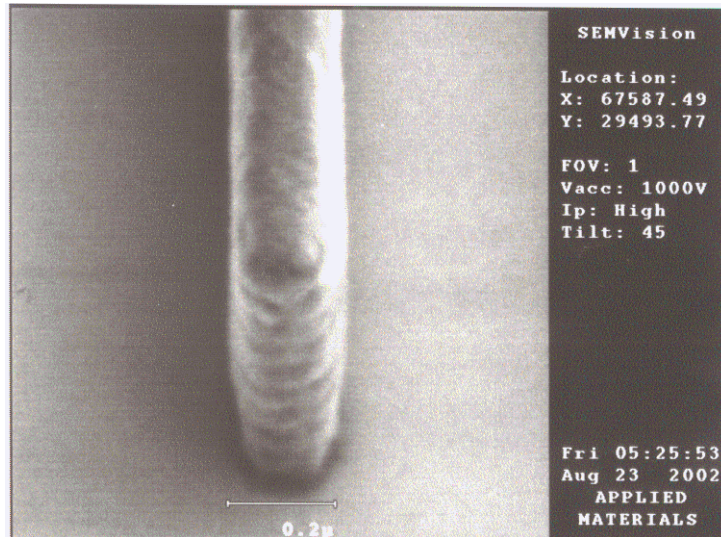
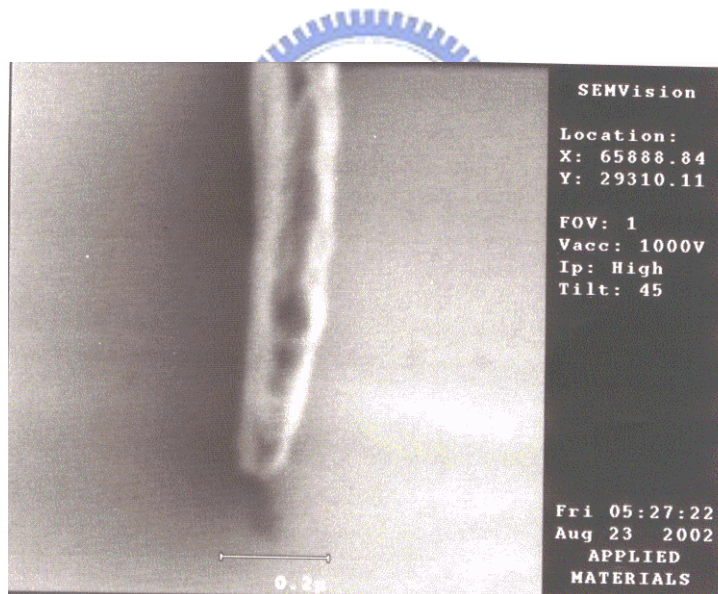


Figure 7.4 Exposure dose becomes too low ( $10 mJ/cm^2$ ) for SEPR-450H PR, observed with the Hitachi SEM at a magnification voltage of 100Kv. PR would not form a pattern.





**Fig. 7.5 (a)**



**Fig. 7.5 (b)**

Figure 7.5 (a) high exposure dose ( $50 \text{ mJ}/\text{cm}^2$ ) makes CD bar become smaller.

(b) Instability of CD bar caused by high exposure dose ( $60 \text{ mJ}/\text{cm}^2$ )

for SEPR-432 PR, by Applied Materials SEM Vision.

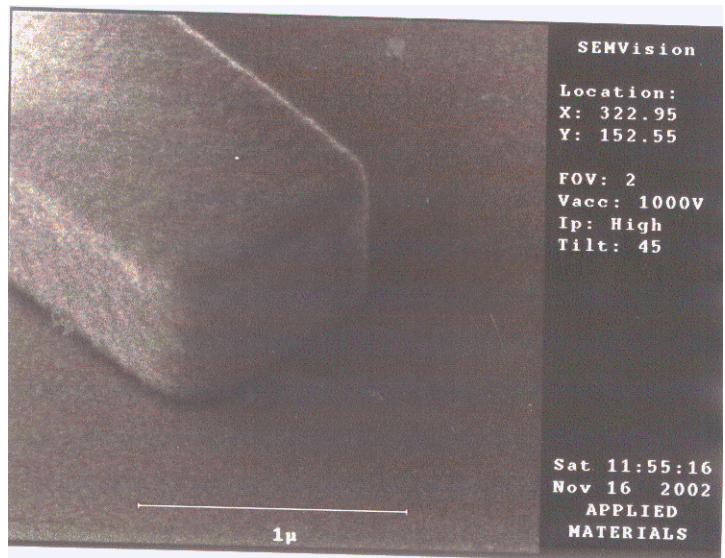


**Fig. 7.6 (a)**

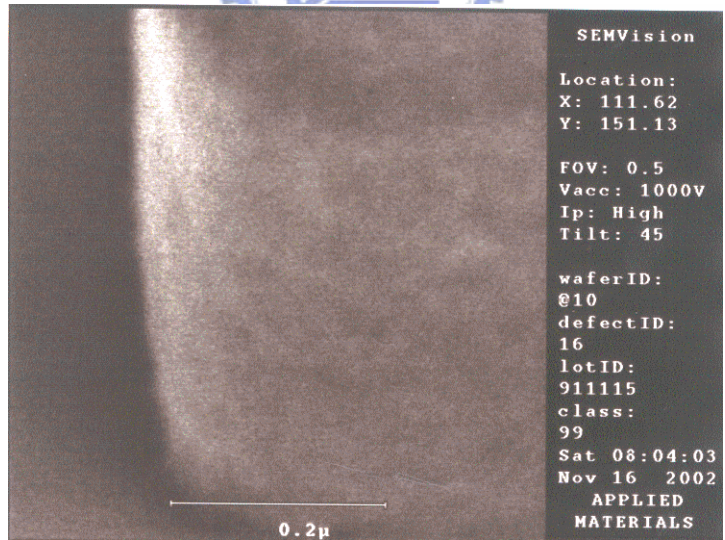


**Fig. 7.6 (b)**

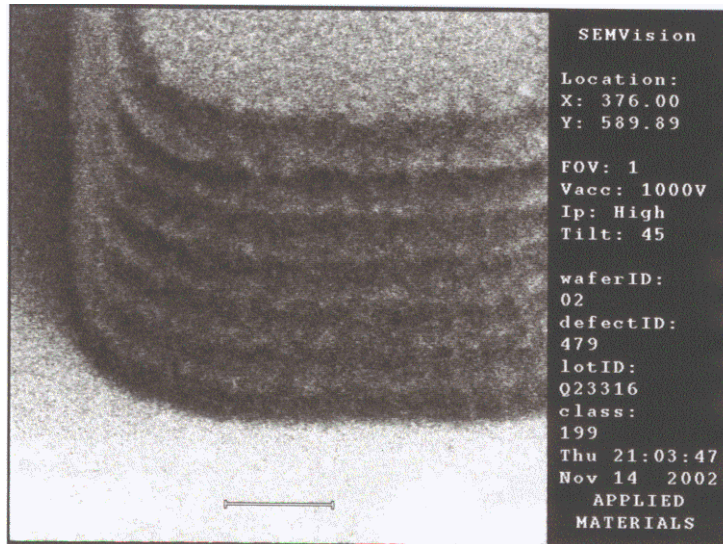


**Fig. 7.6 (c)**

Figure 7.6 (a) add top ARC to SEPR 432, (b) add bottom ARC to SEPR 432,

(c) SEPR 432 without adding any ARC, graphs showing standing wave as side wall of CD bar was observed via Applied Materials SEM Vision.



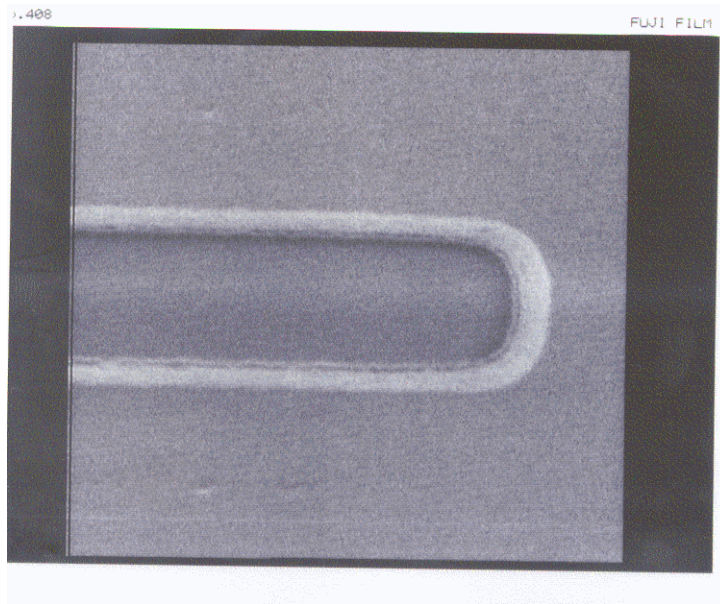


Figure 7.7 DUV light source, SEPR 451 photo resist, exposure time  $=40\text{ mJ} / \text{cm}^2$ , focus= $0\mu\text{m}$ . Observed with the Hitachi SEM at a magnification voltage of 50Kv. i) line-width, ii) white wall.

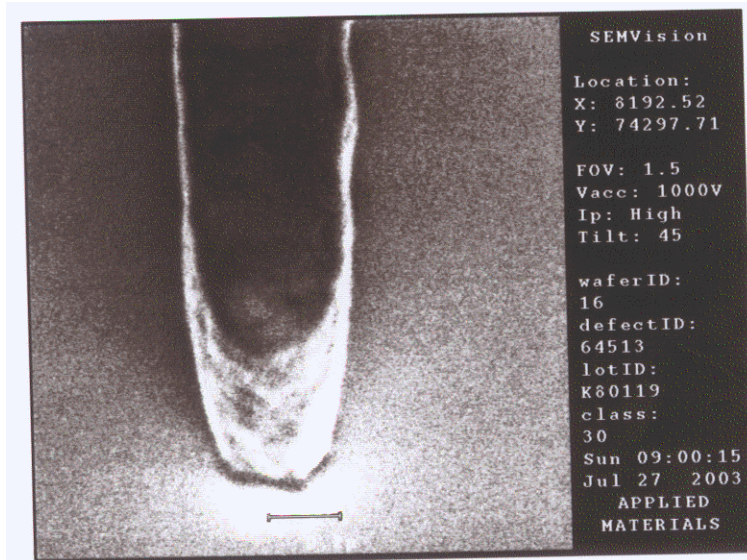


Fig 7.8 (a)

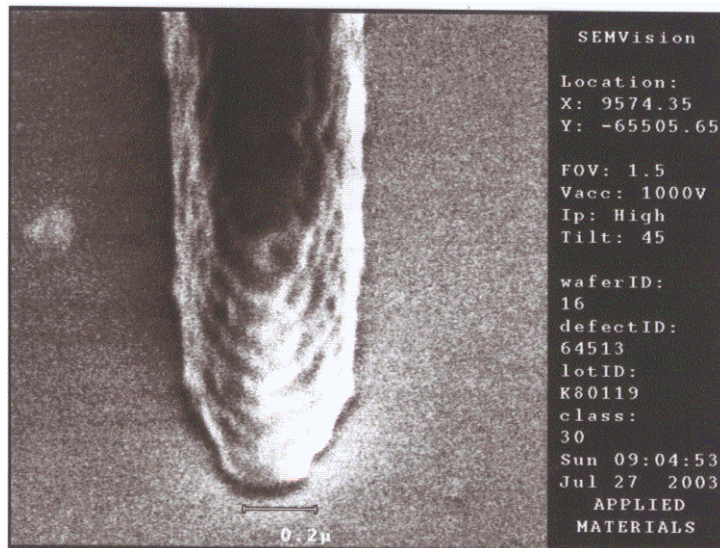


Fig. 7.8 (b)

Figure 7.8 DUV light source, SEPR 432 photo resist, exposure dose  $=30 \text{ mJ/cm}^2$ , Observed with the Applied Materials SEM at a scanning angle of  $+45^\circ$ : (a) focus= $0 \mu\text{m}$ , (b) focus= $+1.0 \mu\text{m}$  CD Bar three -dimensional picture.

## Chapter 8

### Analysis of the Effects of Reflectance and Refraction Generated by Wafers Made from Fused Silica, $AlO_xN_y$ and $TiSi_xN_y$ Under Different Light Sources on Pattern Length and Best Focus

#### ■ Introduction

Wafer throughput in micro-lithography depends on the sensitivity of the resist film to radiation. A lower exposure time required to produce a latent image in the resist corresponds to a higher throughput<sup>17</sup>. The design by Watanabe et al.<sup>18</sup> showed that the focus margin for 0.3 $\mu$ m lithography with a KrF excimer stepper is  $\pm 0.08\mu$ m for a DOF of  $\pm 0.5\mu$ m. It is possible for an ArF excimer laser stepper to achieve 0.13 $\mu$ m lithography with a DOF of  $\pm 0.5\mu$ m by using the recently developed technique of super resolution. The wafer surface profile is structure of the device and has irregularities of 0.3 to 1 $\mu$ m. As optical lithography will not reach the necessary resolution for future demands in microengineering. Now lithographic techniques have to be ready to produce nanostructures in a parallel way. Atoms with thermal kinetic energies have de Broglie wavelengths in the picometer regime and so they do not suffer from diffraction when focused down to a nanometer scale spot size. In the last

decade the investigation of atom light interaction has shown, that the trajectories of neutral atoms can be efficiently manipulated with laser light and that optical elements for neutral atoms can be built using the resonant interaction with laser light <sup>19 - 21</sup> .

The photolithographic process is further limited since a yellow light source does not promote the resist to react chemically. Accordingly, photolithography should be performed in an environment with a yellow light source. The commonly used light sources in the stepper include the G-line, the H-line and DUV (deep ultraviolet). The G-line wavelength is ~436nm, the I-line  $\lambda=350\sim450\text{nm}$ , and DUV  $\lambda=100\sim300\text{nm}$ . DUV wavelengths differ according to the laser gas composition: KrF  $\lambda=248\text{nm}$ , ArF  $\lambda=193\text{nm}$  and F<sub>2</sub>  $\lambda=157\text{nm}$  <sup>6</sup> . In this work, the DUV stepper's laser light source, KrF  $\lambda=248\text{nm}$ , was used.

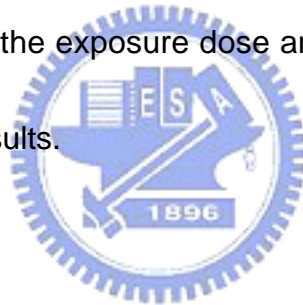
## ▪ Experimental

This investigation used 1) fused silica, 2)  $\text{AlO}_x\text{N}_y$ , 3)  $\text{TiSi}_x\text{N}_y$  wafers as exposure materials and used these three different wafer materials as the bottom reflective materials under a thin film of photo resist . This investigation also divided the wafer surface into a lateral axis and direct axis using matrix exposure. Various combinations of focus and exposure dose then were used

to investigate the variations in wafers made from different materials using the same photo resist.

The focus of PR (Photo Resist) varies with thickness and sensibility. To obtain a reference point for the focus, this investigation used fused silica to coat SPR 432 photo-resist before the experiment to adjust the focus of the wafer via matrix exposure, and fixed the exposure dose at  $35 \text{ mJ}/\text{cm}^2$  (best exposure dose). The focus value is assumed to be below  $\pm 0.1 \mu\text{m}$ , which is considered the best focus of experiment, focus is measured in relation to zero.

This investigation adjusted the exposure dose and focus via matrix exposure to obtain the experiment results.



## ▪ Results and Discussion

### Method used to obtain the best focus

Best focus is the diagram that is best similar with reticle and obtained by altering the focus given fixed exposure dose. Best focus exposes 17 sets of patterns on the surface of the wafer coated with positive resist (SEPR 432), and each pattern set comprises nine sets of horizontal pattern and nine vertical patterns. Each of these nine sets of patterns comprises five rhombus patterns,



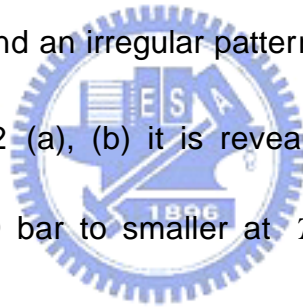
and the ratio of length to width of these rhombus patterns in the reticle is 30:1.

The pattern shapes change with focus variation. The length of each rhombus pattern is measured, revealing an association between long length and good focus. The condition for the experiment to obtain the best focus is SEPR 432 Photo Resist, Exposure Dose =  $36 \text{ mJ/cm}^2$ , Exposure step =  $0.15 \mu\text{m}$ , focus variation ranges from  $+1.4 \mu\text{m}$  to  $-1.4 \mu\text{m}$ .

### Focus Exposure Theory

Figure 8.1 clearly illustrates a cone shaped distribution and positive and negative symmetry of light sources from the lens to the wafer surface. Given focus =  $+1.4 \mu\text{m}$  and focus =  $-1.4 \mu\text{m}$ , the exposure area of CD Bar exceeds focus =  $0 \mu\text{m}$ . Consequently, the size of CD Bar is not different given focus =  $0 \mu\text{m}$  and focus =  $\pm 1.4 \mu\text{m}$ . Pattern length is longest when focus =  $0 \mu\text{m}$ , because exposure area is smallest and pattern length is shortest when focus =  $\pm 1.4 \mu\text{m}$  because exposure area is maximized. However, these phenomenon only occur on positive resist. For negative resist opposite results are obtained. Positive resist is characterized by the lighted area producing photo-acid and alkali developer, which is eliminated following neutralization because of the balance between acid and alkali. DUV light source has a cone shape

distribution, and positive and negative symmetry exists between the lens and the wafer surface. When exposure location is on the top of the cone, then this investigation assumes focus=0 $\mu$ m. The focus distance increases with the distance of the exposure location from the top of the cone., The cone area is smallest when focus=0 $\mu$ m, and thus the lighted area is less than for focus= $\pm$ 1.4 $\mu$ m while the pattern length is longer or bigger. The lighted area of positive resist increases given focus= $\pm$ 1.4 $\mu$ m. Besides, probably because of the serious defocus or the reduced capacity to display diagram borders, pattern length is reduced and an irregular pattern forms given focus= $\pm$ 1.4 $\mu$ m, as illustrated in Figure 8.2 (a), (b) it is revealed that high wafer surface reflectance can cause CD bar to smaller at  $TiSi_xN_y$  wafers, and (c) low reflectance makes CD bar become larger and wafer surface remain Photo Resist. From Figure 8.3, it is found that line-width measured after exposed with high dose is much smaller than that when exposed with low dose, When exposure dose is low, line-width is wider than that exposed at high dose. This can be attributed to the facts that at high exposure dose, the absorption of high energy of PR enhances the reaction capability of neutralization. Therefore, there will be more areas to be neutralized. Those impurities after neutralization can be rapidly washed away by DI water. However, too high of exposure dose



can cause line-width to become very small. As a result, the aspect ratio becomes too large. Therefore, CD bar can't hold back the turbulent force caused by DI water as neutralized area is washed, causing CD bar to collapse.

### **Influence of Wafer Surface Materials on Best Focus Variation**

When the variation of focus is confined within the scope of  $\pm 1.4\mu\text{m}$ , the experiment found that wafers made from different materials produced different focus variation even if they were coated using the same SPR 432 photo resist. From the comparisons of focus variation curves in Figure 8.3 (a), (b) and (c), three kinds of wafers have different materials and different best focuses even given identical exposure and PR conditions. The best focus is  $0.061\mu\text{m}$  for wafers with fused silica surface,  $0.200\mu\text{m}$  for wafers with  $\text{AlO}_x\text{N}_y$  surface, and  $0.061\mu\text{m}$  for wafers with  $\text{TiSi}_x\text{N}_y$  surface. From the analysis of Figure 8.1, when laser light projects into photo resist, the light go through the PR thin film area and produces refractive and reflectance because PR comprises sensitive doses. This investigation did not consider the influence of refractive and reflectance in the thin film area on the experiment, because SEPR 432 PR was required in all experiments. The reflectance varies with wafer surface materials.

The experiment results found that the three wafers had different best focuses. Comparing these three experimental conditions, reflectance=11.82% and best focus=0.200 $\mu\text{m}$  if the wafer is coated by  $\text{AlO}_x\text{N}_y$ , while reflectance=17.63% and best focus=0.245 $\mu\text{m}$  if the wafer surface is coated by  $\text{TiSi}_x\text{N}_y$ . The difference between the two reflectances is 5.81%, while that of best focuses is only +0.045 $\mu\text{m}$ . Comparing reflectances when using  $\text{AlO}_x\text{N}_y$  and fused silica as the wafer surface materials, the difference is only 0.26% , but the difference in best focus is 0.139 $\mu\text{m}$ . Therefore, no necessary relation exists between best focus and material reflectance. To analyze the influences on best focus is the refractive phenomenon of auto focus light sources. The experiment used a halogen lamp as an auto focus light source because halogens light source refractive phenomenon caused the light source to refract at an angle when the sensor received the plane with the best focus. Consequently, the planes of best focus differ for different materials. After reflecting different wafer materials with halogen light sources, this investigation found the planes of auto focus via PR film refraction, as follows: fused silica=0.023 $\mu\text{m}$ ,  $\text{AlO}_x\text{N}_y$  =0.199 $\mu\text{m}$ ,  $\text{TiSi}_x\text{N}_y$  =0.210 $\mu\text{m}$ . The factor of influence on best focus thus is the refraction on the wafer by the auto focus (halogens lamp) light source, not the reflectance on the wafer by the exposure

(laser) light source.

### **Influence of Wafer Surface Materials on DOF (Depth of Focus) Variation**

DOF indicates that focus changes under fixed exposure dose; that is, focus changes from positive to negative with zero as datum. The experiment can accept some values within a certain scope. The scope of focus in the experiment is  $\pm 1.4\mu\text{m}$ . Any measured point in this scope is considered acceptable by the experiment. From Figure 8.4, wafers made from different materials, even given identical PR and exposure conditions, obtain different DOF. Improving imaging effects requires deeper DOF. From Equation (1), possible influences on DOF include wavelength ( $\lambda$ ), numerical aperture (NA) and  $K_2$  ( $K_2 = NA^2 / \lambda$ ). Meanwhile, from Equation (2), the only method of changing DOF under the same conditions of NA with  $\lambda$  is to control  $K_2$ . Previously, many researches in this field proposed only that potential influences on DOF include photo resist and some process parameters. However, this investigation found that wafer surface material is an important influence on DOF. Three kinds of wafer are compared, with exposure dose =  $56 \text{ mJ}/\text{cm}^2$ , fused silica DOF =  $0.9\mu\text{m}$ ,  $\text{AlO}_x\text{N}_y$  DOF =  $1.2\mu\text{m}$ , and  $\text{TiSi}_x\text{N}_y$  DOF =  $0.75\mu\text{m}$ . Wafer material influences the results of DOF.

$$R = \frac{K_{PR} I}{NA} \dots\dots\dots \text{Eqn. (1)}$$

$$DOF = (K_{PR} + K_{\text{wafer surface material}} + K_{\text{other}}) \frac{I}{NA^2} \dots\dots\dots \text{Eqn. (2)}$$

### **Influence of Exposure Dose on Pattern Length Variation for Different Wafer Surface Materials**

From Figure 8.4, exposure dose is a key influence on pattern length. This research investigation found that pattern length decreased with increasing exposure dose, regardless of wafer material. From the mutual comparisons in Figure 8.4, wafers made from three different materials display different pattern lengths given the same exposure dose. However, these wafers display the same curve trends. Given the same PR thickness, the most important influence on pattern length is PR sensitivity. However, because the experiment used the same PR, this investigation did not consider the influences of sensitivities on the experiment results. To reduce the influence of PR film on the experiment results, the PR film of these wafers is limited to  $6500 \pm 200 \text{ \AA}$ , and the homogeneity of PR film is  $3\sigma < 0.03 \mu\text{m}$ .

Figure 8.4 selects the best focus for analyzing the relationship between exposure dose and pattern length. The same exposure dose is compared for

different wafer surface materials, with exposure dose= $26 \text{ mJ/cm}^2$  and  $56 \text{ mJ/cm}^2$  being selected as the analytic condition. Given exposure dose= $26 \text{ mJ/cm}^2$ , fused silica wafer pattern length  $X=12.622\mu\text{m}$  and  $Y=12.339\mu\text{m}$ ,  $\text{AlO}_x\text{N}_y$  wafer pattern length  $X=12.850\mu\text{m}$  and  $Y=12.365\mu\text{m}$ , and  $\text{TiSi}_x\text{N}_y$  wafer pattern length  $X=9.257\mu\text{m}$  and  $Y=8.327\mu\text{m}$ . Pattern lengths  $X$  and  $Y$  indicate the longest measures of 1:30 rhombus pattern measured on wafer surface under vertical and horizontal exposure, respectively. The measurements of pattern lengths  $X$  and  $Y$  differ because of the astigmatism. Fused silica reflectance= $12.03\%$ ,  $\text{AlO}_x\text{N}_y$  reflectance= $11.82\%$ ,  $\text{TiSi}_x\text{N}_y$  reflectance= $17.63\%$ . The reflectance of fused silica/ $\text{AlO}_x\text{N}_y$  is 1.017, while the value of pattern length  $X$  of  $\text{AlO}_x\text{N}_y$ /fused silica is 1.018, and the value of  $Y$  is 1.00. The reflectance of fused silica/ $\text{TiSi}_x\text{N}_y$  is 0.682, the value of pattern length  $X$  of  $\text{TiSi}_x\text{N}_y$ /fused silica is 0.733, and the value of  $Y$  is 0.674. Given exposure dose= $56 \text{ mJ/cm}^2$ , pattern length  $X$  is  $7.931\mu\text{m}$ , fused silica wafer  $Y=7.699\mu\text{m}$ ,  $\text{AlO}_x\text{N}_y$  wafer pattern length  $X=8.930\mu\text{m}$   $Y=8.263\mu\text{m}$ , and  $\text{TiSi}_x\text{N}_y$  wafer pattern length  $X=4.947\mu\text{m}$   $Y=4.494\mu\text{m}$ . The value of pattern length  $X$  of  $\text{AlO}_x\text{N}_y$ /fused silica is 1.125, while the value of  $Y$  is 1.073; moreover, the value of  $\text{TiSi}_x\text{N}_y$ /fused silica pattern length  $X$  is 0.623, while the value of  $Y$  is 0.583. The experimental data

demonstrates that an inverse relationship exists between reflectance and pattern length; pattern length decreases with increasing wafer surface reflectance, while energy reflected by the wafer surface increases. The energy absorbed by the photo resist increases reflectance, enabling PR to absorb more energy and decreasing pattern length.

The pattern length measured by high exposure dose is less than that measured by low exposure dose. The key reason for this difference is that the PR is made of sensitive materials which produce a more sensitive reflection on encountering strong light. When using high exposure dose, PR absorbs high energy and enhances the neutralization capability. Therefore, more areas are neutralized and impurities are quickly washed out by DI water.



### **Astigmatism**

From Figure 8.4 (a), (b) and (c), pattern lengths X and Y are different, meaning that the curves of the active line and the dotted line do not overlap. Pattern lengths X and Y indicate the longest measurements of a 1:30 rhombus pattern on the wafer surface under vertical and horizontal exposure, respectively. A difference between the measures indicates that the focuses of lenses X and Y of the Stepper exposure machine do not share the same



location, causing the experimental difference in the X and Y focuses, which is an unavoidable error. The only way to solve the problem of astigmatism is to enhance the lens quality or turn the lens angle to the optimum area of the X and Y ball surface of the lens. Figure 8.4 has given the phenomenon that different exposure materials cannot improve astigmatism. The observed  $X/Y=1$  in some areas do not mean improved astigmatism because the change of focus may reduce the measures. Precise measurements of astigmatism should use best focus as a reference point.

#### ▪ Conclusions



The components of photo resist influence the measures of best focus. However, the experiment found that the same PRs coated on the wafers of different materials and also influence best focus. The PR focus shift results mainly from sensitivity, while the wafer focus shift results from the refraction factor. Pattern length changes according to measured exposure dose. However, pattern length also changes if wafers made from different materials are exposed under the same exposure dose. The experiment found that wafer reflectance was a key factor. An inverse relationship exists between reflectance and pattern length, with wafer reflectance increasing with

decreasing pattern length. The more reflectance, the more energy will be reflected by wafer surface. The reflected energy is absorbed by photo resist. Consequently, energy absorption by PR increases with increasing reflectance, thus reducing the pattern length. To prevent these two effects, the wafer surface can be coated with a layer of totally reflective photo resist. Industry currently is using the photo resist of bottom ARC (Anti-Reflection Coating), but the reflectance of bottom ARC is approximately 60~70% and cannot be improved. Presently, improvements in this field are being researched.



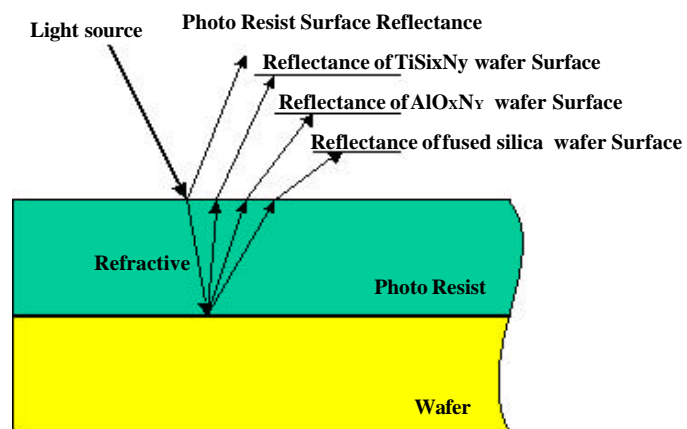


Figure 8.1 Stepper Exposure Diagram, Best Focus Locations following Refraction on Photo Resist and Wafer Surface by Auto Focus Light Source.



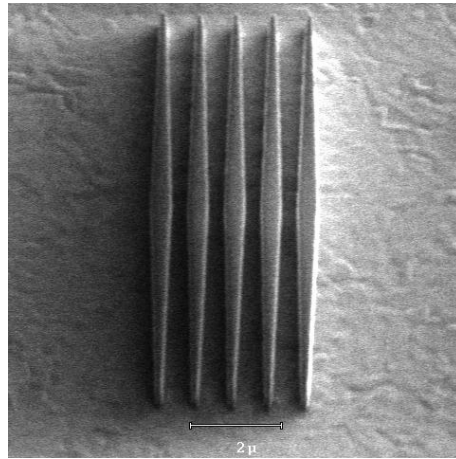


Fig 8.2 (a)

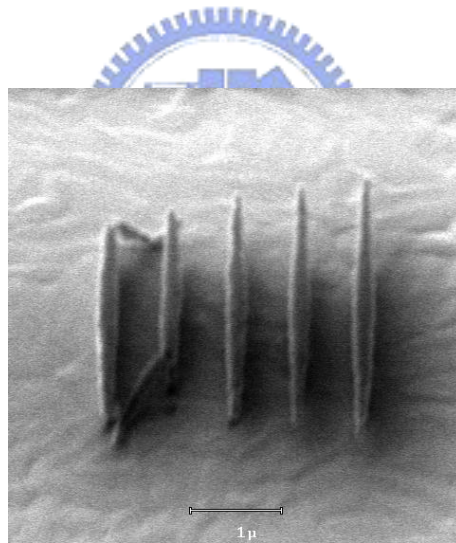


Fig 8.2 (b)

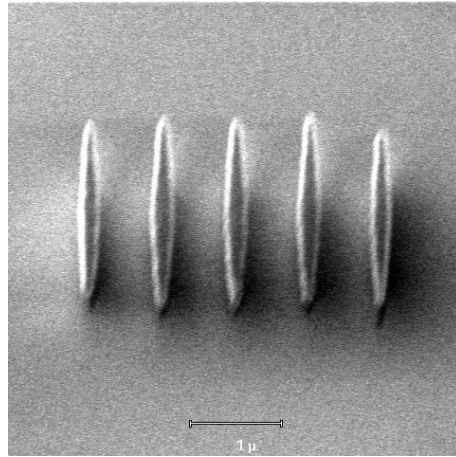


Fig 8.2 (c)

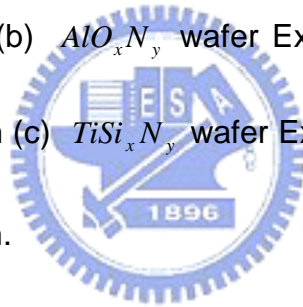
Figure 8.2 Observed with the Applied Materials SEM at a scanning angle of

+45°, (a) Fused silica wafer Exposure Dose= $46 \text{ mJ/cm}^2$  and

focus= $0.0 \mu\text{m}$ , (b)  $\text{AlO}_x\text{N}_y$  wafer Exposure Dose= $56 \text{ mJ/cm}^2$  and

focus= $-0.45 \mu\text{m}$  (c)  $\text{TiSi}_x\text{N}_y$  wafer Exposure Dose= $56 \text{ mJ/cm}^2$  and

focus= $-0.15 \mu\text{m}$ .



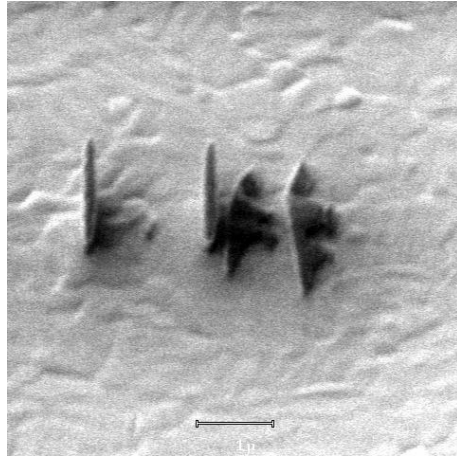


Fig 8.3 (a)

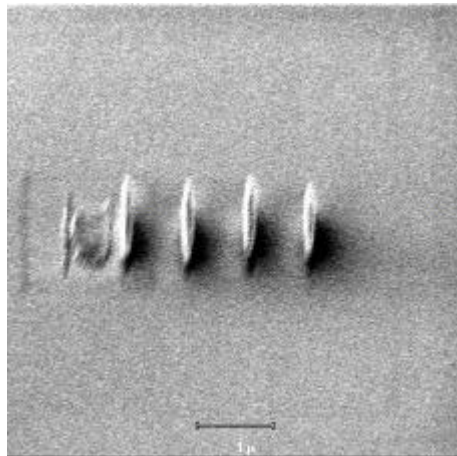
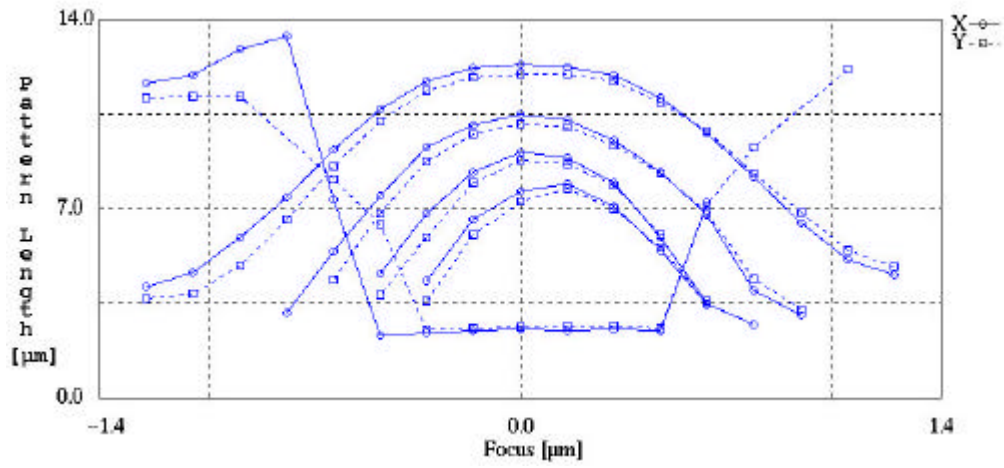


Fig 8.3 (b)

Figure 8.3 Collapse of CD bar for (a)  $AlO_xN_y$  wafer at exposure dose of  $56\text{ mJ/cm}^2$  and focus= $-0.65\mu\text{m}$  (b)  $TiSi_xN_y$  wafer at exposure dose of  $56\text{ mJ/cm}^2$  and focus= $-0.45\mu\text{m}$ , picture taken by Applied Materials SEM Vision.



*Fused Silica*

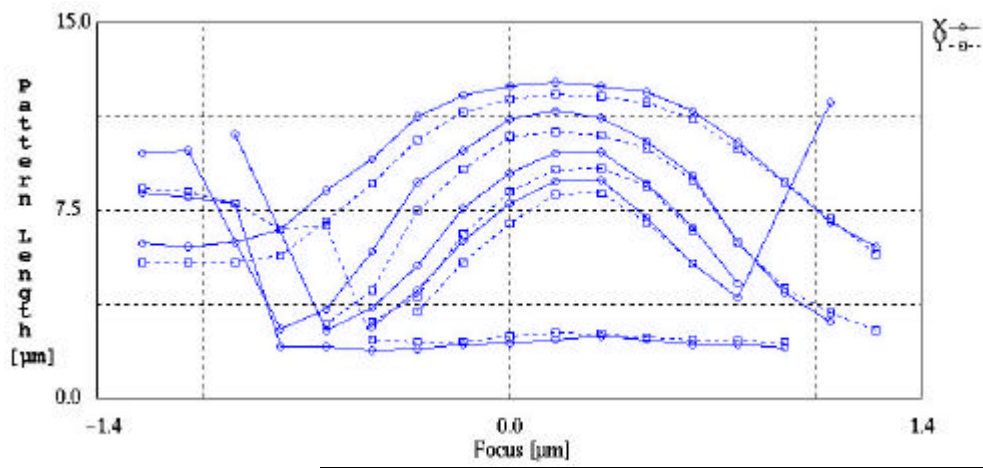
$I = 248\text{nm}$

reflectance = 12.03%

Fused Silica Best Focus Pattern Length			
Exposure (mJ/cm <sup>2</sup> )	X(μm)	Y(μm)	X/Y
16	13.495	0	no good
26	12.622	12.339	1.023
36	10.611	10.264	1.034
46	9.281	8.912	1.041
56	7.931	7.699	1.030



Fig. 8.4 (a)



$AlO_xN_y$

$I = 248nm$

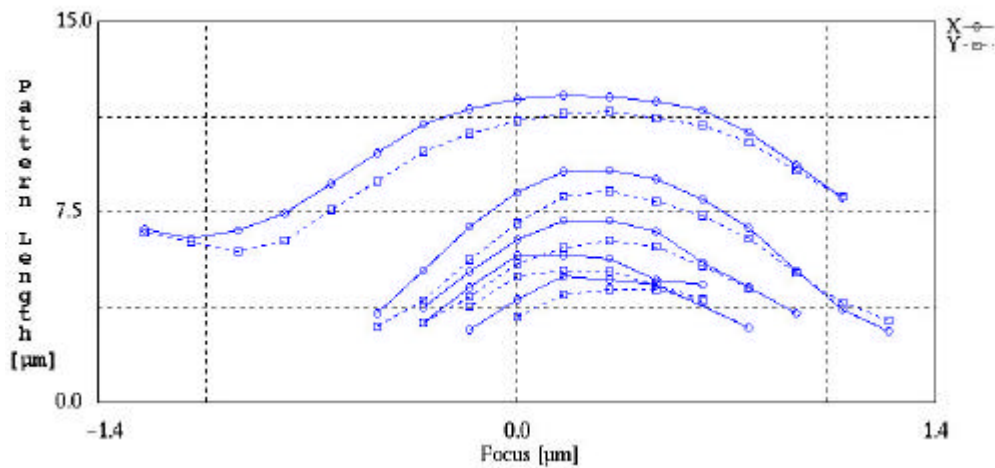
reflectance = 11.82%

AL <sub>x</sub> O <sub>y</sub> N <sub>z</sub> Best Focus Pattern Length			
Exposure(mJ/cm <sup>2</sup> )	X(μm)	Y(μm)	X/Y
16	0	8.577	0.000
26	12.85	12.365	1.039
36	11.518	10.961	1.051
46	10.014	9.411	1.064
56	8.93	8.263	1.081



Fig. 8.4 (b)





TiSixNy Best Focus Pattern Length			
Exposure(mJ/cm2)	X(μm)	Y(μm)	X/Y
16	12.34	11.61	1.063
26	9.257	8.327	1.112
36	7.258	6.401	1.134
46	5.97	5.276	1.132
56	4.947	4.494	1.101

$TiSi_xN_y$

$\lambda = 248nm$

reflectance = 17.63%



**Fig. 8.4 (c)**

Figure 8.4 Pattern Length Focus Process Latitude Smiley Curve Obtained by

Deep UV Together with SEPR 432 Photo Resist from Wafers

Made using (a) fused silica, (b)  $AlO_xN_y$  or (c)  $TiSi_xN_y$  via

Matrix Exposure.

## Chapter 9

### Conclusions

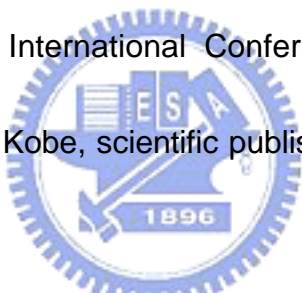
The stability of nano photo-lithography is the key factor of success and the reticle is one of important factors. The reticle currently used in manufacturing industry is very expensive and the effect of heat-radiation is not good. In the past micron process era, reticle needed not function of heat radiation because the microscale thermal shape-changing is tolerable for micron. But in nano era, microscale shape-changing of reticle may cause the decline of wafer yield. So we took advantage of characteristics of thermal conductivity of diamond to solve the problem of thermal effects. However, while the increasing of diamond film on reticle solves the problem of thermal effects, it also reduces the intensity of light that penetrates through reticle. Until today, we still have not yet developed technology that enables light to penetrate diamond completely. As soon as there is a breakthrough, diamond film reticle may be applied to entire manufacturing technology of semi-conductor lithography.

In the thesis, we compare relations of focus and exposure dose that were made from same materials and reflectance and refraction that were made from different wafer materials with line width and white wall to respond reference factors of future nano manufacturing process. The results of experiment found

that focus would affect line width and form a curve that had symmetry of positives and negatives while different wafer materials would enable optical beam to generate reflectance and refraction that in turn enable best focus to generate shift. Therefore, the control of focus in the nano manufacturing process should be very strict. Besides, in the research of effects of exposure dose on line width and white wall, we found that there were correlations among exposure dose, line width and white wall. High exposure dose may lead to the smaller line width and white wall. The relationship of variation among them was decided by sensitivity of photo resist.



## ■ References

- [1] J. E. Graebner, Diamond Films Technol. 3 (1997) 77.
- [2] D. Fournier, K. Plaman, Diamond Relat. Mater. 4 (1995) 809.
- [3] J. E. Graebner, Recent developments in the thermal conductivity of CVD diamond, Adv. New diamond Sci. technol. (1994) 345-351.
- [4] Y. Q. Gunge et al., thermal diffusivity measurement of thin films, High temp.-high pressures 25 (1993) 553-559.
- [5] GD. Lu, R. Enck, A. Feldman et al., thermal conductivity round robin testing, in: Proceedings Fourth International Conference on the new diamond science and technology, Kobe, scientific publishing division of MYO, Tokyo (Japan), 1994, p. S8-2.
- 
- [6] S. Albin, thermal diffusivity of diamond films, SPIE J. 1145 (1989) 85-94.
- [7] C. M. Vest, Holographic Interferometry, Wiley, New York, 1979.
- [8] W. Chen, J. Carroll, G. Storm, R. Ivancich, J. Maloney, O. Maurin, E. Souleillet, Pellicle-induced reticle distortion: an experimental investigation, SPIE 3546 (1998) 167-172
- [9] K. D. Roth, T. Struck, Pellicle-induced distortions on photo masks, SPIE 3412 (1998) 440-446.
- [10] A. Mikkelsen, R. Engelstad, E. Lovell, Pattern transfer distortions in optical

photomasks, *Microelectronic Engineering* (2001) 489-495

[11] R. Leuschner, H. Borndorfer, E. Kuhn, M. Sebald, R. Sezi, M. Byer and CH.

Nolscher, *Polymer Engineering and Science*, 1558 (1998).

[12] Y. Matsuoka, K. Yokota, S. Ogitani, A. Ikeda, H. Takahashi and H. Ai,

*Polymer Engineering and Science*, 1618 (1992).

[13] Cesar M. Garza, Eric J. Solowiej and Mark A. Boehm, *Polymer*

*Engineering and Science*, 1600 (1992).

[14] Allan E. Nader, Kazunori Imai, John D. Craig, Christina N. Lazaridis,

Daniel O. Murray III, Michael T. Pottiger, Stephen A. Dombchik and

William J. Lautenberger, *Polymer Engineering and Science*, 1613 (1992).

[15] Hiroshi Nishizawa, Kuniaki Sato, Mitsumasa Kojima and Hidetaka Satou,

*Polymer Engineering and Science*, 1610 (1992).

[16] Birol Kuyel and Harry Sewell, *J. Vac. Sci. Technol.* 1385 (1990).

[17] Treva Long, S. Kay Obendorf and Ferdinand Rodriguez, *Polymer*

*Engineering and Science*, 1589 (1992).

[18] M. Watanabe et al., *SPIE* . vol. 2179 (1994)

[19] C. S. Adams, M. Sigel, and J. Mlynck, *Phys. Rep.* 3, 240 (1994)

[20] Shi, Frank F. and Yu, Shuhuan, *Thin Solid Films*, June 8, pp. 254-258

(1998)

- [21] Fay, Bernard, Microelectronic Engineering, Volume: 61-62, July, 2002, pp. 11-24 (2002)
- [22] Lawes, R.A., Applied Surface Science, Volume: 154-155, February 1, 2000, pp. 519-526
- [23] Wada, Y., Microelectronics Journal, Volume: 29, Issue: 9, September, 1998, pp. 601-611
- [24] Matsuzaka, T., Microelectronic Engineering, Volume: 35, Issue: 1-4, February, 1997, pp. 3-9
- [25] Deguchi, Kimiyoshi; Haga, Tsuneyuki, Comptes Rendus de l'Academie des Sciences Series IV Physics, Volume: 1, Issue: 7, September, 2000, pp. 829-842
- [26] Chou, Stephen Y.; Krauss, Peter R., Microelectronic Engineering, Volume: 35, Issue: 1-4, February, 1997, pp. 237-240
- [27] Seo, Yongduck; Lee, Kyoungho; Yi, Moonsuk; Seo, Eunsung; Choi, Bo Kyung; Kim, Ohyun; Raptis, Ioannis; Argitis, Panayiotis; Hatzakis, Michael., Microelectronic Engineering, Volume: 46, Issue: 1-4, May, 1999, pp. 461-464
- [28] Smith, Henry I. Physica E, Volume: 11, Issue: 2-3, October, 2001, pp. 104-109



- [29] Fisher, A.; Tejeda, R.; Sprague, M.; Engelstad, R.; Lovell, E.,  
Microelectronic Engineering, Volume: 41-42, March, 1998, pp. 245-248
- [30] Sohda, Y.; Ohta, H.; Murai, F.; Yamamoto, J.; Kawano, H.; Satoh, H.; Itoh,  
H., Microelectronic Engineering, Volume: 67-68, June, 2003, pp. 78-86
- [31] Ronse, K., Microelectronic Engineering, Volume: 67-68, June, 2003, pp.  
300-305
- [32] Hector, Scott, Microelectronic Engineering, Volume: 41-42, March, 1998,  
pp. 25-30
- [33] Kudryashov, V.A.; Lee, Sing, Microelectronic Engineering, Volume: 57-58,  
September, 2001, pp. 819-823
- [34] Yomazzo, M.; Van Den Broeke, D., Microelectronic Engineering, Volume:  
41-42, March, 1998, pp. 53-58
- [35] Azam Ali, M.; Gonsalves, K.E.; Golovkina, V.; Cerrina, F., Microelectronic  
Engineering, Volume: 65, Issue: 4, May, 2003, pp. 454-462
- [36] Selzer, Robert (Bob); Heaton, John, Microelectronic Engineering, Volume:  
53, Issue: 1-4, June, 2000, pp. 591-594
- [37] Ausschnitt, Christopher P., Microelectronic Engineering, Volume: 41-42,  
March, 1998, pp. 41-46
- [38] Groves, T.R.; Pickard, D.; Rafferty, B.; Crosland, N.; Adam, D.; Schubert,

- G., *Microelectronic Engineering*, Volume: 61-62, July, 2002, pp. 285-293
- [39] Arnold, William H, *Microelectronic Engineering*, Volume: 46, Issue: 1-4,  
May, 1999, pp. 7-9
- [40] Ki-Ho, Baik, *Microelectronic Engineering*, Volume: 35, Issue: 1-4, February,  
1997, pp. 11-20
- [41] Peuker, M.; Lim, M.H.; Smith, Henry I.; Morton, R.; van Langen-Suurling,  
A.K.; Romijn, J.; van der Drift, E.W.J.M.; van Delft, F.C.M.J.M.,  
*Microelectronic Engineering*, Volume: 61-62, July, 2002, pp. 803-809
- [42] Rosolen, Grahame C., *Applied Surface Science*, Volume: 144, Issue: 1,  
April, 1999, pp. 467-471
- [43] Hirscher, S.; Kümmel, M.; Wolter, A.; Kaesmaier, R.; Jaeschke, A.,  
*Microelectronic Engineering*, Volume: 61-62, July, 2002, pp. 351-355
- [44] Van den hove, L.; Ronse, K., *Microelectronic Engineering*, Volume: 27,  
Issue: 1-4, February, 1995, pp. 357-365
- [45] Choi, Yang-Kyu; King, Tsu-Jae<sup>a</sup>; Hu, Chenming, *Solid-State Electronics*,  
Volume: 46, Issue: 10, October, 2002, pp. 1595-1601
- [46] Ngô, C.; Rosilio, C., *Nuclear Instruments and Methods in Physics  
Research Section B: Beam Interactions with Materials and Atoms*,  
Volume: 131, Issue: 1-4, August, 1997, pp. 22-29



- [47] Deguchi, K.; Miyoshi, K.; Matsuda, T., Journal of Electron Spectroscopy and Related Phenomena, Volume: 80, May, 1996, pp. 321-327
- [48] Shamaly, John J.; Bunze, Victor F., Microelectronic Engineering, Volume: 30, Issue: 1-4, January, 1996, pp. 87-93
- [49] Martin, Olivier J.F., Microelectronic Engineering, Volume: 67-68, June, 2003, pp. 24-30
- [50] Damm, Christoph; Peschel, Thomas; Risse, Stephan; Kirschstein, Ulf C., Microelectronic Engineering, Volume: 57-58, September, 2001, pp. 181-185
- [51] Pantenburg, F.J.; Mohr, J., Nuclear Instruments and Methods in Physics Research Section A: Accelerators, Spectrometers, Detectors and Associated Equipment, Volume: 467-468, Part 2, July 21, 2001, pp. 1269-1273

